Review

Contribution of Electrochemistry to Organometallic Catalysis

Anny Jutand

Chem. Rev., **2008**, 108 (7), 2300-2347 • DOI: 10.1021/cr068072h • Publication Date (Web): 08 July 2008

Contribution of Electrochemistry to Organometallic Catalysis

Anny Jutand*

Ecole Normale Supérieure, Département de Chimie, CNRS - UPMC, 24 Rue Lhomond, F-75231 Paris Cedex 5, France

Received October 31, 2007

Contents

* To whom correspondence should be addressed. Fax: 33 (0)1 44 32 24 02. E-mail: Anny.Jutand@ens.fr.

10.1021/cr068072h CCC: $71.00
Published on Web 07/08/2008

1. Introduction

Many reactions are nowadays catalyzed by a transition metal, which not only accelerates the reactions but allows, via its ligand(s), a fine control of the chemo-, regio-, and enantioselectivity of the catalytic reactions.[1,2]

The active catalytic species M_1, which initiates the catalytic cycle, is generally introduced via a precursor (precatalyst) M_0, which is often a stable and unreactive transition metal complex or salt (Scheme 1).

The active catalytic species M_1 may be generated in situ by reaction of the precursor M_0 with a reagent of the catalytic reaction or with an additive. Such reactions are chemical reductions or oxidations when M_1 and M_0 do not have the same oxidation state. When they have the same oxidation state, the active catalytic species M_1 may be delivered at a very low thermodynamic concentration from the precursor M_0 via an endergonic equilibrium, which lies in favor of the more stable M_0.

The catalytic cycle is a succession of elemental steps (i) involving catalytic species M_i at various oxidation states. Each elemental step is characterized by a rate constant k_i. When taken independently from each other, each step has its own reaction rate. However, when they are involved in a catalytic cycle, the effective rates of the successive steps are not independent from each other. Indeed, the rate of the step i is expressed as $\text{rate}_i = k_i[R_i][M_i]$ where k_i is the rate constant of step i, R_i the reagent involved in step i, and M_i is the catalytic species involved in step i, whose concentration $[M_i]$ is controlled and modulated by the rate of the previous reaction $(i - 1)$ in which M_i is generated (Scheme 1).[3,4] All steps will have the same rate as soon as the stationary regime is attained. It will be more easily reached and the efficiency of the catalytic cycle will be higher if the reaction rates of all elemental steps are made as close as possible to each other. This is illustrated in Scheme 2A,B where M* is the catalytic species of highest energy, which must be recovered at the end of each catalytic cycle, making this last reaction potentially very slow. The catalytic reaction whose energy diagram is represented in Scheme 2B will be more efficient than that in Scheme 2A because the value of the energy span, δG^0, has been minimized. In other words, to increase the efficiency of a catalytic cycle, one must accelerate the rate-determining step, that is, destabilize the most stable catalytic species, and also decelerate the fastest step by stabilizing the transition state of highest energy.[3,4]

It is thus worthwhile to investigate the rate and mechanism of all steps of a catalytic cycle to determine factors that control the efficiency of a catalytic reaction, to understand how and why a catalytic reaction works, so as to increase its efficiency in terms of turn-over and selectivities. This can be achieved by means of electrochemical techniques associated with spectroscopic techniques.

The contribution of electrochemistry to the determination of the mechanism of transition metal-catalyzed reactions is first presented. It is followed by a second contribution of electrochemistry to catalytic reactions in which intermediate organometallic species can be reactive only after activation by electron transfer or when the active organometallic species that initiates the catalytic cycle must be recycled from a nonreactive one formed in the catalytic cycle. In such transition metal-catalyzed electrosyntheses, the electrons play

Anny Jutand was born in France. She received her M.S. degree in Chemistry from the Ecole Nationale Supérieure de Chimie de Paris (ENSCP, University Paris VI) in 1971. She has obtained her "Doctorat d'Etat" (Ph.D.) under the supervision of Professor J.-F. Fauvarque at the University Paris XIII in Villetanneuse. After a postdoctoral stay with Professor B. Åkermark at the Royal Institute of Technology in Stockholm in 1980−1981, she moved back to the University Paris XIII where she was appointed as a "Chargée de Recherche" at CNRS. In 1985, she joined Dr. C. Amatore's group at the Ecole Normale Supérieure in Paris. She became Director of Research at CNRS (a position equivalent to full Professor) in 1992. She has received the 2003 Award from the Organic Chemistry Division of the French Chemical Society. Throughout her career, she has been interested in transition metal-catalyzed reactions from a synthetic and mechanistic point of view. From her postdoctoral stay in Sweden, she became interested in electrochemistry, first used for transition metal-catalyzed electrosyntheses and then to explore the mechanism of catalytic electrosyntheses or syntheses. She is author of 131 publications, 7 book chapters, and 7 patents.

Scheme 1

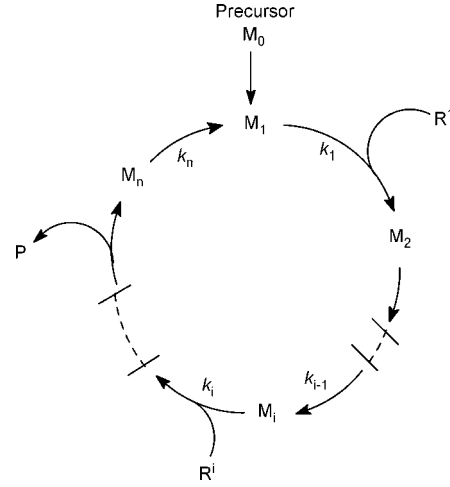

Scheme 2

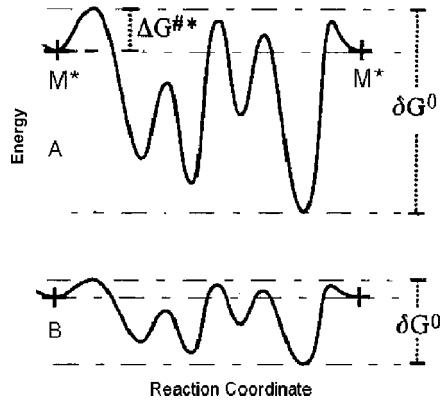

the role of a reagent (oxidant or reductant) and are used in stoichiometric amount.

2. Elucidation of the Mechanism of Transition Metal-Catalyzed Reactions by Using Electrochemical Techniques

2.1. General Features

The determination of the mechanism of a catalytic cycle requires the investigation of all steps of the catalytic cycle, separately from each other and then in the context of the real catalytic reaction, that is, taking into account for all steps the presence of all reagents and additives of the catalytic reaction. A mechanistic investigation requires kinetic data and characterization of the reactive species as well. Organometallic species may be characterized by most spectroscopic techniques (UV, NMR), provided they are stable enough. Kinetic data on their reactivity are also available through these techniques, provided the reactions are not too fast (half-reaction time, $t_{1/2}$, higher than some minutes). All these techniques are well-adapted for the reactivity of long-lived species. The investigation of more reactive species is problematic, but electrochemical techniques can fill in this gap.

Electroactive organometallic species involved in a catalytic cycle can be detected and characterized by their reduction or oxidation potentials. Moreover, since reduction or oxidation currents are proportional to the concentration of the electroactive species, their reactivity can be followed by using electrochemical techniques.[5–8] Kinetic data are thus available via two strategies, according to the lifetime of organometallic species.

Short-lived species can be generated by electrochemical reduction or oxidation of known organometallic complexes in transient *cyclic voltammetry* (Figure 1a,b) or *double potential step chronoamperometry* (Figure 1e,f) performed at a *steady disk electrode*.[5,6] The reactivity of the electrogenerated species can be followed by the evolution of their oxidation or reduction currents with scan rate (υ) or duration of potential steps (θ).[5,6] Time scales from 10^{-1} to 10^{-6} seconds are thus available, and electrochemistry is used for both its synthetic and its analytical abilities.

The reactivity of *long-lived* species ($t_{1/2}$ higher than a few seconds) can be followed by *chronoamperometry at a rotating disk electrode* (RDE; Figure 1a,c) by the evolution of their oxidation or reduction plateau currents with time.[5,6] Electrochemistry is thus simply used as an analytical technique to follow the concentration of organometallic species involved in slow steps.

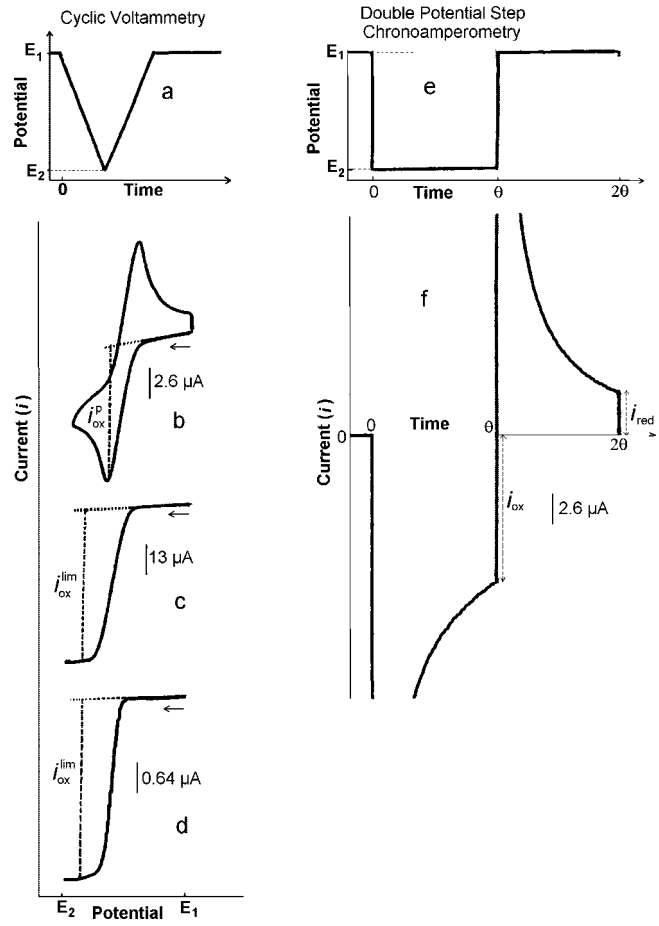

Figure 1. Electrochemical techniques used for the investigation of the mechanism of transition metal-catalyzed reactions, illustrated with the oxidation of ferrocene (2.8 mM) in THF containing nBu$_4$NBF$_4$ (0.3 M). The reference is a saturated calomel electrode (SCE). (a) Cyclic voltammetry: variation of the potential (E) versus time, from E_1 (0 V vs SCE) to E_2 (+1.0 V) (oxidation), then back to E_1 (reduction). The scan rate υ is the slope of the straight lines expressed in V s^{-1}. (b) Cyclic voltammetry at a steady gold disk electrode (d = 1 mm) at the scan rate υ = 0.5 V s^{-1}. The current i_{ox}^{p} is the oxidation peak current corresponding to the oxidation peak potential E_{ox}^{p}. (c) Cyclic voltammetry at a rotating gold disk electrode (RDE; d = 2 mm, angular velocity ω = 105 rad s^{-1}) at the scan rate υ = 0.02 V s^{-1}. The current i_{ox}^{lim} is measured as indicated in the figure. (d) Cyclic voltammetry at a gold disk ultramicroelectrode (d = 50 μm) at the scan rate υ = 0.02 V s^{-1}. The current i_{ox}^{lim} is measured as indicated in the figure. (e) Double potential step chronoamperometry at a steady gold disk electrode (d = 1 mm). The potential is first held at E_2 (+ 1 V) during θ = 200 ms. The corresponding oxidation current is i_{ox} as indicated in panel f. The potential is then held at E_1 (0 V) during the same time θ. The corresponding reduction current is i_{red} as indicated in panel f. (f) Response of the current versus time in the double potential step chronoamperometry of panel e. A single potential step chronoamperometry experiment corresponds to a single step at E_2 during θ, giving the current i_{ox}.

Electrochemical experiments require a solvent and a supporting electrolyte. Conducting polar solvents such as THF, DMF, NMP, HMPA, TMU, acetone, acetonitrile, dichloromethane, or acetic acid, which are currently used in catalytic reactions, are well-adapted to electrochemical techniques. Considerably less conducting solvents such as toluene have been recently made compatible with electrochemical techniques thanks to the use of disk ultramicroelectrodes whose small size (radius <50 μm) allows per-

formance voltammetry in highly resistive solvents, as pioneered by Amatore.[8] The use of a supporting electrolyte (usually tetraalkylammonium tetrafluorobarate) imposes an ionic strength, which may modify the rate and mechanism of some elemental reactions involving ionic organometallic species. It is worthwhile to note that most palladium-catalyzed reactions are performed at significant ionic strength in polar solvents due to the introduction of anions and cations via ionic reagents, additives, bases, etc. and the release of ions from neutral reagents in the course of the catalytic reactions.

Electrochemical techniques cannot give any structural information (except the oxidation state of the metal) unless by comparison to authentic samples. When the latter are not available, the association of electrochemical techniques (which provide kinetic data) with other techniques such as ^{1}H or ^{31}P NMR spectroscopy (which provide structural information) is quite advantageous for the investigation of any reaction involving electroactive organometallic species. Whenever ionic organometallic species are formed in a catalytic cycle, they can be characterized by conductivity measurements[9] and their formation or evolution with time followed by the same technique.

Electrochemical techniques can be used for the determination of the mechanism of transition metal-catalyzed reactions whatever the transition metal, provided some of the organometallic species involved in the catalytic cycle are electroactive. Since palladium is one of the most useful catalysts involved in many different reactions, electrochemical techniques have been intensively used to investigate the mechanism of palladium-catalyzed reactions, as illustrated in the following.[10] In the 1970s and 1980s, most palladium-catalyzed reactions involving C−C bond formation from aryl halides ArX were discovered:[11] (i) arylation of alkenes by Mizoroki et al.[12] and Heck and Nolley[13] in 1971 and 1972, respectively (Scheme 3); (ii) arylation of alkynes independently by Cassar[14] and Heck and Dieck[15] in 1975 (Scheme

Scheme 3

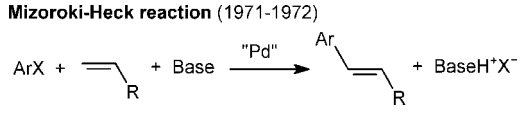

4) and improved by Sonogashira et al.[16] upon addition of

Scheme 4

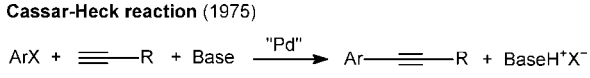

catalytic copper salts in 1975 (Scheme 5); (iii) cross-coupling

Scheme 5

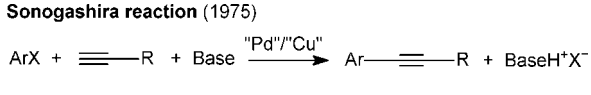

reactions with RLi and RMgBr by Fauvarque and Jutand[17] in 1976 (Scheme 6), with RZnX by Negishi et al.[18] in 1977 (Scheme 6), with $BrZnCH_2CO_2Et$ by Fauvarque and Jutand[19] in 1977 (Scheme 6), with R_4Sn by Milstein and Stille[20] in 1979 (Scheme 7), with $RB(OH)_2$ by Miyaura and Suzuki[21] in 1981 (Scheme 8), and with $RSiMe_3F^-$ by Hatanaka and Hiyama[22] in 1988 (Scheme 9).

Scheme 6

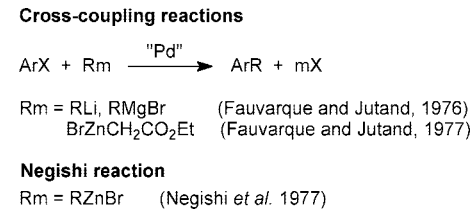

Scheme 7

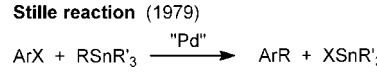

Scheme 8

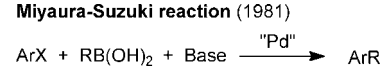

Scheme 9

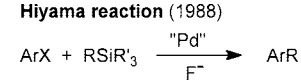

It is first shown how the mechanism of elemental steps of catalytic cycles can be elucidated by using electrochemical techniques. The strategy is to investigate the rate and mechanism of the first step of a catalytic cycle and then the following steps, in the context of the catalytic reaction, that is, using the same precursor, ligands, reagents, solvent, and additives, so as to construct catalytic cycles for real palladium-catalyzed reactions.

2.2. Characterization of Reactive Organometallic Species in Equilibrium with Precursors by Chronoamperometry at a Rotating Disk Electrode (RDE)

2.2.1. Oxidative Addition from Pd^0L_4

2.2.1.1. Oxidative Addition of Aryl Halides, Triflates, or Anhydrides to $Pd^0(PPh_3)_4$. The oxidative addition of aryl halides to a Pd(0) complex is a key step because it is the first one in all palladium-catalyzed reactions involving aryl halides.[10–22] In 1968, Fitton et al. reported the first oxidative additions of aryl halides to a stable, isolated Pd(0) complex, $Pd^0(PPh_3)_4$ (tetrakis-triphenylphosphine)palladium (Scheme 10).[23,24]

The complexes, *trans*-σ-$ArPd^{II}XL_2$ ($L = PPh_3$), formed in the reactions have been well characterized, but no kinetic data were available. From their synthetic work, Fitton and Rick had however observed the following reactivity orders:[24] ArI > ArBr ≫ ArCl and 4-EWG-C_6H_4-X > 4-EDG-C_6H_4-X. At that time, the structure of the reactive Pd(0) complex was not known. It was however established by Mann and Musco[25] that $Pd^0(PPh_3)_4$ quantitatively dissociates to PPh_3 and $Pd^0(PPh_3)_3$, which is the major species in solution.

The very first use of electrochemical techniques to follow the reactivity of an organometallic species in an elemental step, such as oxidative addition of aryl iodides to $Pd^0(PPh_3)_4$, was reported by Fauvarque et al. in 1981.[26] The voltammogram of $Pd^0(PPh_3)_4$ ($C_0 = 2$ mM) in THF or DMF at a rotating gold disk electrode (RDE) at the scan rate of 0.02 V s^{-1} exhibits the oxidation wave of $Pd^0(PPh_3)_3$ whose oxidation plateau current (i_0) is proportional to the initial Pd(0) concentration: $i_0 = \alpha C_0$ (Figure 2a; for an illustration

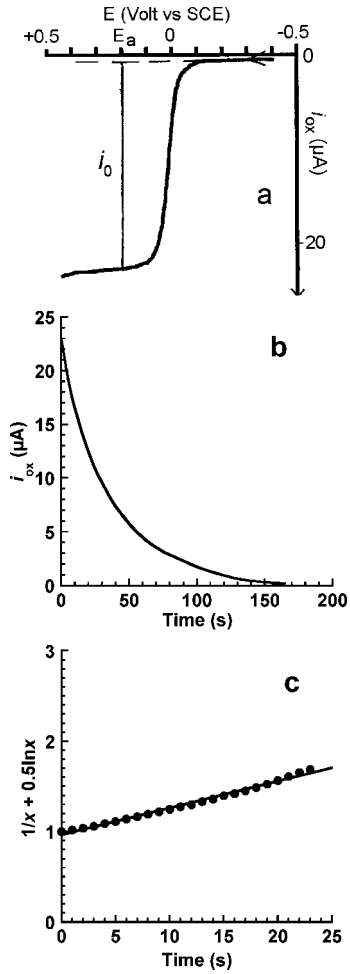

Figure 2. (a) Voltammetry of $Pd(PPh_3)_4$ (2 mM) in DMF (containing nBu$_4$NBF$_4$, 0.3 M) at a rotating gold disk electrode (d = 2 mm, angular velocity ω = 105 rad s^{-1}) at the scan rate of 0.02 V s^{-1} at 22 °C, (b) kinetics of the oxidative addition of PhI (2 mM) to $Pd(PPh_3)_4$ (2 mM) showing a decrease with time of the oxidation plateau current of $Pd(PPh_3)_3$ measured at the RDE polarized at +0.2 V, and (c) plot of $1/x + 0.5 \ln x$ against time (x = molar fraction of $Pd^0(PPh_3)_3$ at t; $x = [Pd^0]_t/[Pd^0]_0 = i/i_0$). The kinetic law takes into account the variation of the concentration of PPh_3, which is released during the oxidative addition (Scheme 11). $1/x + 0.5 \ln x = 1 + 0.5k^{oa}K_L t$.

of the technique, see Figure 1a,c). The oxidation plateau current decreases with time upon addition of iodobenzene because of the oxidative addition depicted in Scheme 10.

Scheme 10

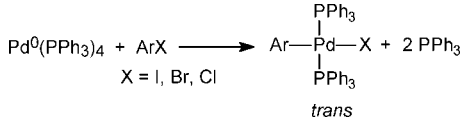

The RDE is polarized at a potential E_a on the plateau of the oxidation wave of $Pd^0(PPh_3)_3$ (Figure 2a) and the decrease of the oxidation plateau current with time is recorded after addition of PhI (Figure 2b). Such a curve characterizes the kinetics of the oxidative addition.

Fauvarque et al. have observed that the oxidative addition is retarded by excess PPh_3 and have determined the reaction orders for PhI (+1) and PPh_3 (−1) in THF, establishing that the low-ligated $Pd^0(PPh_3)_2$ is the reactive species, according to the mechanism depicted in Scheme 11.[26] Even if $Pd^0(PPh_3)_2$ is intrinsically very reactive (high value of k^{oa}),

Scheme 11

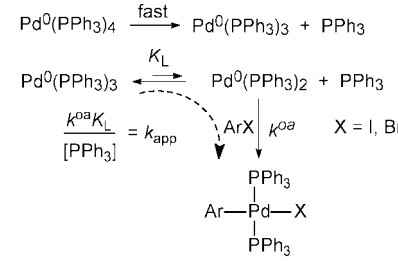

$$rate = k^{oa}[ArX][Pd^0L_2] = k^{oa}K_L[ArX][Pd^0L_3]/[L] = k_{app}[ArX][Pd^0L_3]$$

the reaction rate is controlled by its concentration, which is very low in its endergonic fast equilibrium with the unreactive $Pd^0(PPh_3)_3$ ($K_L/[L] \ll 1$). Higher concentration of PPh_3 leads to slower overall oxidative addition of aryl halides to $Pd(PPh_3)_4$, according to the kinetic law given in Scheme 11. $k^{oa}K_L$ characterizes the reactivity of aryl halides with $Pd^0(PPh_3)_4$ via $Pd^0(PPh_3)_2$.

The same mechanism has been established in DMF by Amatore, Jutand, et al. by using the same technique, chronoamperometry at a rotating disk electrode (Figure 2c).[27] The kinetics of the oxidative addition in toluene, a considerably less polar solvent than THF or DMF, has been investigated thanks to a disk ultramicroelectrode (d = 10 μm) whose small size allows performance of voltammetry in highly resistive media (for an illustration of the technique, see Figure 1a,d) (Amatore et al.).[8,28] A steady-state voltammogram is obtained at low scan rates (0.2 V s^{-1}) whose plateau current (proportional to the concentration of $Pd^0(PPh_3)_3$) decreases with time after addition of excess PhI.[28] Whatever the solvent, THF,[26] DMF,[27] or toluene,[28] the values of $k^{oa}K_L$ are very similar (Table 1). The energy parameters determined in the polar THF and in the less polar toluene are very close: $\Delta H^{\ddagger}$ = 77 kJ mol^{-1} and $\Delta S^{\ddagger}$ = 13 J mol^{-1} K^{-1} in THF;[26] $\Delta H^{\ddagger} = 75 \pm 5$ kJ mol^{-1} and $\Delta S^{\ddagger} = 7 \pm 5$ J mol^{-1} K^{-1} in toluene.[28] The Hammett plots obtained for *para*-*Z*-substituted aryl iodides deliver a positive slope with similar values at 25 °C: ρ = +2.0 in THF;[26] $\rho = +2.3 \pm 0.2$ in toluene.[28] These results confirm the experimental reactivity (4-EWG-C_6H_4-X > 4-EDG-C_6H_4-X) observed by Fitton and Rick[24] and establish that the oxidative addition from $Pd^0(PPh_3)_4$ is not significantly sensitive to the solvent polarity. A mechanism proceeding by electron transfer, as established by Tsou and Kochi for the oxidative addition of aryl halides to $Ni^0(PEt_3)_4$, is therefore excluded.[29]

Scheme 12

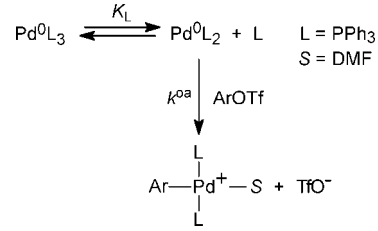

Chronoamperometry at a rotating disk electrode has been used by Jutand and Mosleh to investigate the reactivity of aryl triflates, ArOTf (Ar-OSO_2CF_3), in their oxidative addition to $Pd^0(PPh_3)_4$ in DMF (Scheme 12).[30] As for aryl iodides, the Hammett plot has a positive slope: ρ = +2.55 (DMF, 20 °C). Aryl triflates exhibit the originality to deliver cationic complexes, *trans*-ArPd(DMF)$(PPh_3)_2^+$ (Scheme 12,

Table 1. Comparative Reactivity of $Pd^0(PPh_3)_4$ in the Oxidative Addition to Aryl/Vinyl Halides/Triflates[c]

RX	$k^{oa}K_L$ (s^{-1}) DMF 20 °C	DMF 25 °C	THF[a] 25 °C	Toluene 25° C
PhI	5.4 (±0.2)×10^{-2}	7.5 (±0.2)×10^{-2}	8.7 (±0.2)×10^{-2}	6.9 ×10^{-2} s^{-1}
PhOTf	5.1×10^{-6}			
PhBr	3.0×10^{-6}			
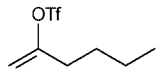	16[b]			
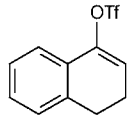	4.6[b]			
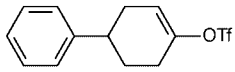	2.0[b]			
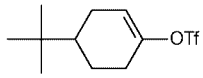	1.6[a]			
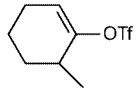	0.52[b]			
	0.091[b]			
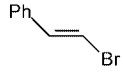	0.038[b]			
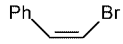	0.0011[b]			
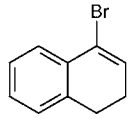	0.0004[b]			

[a] $k^{oa}K_L = (5.1 \pm 0.4) \times 10^{-2}$ s^{-1} in THF at 20 °C. [b] Oxidative addition performed at 30 °C. [c] For the definition of $k^{oa}K_L$, see Schemes 11, 12, and 15.

Scheme 13

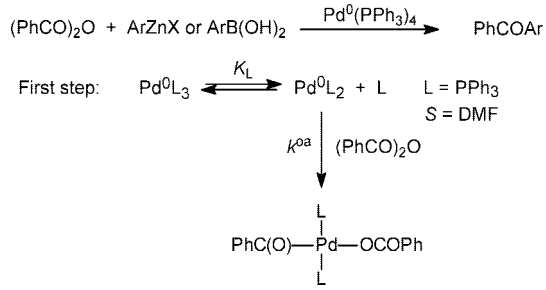

see section 2.6.1),[30] in contrast to aryl halides, which deliver neutral complexes, *trans*-$ArPdX(PPh_3)_2$ (X = I, Br, Cl) (Scheme 11).

Since aryl triflates are often used as an alternative to aryl halides in Pd-catalyzed reactions,[10,31] their reactivity in oxidative additions to $Pd^0(PPh_3)_4$ has been compared with that of aryl halides (Table 1).[30] The oxidative addition of $Pd^0(PPh_3)_4$ to benzoic anhydride used as acylating agent in Pd-catalyzed cross-coupling reactions[32,33] has also been investigated by chronoamperometry at a RDE (Scheme 13).[34]

The following decreasing reactivity order has been established in DMF:[30,32] PhI ≫ $(PhCO)_2O$ > PhOTf > PhBr ≫ PhCl.

Chronoamperometry at a RDE was recently used to compare the reactivity of (η^5-C_5H_4-I)ML_n (**1a**−**c**) in their oxidative addition to $Pd^0(PPh_3)_4$ in DMF by Jutand et al. (Scheme 14).[35] The electronic properties of ML_n moieties

Scheme 14

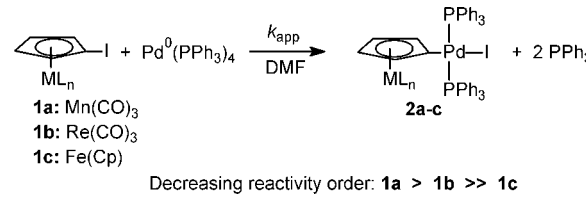

ligated to iodocyclopentadienyl, which determine the rate of the oxidative additions, can now be compared.

2.2.1.2. Oxidative Addition of Vinyl Halides or Triflates to Pd^0L_4 (L = PPh_3). The first $Pd^0(PPh_3)_4$-catalyzed cross-coupling reaction of vinyl halides with organolithium or Grignard reagents was reported by Murahashi et al. in 1975.[36] The kinetics of the oxidative addition of (*E*)- and (*Z*)-PhCH=CHBr to $Pd(PPh_3)_4$ was followed by chronoamperometry at a rotating disk electrode by Fauvarque and Jutand in 1981.[37] The (*E*) isomer was found to be more reactive than the (*Z*) isomer in the oxidative addition, as in their Pd-catalyzed cross-coupling reactions with $BrZnCH_2CO_2Et$, indicating that the oxidative addition is rate-determining.[37]

More recently, the reactivity of $Pd^0(PPh_3)_4$ with vinyl triflates has been investigated in DMF by Jutand and Negri, with the same electrochemical technique.[38] The oxidative additions of vinyl triflates to $Pd^0(PPh_3)_4$ (C_0 = 2 mM) are so fast, even under stoichiometric conditions, that they cannot be investigated as such. To bypass such problem, the kinetics have been investigated in the presence of a known excess of PPh_3, which slows down the reaction (Scheme 15). The

Scheme 15

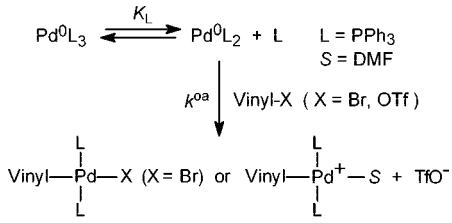

determination of $k^{oa}K_L$ allows comparison of the reactivity of vinyl halides and triflates in oxidative additions (Scheme 15, Table 1).[38]

Vinyl triflates are considerably more reactive than vinyl bromides when the same vinylic structure is considered (by a factor ca 10^5, Table 1).[38] Vinyl triflates are considerably more reactive than aryl triflates:[30,38] vinyl-OTf ≫ vinyl-Br > PhBr; vinyl-OTf ≫ PhOTf

2.2.2. Oxidative Addition of Pd(0) Complexes Generated in Situ from $Pd^0(dba)_2$ and Ligands

As reported above, the low-ligated $Pd^0(PPh_3)_2$ has been found to be the reactive species in oxidative additions from kinetic data. However, it has never been characterized by spectroscopic techniques due to its low concentration in its fast equilibrium with $Pd^0(PPh_3)_3$. Indeed, ^{31}P NMR spectra of $Pd^0(PPh_3)_4$ in THF or DMF at 22 °C always exhibit a broad signal due to the fast equilibrium among $Pd^0(PPh_3)_3$, $Pd^0(PPh_3)_2$, and PPh_3 (Scheme 11).[27] It is shown in the following how the low-ligated complex $Pd^0(PPh_3)_2$ has been detected and characterized by cyclic voltammetry at a steady electrode (for an illustration of the technique, see Figure 1a,b).

The precursor $Pd^0(dba)_2$ (or $Pd^0{}_2(dba)_3$) (dba = (*E*,*E*)-dibenzylideneacetone) associated with PPh_3 (PPh_3/Pd = 2) was long considered as a quantitative source of $Pd^0(PPh_3)_2$. In other words, dba was expected to be a very labile ligand with considerably less affinity for the Pd(0) center than the phosphine.

As reported by Amatore, Jutand et al., the ^{31}P NMR spectrum of a mixture of $Pd^0(dba)_2$ and PPh_3 (2 equiv) in THF or DMF exhibits two signals of equal magnitude (Figure 3a), which characterize the two magnetically nonequivalent phosphorus atoms in the complex $Pd^0(dba)(PPh_3)_2$ formed

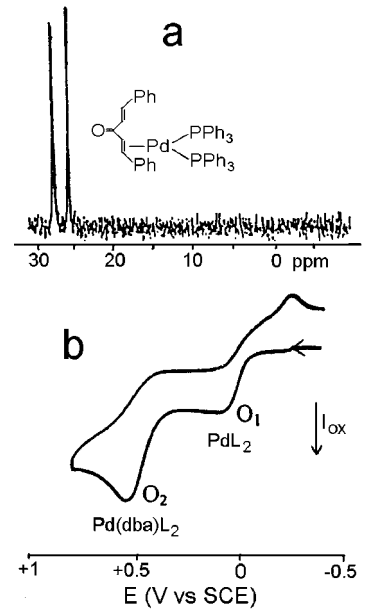

Figure 3. (a) ^{31}P NMR (101 MHz) of $Pd^0(dba)(PPh_3)_2$ generated from $Pd^0(dba)_2$ and PPh_3 (2 equiv) in THF and (b) cyclic voltammetry of a mixture of $Pd(dba)_2$ (2 mM) and PPh_3 (4 mM) in THF (containing nBu_4NBF_4, 0.3 M) at a steady gold disk electrode (d = 0.5 mm) at the scan rate of 0.2 V s^{-1} at 20 °C.

as the main species (Scheme 16, upper equation). The dba

Scheme 16

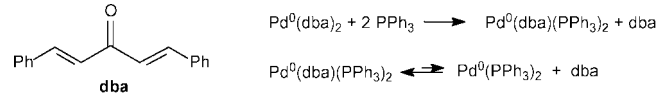

is coordinated to $Pd^0(PPh_3)_2$ by one C=C bond (Figure 3a).[27]

However, when the cyclic voltammetry is performed on a mixture of $Pd(dba)_2$ (2 mM) and PPh_3 (4 mM) in THF at a steady gold disk electrode (d = 0.5 mm, scan rate 0.2 V s^{-1}), two successive oxidation peaks, O_1 and O_2, are observed (Figure 3b), suggesting the formation of two different Pd(0) complexes. Since the oxidation peak current of O_2 increases at the expense of that of O_1 upon addition of dba, O_1 and O_2 characterize $Pd^0(PPh_3)_2$ and $Pd^0(dba)(PPh_3)_2$, respectively, which are in equilibrium with the dba ligand (Scheme 16). Despite the low concentration of $Pd^0(PPh_3)_2$ in that equilibrium, it is nevertheless observed by cyclic voltammetry at low scan rate because its consumption in the diffusion layer by its oxidation at the electrode results in a shift of the equilibrium in Scheme 16 toward its right-hand side. Consequently, what is given by the measurement of the oxidation peak current at O_1 is not the thermodynamic concentration of $Pd^0(PPh_3)_2$ but a higher dynamic concentration due to the shift of the equilibrium toward $Pd^0(PPh_3)_2$ during the slow voltammetric scan (CE mechanism).[6] The relative peak currents at O_1 and O_2 indeed depend on the scan rate, that is, on the time scale of the oxidation process.

Thanks to cyclic voltammetry, the existence of $Pd^0(PPh_3)_2$ was established for the first time in 1993 by Amatore, Jutand et al.[27]

The kinetics of the reaction of iodobenzene with the Pd(0) complexes formed in situ from $Pd^0(dba)_2$ associated to PPh_3 (2 equiv) has been followed by chronoamperometry at a rotating disk electrode, as done previously for $Pd^0(PPh_3)_4$ (see section 2.2.1). The decrease of the oxidation current plateau i, measured at the RDE polarized at +0.8 V on the

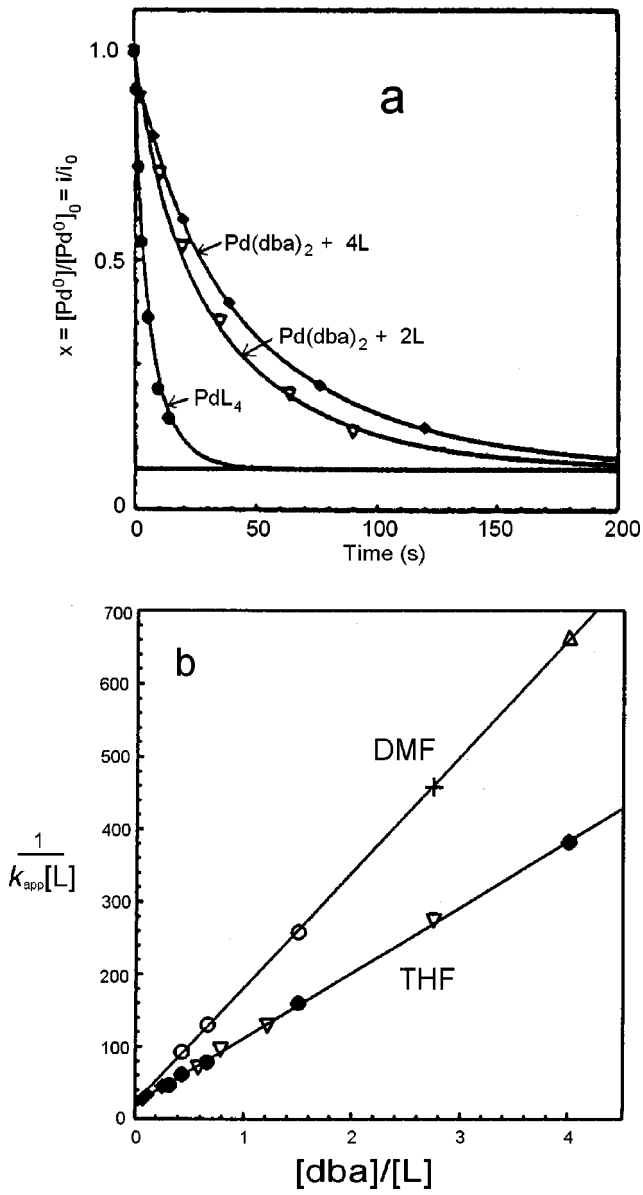

Figure 4. (a) Kinetics of the oxidative addition of PhI (10 mM) to the Pd(0) generated from $Pd^0(PPh_3)_4$ (2 mM) or $Pd^0(dba)_2$ (2 mM) + 2 PPh_3 or 4 PPh_3, as indicated by the arrows, in THF (containing nBu_4NBF_4, 0.3 M) at 20 °C, followed by chronoamperometry at a gold rotating disk electrode (d = 2 mm, ω = 105 rad s^{-1}). Plot of x against time, x = molar fraction of Pd(0) at t ($x = [Pd^0]_t/[Pd^0]_0 = i/i_0$). (b) Plot of $1/(k_{app}[PPh_3])$ versus [dba]/[PPh_3] (see equation in Scheme 17).

plateau of the oxidation wave of $Pd^0(dba)(PPh_3)_2$, is recorded with time after addition of excess PhI. Figure 4a exhibits the comparative reactivity of PhI with the Pd(0) generated from the precursors: $Pd^0(PPh_3)_4$, {$Pd^0(dba)_2$ + 2 PPh_3}, and {$Pd^0(dba)_2$ + 4 PPh_3} with the decreasing reactivity order:[27] $Pd^0(PPh_3)_4$ > {$Pd^0(dba)_2$ + 2PPh_3} > {$Pd^0(dba)_2$ + 4PPh_3}.

This unexpected reactivity order is in agreement with the mechanism in Scheme 17. The only reactive species is the minor complex $Pd^0(PPh_3)_2$ whose concentration is controlled by the dba concentration in the left equilibrium (K_{dba}) and by the PPh_3 concentration in the right equilibrium (K_L), which is operative only in the presence of 4 equiv of PPh_3.[27]

The low values of $K = K_{dba}/K_L = 0.18$ in THF and 0.12 in DMF (20 °C) for the overall equilibrium between $Pd^0(dba)(PPh_3)_2$ and $Pd^0(PPh_3)_3$ deduced from the kinetic law

Scheme 17

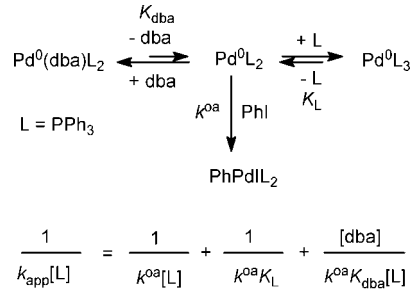

$$\frac{1}{k_{app}[L]} = \frac{1}{k^{oa}[L]} + \frac{1}{k^{oa}K_L} + \frac{[dba]}{k^{oa}K_{dba}[L]}$$

20 °C	THF	DMF
$10^2 k^{oa}K_{dba}$ (s^{-1})	0.94	0.63
$10^2 k^{oa}K_L$ (s^{-1})	5.1	5.4

in Scheme 17 and the plot depicted in Figure 4b indicate that dba is a better ligand than PPh_3 for $Pd^0(PPh_3)_2$ at identical concentrations. In other words, the thermodynamic concentration of $Pd^0(PPh_3)_2$ in its equilibrium with $Pd^0(dba)(PPh_3)_2$ is lower than in its equilibrium with $Pd^0(PPh_3)_3$ ($K_{dba} < K_L$). This is why the oxidative addition of PhI performed from the precursor $Pd^0(PPh_3)_4$ is faster than the one performed from {$Pd^0(dba)_2$ + 2 PPh_3} at identical Pd(0) and PhI concentrations, even if they both involve the common reactive species $Pd^0(PPh_3)_2$. This rationalizes a few results in literature where some $Pd^0(PPh_3)_4$-catalyzed reactions are faster than the ones catalyzed by {$Pd^0(dba)_2$ + 2 PPh_3}.[10] The respective values of $k^{oa}K_{dba}$ and $k^{oa}K_L$ are given in the table of Scheme 17 (for a comparison with the reactivity of anionic $Pd^0(PPh_3)_2X^-$ (X = Cl, OAc), see Table 3).

This study has been extended to various monodentate ligands L:[39] phosphines PAr_3 ($P(4\text{-}Z\text{-}C_6H_4)_3$,[40] TFP (tri-2-furylphosphine),[41] DBP (1-phenyl-dibenzophosphole, **3** in Chart 1),[42] and arsine such as $AsPh_3$.[43] In all cases, $Pd^0(dba)L_2$ is the major complex formed from {$Pd^0(dba)_2$ + 2L} in THF or DMF, but the minor complex Pd^0L_2 is the reactive species in oxidative additions (Scheme 18).

Scheme 18

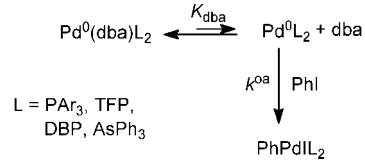

Interestingly, in the case of the bulky monophosphine ligand **4** (Chart 1), the major complex $Pd^0(dba)$(**4**) is produced, as reported by Buchwald et al.[44]

As far as bidentate ligands L^L are concerned, such as dppf (1,1′-bis(diphenylphosphino)ferrocene),[45] Binap (2,2′-bis(diphenylphosphino)-1,1′-binaphthyl),[45] diop (*O*-isopropylidene-2,3-dihydroxy-1,4-bis(diphenylphosphino)butane),[45] dppe ($Ph_2P\text{-}(CH_2)_2\text{-}PPh_2$),[46] and pte ($PhS\text{-}(CH_2)_2\text{-}SPh$),[46] the situation slightly differs in the sense that the major complex $Pd^0(dba)(L\text{^}L)$ reacts with PhI in parallel with the more reactive but minor complex $Pd^0(L\text{^}L)$ in equilibrium with dba (Scheme 19). Once again, the reactivity is influenced by dba whose concentration controls the concentration of the more reactive complex $Pd^0(L\text{^}L)$.[45]

All reactions have been followed by chronoamperometry at a RDE. In summary, the decreasing reactivity orders with

Table 2. Comparative Reactivity of Pd^0L_2 Complexes in Their Oxidative Additions to Aryl Halides or Triflates in THF at 25 °C[a]

	k_A^{oa} (M^{-1} s^{-1})			
Pd^0L_2	PhI	PhOTf	PhBr	PhCl
$Pd^0(PPh_3)_4$ via $Pd^0(PPh_3)_2$	(29)[b]	(0.0017)[b,c]	(0.001)[b,c]	no[b,c]
$Pd^0(PCy_3)_2$	15	0.26	0.025	0.01
$Pd^0(PMetBu_2)_2$	6.2	0.39	0.105	0.05
$Pd^0(PEttBu_2)_2$	0.022	*e*	*e*	*e*
$Pd^0(PCy_2tBu)_2$	0.0045[d]	*e*	*e*	*e*

[a] For the definition of k_A^{oa}, see Scheme 24. [b] To allow comparison, the value given in parentheses is that of the rate constant k_{app} of the overall reaction from $Pd^0(PPh_3)_4$ expressed in M^{-1} s^{-1} (see Scheme 11). [c] In DMF at 20 °C. [d] In benzene at 22 °C. [e] Not determined.

Chart 1

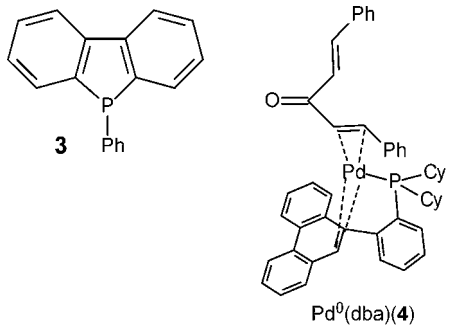

Scheme 19

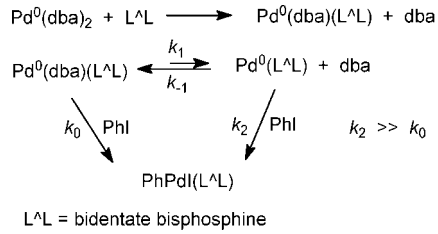

PhI have been established: {$Pd(dba)_2$ + 2PPh_3} ≫ {$Pd(dba)_2$ + 1diop} > {$Pd(dba)_2$ + 1dppf} > {$Pd(dba)_2$ + 1Binap} (THF, 20 °C); {$Pd(dba)_2$ + 1pte} > {$Pd(dba)_2$ + 1dppe} (DMF, 10 °C).

Therefore, the dba ligand is not as labile as expected and its affinity for Pd(0) complexes ligated to phosphines or arsines is quite high. Except for some bulky monophosphine ligands (**4**)[44] or some P^N ligands,[47] whatever the ligand, monodentate (L) or bidentate (L_2), the major species is always $Pd^0(dba)L_2$ in equilibrium with dba and the minor but more reactive Pd^0L_2.[27,40–43] This stresses the importance of thermodynamic factors since dba controls the concentration of the more reactive Pd^0L_2 complex in oxidative additions. The ligand dba slows down the oxidative addition of aryl halides by complexation of the more reactive complex Pd^0L_2 to form the unreactive or less reactive $Pd^0(dba)L_2$.[39]

Since dba plays such an important role in oxidative addition, the two different precursors, $Pd^0{}_2(dba)_3$ and $Pd^0(dba)_2$, associated with PPh_3 (PPh_3/Pd = 2) should not have the same reactivity when considered at the same Pd(0) concentration, due to different dba concentrations. Indeed, the reaction with PhI is faster when starting from $Pd^0{}_2(dba)_3$ instead of $Pd^0(dba)_2$ at identical PhI concentrations, as established by Fairlamb, Jutand, et al. by means of chronoamperometry at a RDE (Scheme 20).[48] Moreover, the rate of the reaction is affected by the electron-donating or -accepting properties of groups Z-substituted on the aromatic rings of dba in Pd^0(dba-4,4′-Z)$_2$ (Z = Br, Cl, H, CH_3, OMe) associated with 2 PPh_3 (Scheme 20).[48]

Whatever Z, the reactive species is always $Pd^0(PPh_3)_2$ (Scheme 20). However, the reaction with PhI is faster when

Scheme 20

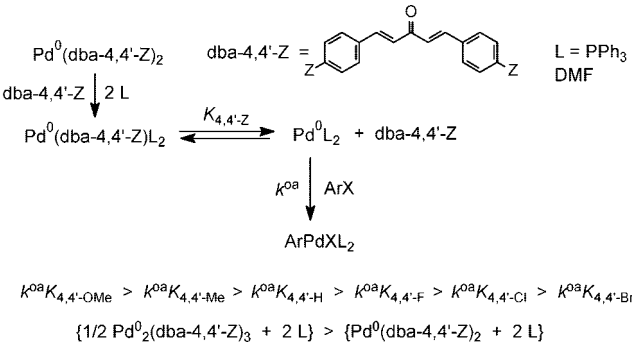

Z becomes more electron-donating, in agreement with the fact that the affinity of dba-4,4′-Z for the electron-rich $Pd^0(PPh_3)_2$ is lower for electron-donating Z. In other words, the concentration of the common $Pd^0(PPh_3)_2$ is higher in its equilibrium with Pd^0(dba-4,4′-Z)$(PPh_3)_2$ when Z is an electron-donating substituent and consequently the oxidative addition is faster:[48] $K_{4,4'\text{-OMe}} > K_{4,4'\text{-Me}} > K_{4,4'\text{-H}} > K_{4,4'\text{-F}} > K_{4,4'\text{-Cl}} > K_{4,4'\text{-Br}}$.

Therefore, the rate of the oxidative addition can be modulated by changing the electronic properties of the dba ligand via substituents Z on its phenyl groups and by changing the structure of the precursor: $Pd^0{}_2(dba)_3$ versus $Pd^0(dba)_2$.

2.2.3. Oxidative Addition of Pd(0) Complexes in the Presence of Unsaturated Substrates

As for dba, which coordinates Pd^0L_2 complexes via one C═C bond and induces such a decelerating effect on the oxidative addition, the effect of other unsaturated substrates, which are reagents in Pd-catalyzed reactions, has been investigated by Amatore, Jutand, et al. The reactivity of PhI with $Pd^0(PPh_3)_4$ in the presence of alkenes CH_2═CH−R (R = Ph, CO_2Me) involved in Heck reactions (Scheme 3) has been followed by chronoamperometry at a rotation disk electrode, as described in section 2.2.1. The oxidative addition is slower when performed in the presence of alkenes because the concentration of the reactive Pd^0L_2 decreases by formation of unreactive complexes, $Pd^0(\eta^2$-CH_2═CH−R)L_2 (Scheme 21, Figure 5a).[49] The affinity of the alkenes for Pd^0L_2 can be compared from the values of the equilibrium constant of the overall equilibrium $K = K_L K_{C=C}$ (Scheme 21). As expected, the electron-deficient CH_2═CH−CO_2Et is a better ligand for the electron-rich $Pd^0(PPh_3)_2$ than CH_2═CH−Ph and the decelerating effect of CH_2═CH−CO_2Me in the oxidative addition is more pronounced than that of CH_2═CH−Ph at the same concentration.[49]

The oxidative addition is also slower when performed in the presence of terminal alkynes (HC≡C−R, R = Ph, CO_2Et)

Scheme 21

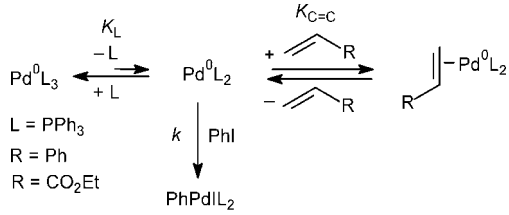

$K_LK_{C=C}$ = 0.0048 (R = Ph); 7.5 (R = CO_2Et) in DMF, 25 °C

involved in Cassar−Heck−Sonogashira reactions (Schemes 4 and 5), due to complexation of Pd^0L_2 by the alkyne. However, the new complex as $Pd^0(\eta^2\text{-HC}{\equiv}\text{C}-CO_2Et)(PPh_3)_2$ may be reactive (Scheme 22, Figure 5b).[50]

Scheme 22

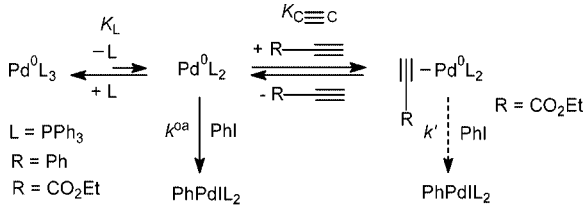

$K_LK_{C\equiv C}$ = 0.012 (R = Ph); 29 (R = CO_2Et)

k' = 0.2 $M^{-1}s^{-1}$ (R = CO_2Et) in DMF, 25 °C

Vinyl(tributyl)stannane, $CH_2{=}CH-SnBu_3$, involved in Stille reactions catalyzed by $Pd(dba)_2$ associated with $2AsPh_3$ (Scheme 7), also competes with dba for the coordination of $Pd^0(AsPh_3)_2$. The oxidative addition to PhI is slower when performed in the presence of $CH_2{=}CH-SnBu_3$ by formation of the unreactive $Pd^0(\eta^2\text{-}CH_2{=}CH-SnBu_3)(AsPh_3)_2$ (Scheme 23).[43]

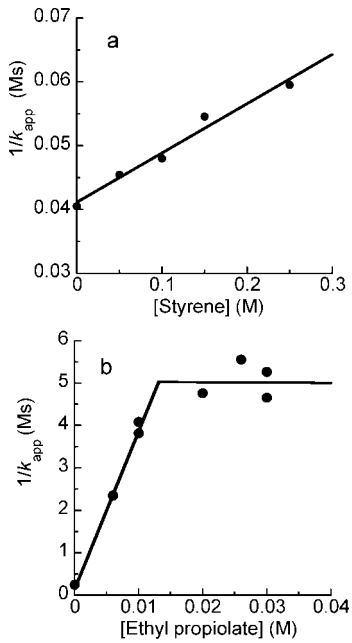

Figure 5. Oxidative addition of PhI (2 mM) to $Pd^0(PPh_3)_4$ (2 mM) in DMF monitored by chronoamperometry at a rotating gold disk electrode (d = 2 mm, ω = 105 rad s^{-1}) polarized at +0.2 V vs SCE at 25 °C: (a) in the absence and presence of styrene, plot of $1/k_{app}$ versus styrene concentration, $1/k_{app} = [L]/(kK_L) + K_{C=C}[CH_2{=}CHR]/k$; (b) in the absence and presence of ethyl propiolate, plot of $1/k_{app}$ versus ethyl propiolate concentration, $1/k_{app} = [L]/(kK_L) + K_{C\equiv C}[HC{\equiv}C-CO_2Et]/k$.

Scheme 23

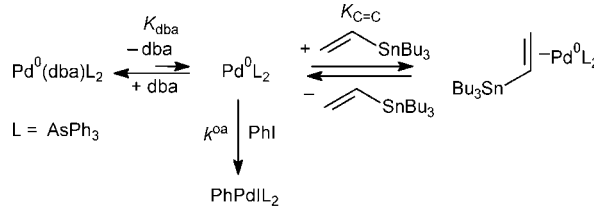

$K_{dba}K_{C=C}$ = 0.21 (DMF); 0.06 (THF), 20 °C

From the values of the equilibrium constant of the overall equilibrium $K = K_{dba}K_{C=C}$ in THF and DMF (Scheme 23), it emerges that the affinity of $CH_2{=}CH-SnBu_3$ for $Pd^0(AsPh_3)_2$ is weaker than that of dba at identical concentrations. However, in catalytic reactions where the concentration of $CH_2{=}CH-SnBu_3$ is considerably higher than that of dba (released in catalytic amounts), the concentration of the unreactive $Pd^0(\eta^2\text{-}CH_2{=}CH-SnBu_3)(AsPh_3)_2$ becomes higher than that of $Pd^0(dba)(AsPh_3)_2$ (ten times higher for 2% catalyst in DMF).[43]

In all cases, the oxidative addition is slower when performed in the presence of unsaturated substrates due to the decrease of the concentration of the reactive Pd^0L_2, which is partly stocked under the nonreactive $Pd^0(\eta^2\text{-}C{=}C)L_2$ or $Pd^0(\eta^2\text{-}C{\equiv}C)L_2$ or less reactive $Pd^0(\eta^2\text{-}CH{\equiv}C-CO_2Et)L_2$ complexes.[51] This decelerating effect on the rate of the oxidative addition induced by unsaturated substrates may play a very important role in catalytic reactions, whenever the oxidative addition is much faster than the following slower step, the reaction of $ArPdXL_2$ (formed in the oxidative addition) with the unsaturated substrates (alkene, alkyne, vinyl stannane) of the catalytic reactions. The rate of those two steps are made closer to each other, and the catalytic reaction becomes more efficient.[51] The decelerating effect of unsaturated substrates on the oxidative addition when the latter may be rate-determining as for aryl chlorides or deactivated aryl bromides is of course problematic. This could be solved upon slow addition of the unsaturated substrate via a syringe pump so as to maintain a low concentration of the unsaturated substrate all along the catalytic reaction.

2.2.4. Oxidative Addition to Pd^0L_2 (L = Bulky and Electron-Rich Monophosphine)

The oxidative addition of aryl bromides or chlorides to $Pd^0(PPh_3)_4$ is quite slow when compared with aryl iodides (Table 1). The activation of aryl bromides or chlorides requires a more electron-rich Pd^0L_2, that is, a more electron-donating phosphine ligand and an isolated Pd^0L_2 complex, so as to bypass its equilibrium with Pd^0L_3, which would be responsible for its low concentration (see Scheme 11 for PPh_3). Stable Pd^0L_2 complexes can been isolated when the monophosphines are bulky.[52,53] The reactivity of isolated Pd^0L_2 in oxidative addition to aryl halides or triflates has been investigated by chronoamperometry at a rotating disk electrode, polarized at a potential on the plateau of the oxidation wave of Pd^0L_2 complexes. Brown, Jutand, et al. have observed that the rate of the oxidative addition of PhI or PhOTf to $Pd^0(PCy_3)_2$ (Cy = cyclohexyl), $Pd^0(PMetBu_2)_2$, and $Pd^0(PCy_2tBu)_2$ is not affected upon addition of PCy_3, $PMetBu_2$, and PCy_2tBu, respectively.[54,55] Consequently, $Pd^0(PCy_3)_2$, $Pd^0(PMetBu_2)_2$, and $Pd^0(PCy_2tBu)_2$ do not dissociate to Pd^0L and are the reactive species in an associative mechanism (Scheme 24, Table 2). This contrasts with $Pd^0(Po\text{-}Tol_3)_2$ ($Po\text{-}Tol_3$ = tri-*o*-tolylphosphine), which dissociates to

Table 3. Rate Constant, k^{oa}, of the Oxidative Addition of PhI to Anionic $Pd^0(PPh_3)_2X^-$ (X = I, Br, OAc) (C_0 = 2 mM) in the Absence or Presence of Additives in Comparison with Other Precursors, $Pd^0(PPh_3)_4$ and {$Pd^0(dba)_2$ + 2 PPh_3}

		k^{oa} (M^{-1} s^{-1})	
precursor[a]	reactive Pd(0)	THF, 20 °C	DMF, 25 °C
$Pd^0(dba)_2$ + 2L	Pd^0L_2	(3.1)[b]	
Pd^0L_4	Pd^0L_2	(17)[c]	(25)[c]
$PdBr_2L_2$ + 2e	$Pd^0L_2Br^-$	400	
$PdCl_2L_2$ + 2e	$Pd^0L_2Cl^-$	530	
$PdCl_2L_2$ + 2e + $50Li^{+d}$	$Pd^0L_2Cl^-\cdots Li^+$	1320	
$PdCl_2L_2$ + 2e + $1Zn^{2+e}$	$Pd^0L_2Cl^-\cdots Zn^{2+}$	1480	
$Pd(OAc)_2$ + 3L + $3NEt_3$	$Pd^0L_2(OAc)^-$		65
$Pd(OAc)_2$ + 3L	$Pd^0L_2(OAc)^-\cdots H^+$		140

[a] L = PPh_3. [b] Values of the apparent rate constant: $k_{app} = k^{oa}K_{dba}/[dba]$ expressed in M^{-1} s^{-1} ([dba] = $1.5C_0$, Schemes 17 and 18). [c] Values of the apparent rate constant: $k_{app} = k^{oa}K_1/C_0$ expressed in M^{-1} s^{-1} ([L] = $1.5C_0$, Scheme 11). [d] Introduced as $LiBF_4$. [e] Introduced as $Zn(BF_4)_2$.

$Pd^0(Po\text{-}Tol_3)$, the reactive species in oxidative addition to aryl bromides (dissociative mechanism), as established by Hartwig and Paul[56] who have monitored the slow oxidative addition by ^1H NMR spectroscopy (Scheme 24).

Whatever the Pd^0L_2 complex involved in the associative mechanism, the reactivity order is:[54,55] PhI > PhOTf > PhBr > PhCl.

$Pd^0(PCy_3)_2$ should be more reactive than $Pd^0(PPh_3)_4$ at identical concentrations, since the reactive species $Pd^0(PPh_3)_2$ is less electron-rich than $Pd^0(PCy_3)_2$ and is also present at lower concentration because of its equilibrium with the unreactive $Pd^0(PPh_3)_3$ (Scheme 11). $Pd^0(PCy_3)_2$ is indeed more reactive than $Pd^0(PPh_3)_4$ with PhOTf, PhBr, and PhCl, but the reverse situation is observed when considering PhI (Table 2, Scheme 24). Such inversion of reactivity is also observed for $Pd^0(PMetBu_2)_2$. This suggests a change in the mechanism of the oxidative addition. A specific interaction of Pd^0L_2 with PhI must be considered that does not take place with PhBr, PhOTf, nor PhCl.[54,55]

Interestingly, the oxidative addition of PhI to $Pd^0(PEttBu_2)_2$ is slower than that to $Pd^0(PMetBu_2)_2$. The reaction is retarded by excess ligand $PEttBu_2$ and obeys the kinetic law $k_{obs} = k_A^{oa}[PhI] + k_{+L}$ at high PhI concentrations (0.1−0.3 M) (Scheme 24).[55] In contrast to $Pd^0(PMetBu_2)_2$, which reacts by an associative mechanism, $Pd^0(PEttBu_2)_2$ partly dissociates to $Pd^0(PEttBu_2)$ and $PEttBu_2$ because $PEttBu_2$ is more bulky than $PMetBu_2$. $Pd^0(PEttBu_2)_2$ and $Pd^0(PEttBu_2)$ react in parallel with PhI (Scheme 24). $Pd^0(PEttBu_2)_2$ is intrinsically less reactive than $Pd^0(PMetBu_2)_2$ because it is more sterically hindered (see k_A^{oa} values in Table 2). Even if $Pd^0(PEttBu_2)$ is more reactive than $Pd^0(PEttBu_2)_2$, it is present at low concentration in its endergonic equilibrium with $Pd^0(PEttBu_2)_2$. The reactivity of $Pd^0(PEttBu_2)$ is moreover limited by the dissociation rate at high PhI concentrations (k_{+L} = ca. 5×10^{-4} s^{-1}, Scheme 24).[55]

Therefore, according to increasing bulk of the monophosphine, Pd^0L_2 complexes may react in oxidative additions in an associative mechanism (moderately bulky phosphines, L = PCy_3, $PMetBu_2$, PCy_2tBu),[54,55] in a mixture of associative/dissociative mechanism (Pd^0L_2/Pd^0L, L = $PEttBu_2$),[55] or via Pd^0L in a dissociative mechanism (most bulky phosphine, L = $Po\text{-}Tol_3$)[56] (Scheme 24).

Therefore, the structure of the reactive Pd(0) in oxidative additions, that is, Pd^0L_2 versus Pd^0L, is mainly controlled by the bulk of the phosphine ligand L. However, the reactivity is not necessarily controlled by the structure of the reactive species since a Pd^0L_2 complex (L = $PMetBu_2$) may be more reactive than a Pd^0L_2, which also reacts via Pd^0L (L = $PEttBu_2$).

Therefore, chronoamperometry at a rotating disk electrode can be efficiently used to follow the reactivity of organometallic species in oxidative addition to characterize the true reactive species in equilibrium with nonreactive or less reactive precursors.

2.3. Generation and Reactivity of Highly Reactive Organometallic Species from Stable Precursors by Fast Cyclic Voltammetry

2.3.1. Determination of the Absolute Number of Electron(s) Involved in the Electrochemical Reduction or Oxidation of an Organometallic Species

The active organometallic species that initiates the catalytic cycle (M_1 in Scheme 1) is often generated by the chemical reduction (or oxidation) of a stable precursor M_0 by one of the reagents of the catalytic reaction. This chemical process may be easily mimicked by an electrochemical process, the electrons playing the role of reductant (or oxidant). The electrochemical process is in a sense "purer", since it does

Scheme 24

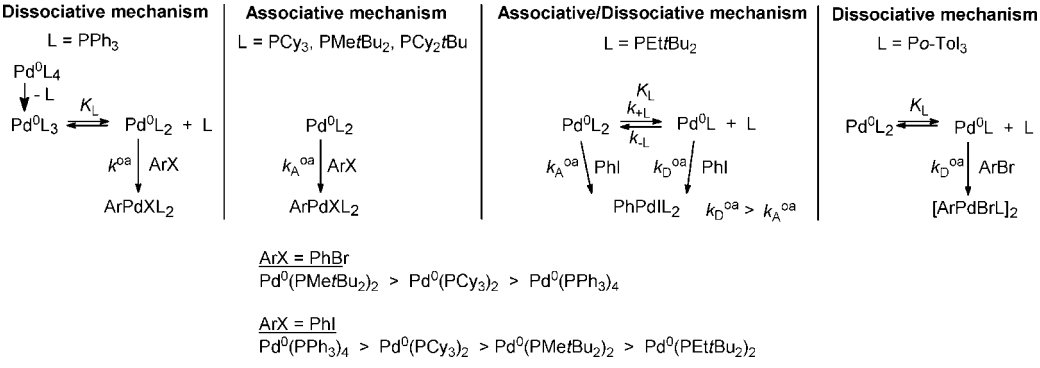

not bring any chemical cocompounds such as cations or anions, which are usually delivered by chemical reductants (or oxidants). Moreover, the electrochemical process is more selective because electrons are transferred at well-defined potentials. They can be transferred successively via a fine-tuning of the electrode potential.

Once an organometallic species has been reduced (or oxidized) at one electrode, it is crucial to know how many electron(s) have been transferred to better define the oxidation state of the electrogenerated new species. Two electrons may be indeed transferred at the same potential. As an example, the electrochemical reduction of $PdCl_2(PPh_3)_2$ exhibits a single irreversible reduction peak at R_1 in THF (Figure 6a).[57,58] Does this reduction deliver a Pd(I) or a Pd(0) complex? Does the oxidation peak observed on the reverse scan characterize a Pd(I) or a Pd(0) complex?

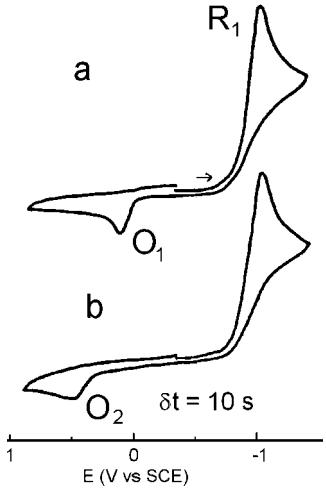

Figure 6. Cyclic voltammetry of (a) $PdCl_2(PPh_3)_2$ (2 mM) in THF (containing nBu$_4$NBF$_4$, 0.3 M) at a steady gold disk electrode (d = 0.5 mm) with a scan rate v = 0.2 V s^{-1}, at 20 °C and (b) the same conditions but in the presence of PhI (20 mM). The oxidation peak, O_2, is assigned to a transient anionic intermediate complex [PhPdI(Cl)$(PPh_3)_2^-$] formed in the oxidative addition on the way to the more stable *trans*-PhPdI$(PPh_3)_2$.

Amatore et al. have developed a new method to determine the absolute number of electron(s) involved in any electrochemical process.[59] It is based on a comparison with an internal standard, such as ferrocene, whose one-electron oxidation is well-known and the use of two electrochemical techniques. The first one is cyclic voltammetry performed at a disk ultramicroelectrode (r = 5 μm) at low scan rate (0.02 V s^{-1}),[8] which gives a limiting oxidation current for ferrocene (for an illustration of the technique, see Figure 1a,d), $i_{Fe}^{lim} = An_{Fe}C_{Fe}D_{Fe}$ (n_{Fe} = 1 = number of electrons involved in the oxidation of ferrocene, C_{Fe} = initial concentration, and D_{Fe} = diffusion coefficient of ferrocene, $A = 4Fr$; r = electrode radius),[8,59] and a limiting reduction current for $PdCl_2(PPh_3)_2$, $i_{Pd}^{lim} = An_{Pd}C_{Pd}D_{Pd}$ (n_{Pd} = number of electron(s) involved in the reduction, C_{Pd} = initial concentration, and D_{Pd} = diffusion coefficient of $PdCl_2(PPh_3)_2$). The ratio $i_{Pd}^{lim}/i_{Fe}^{lim} = n_{Pd}C_{Pd}D_{Pd}/(C_{Fe}D_{Fe})$ contains three unknown parameters: n_{Pd}, D_{Pd}, and D_{Fe}. Consequently, a second electrochemical technique is required that involves a different diffusion mode (linear instead of spheric for ultramicroelectrodes at low scan rates) such as in single potential step chronoamperometry at a steady disk microelectrode (d = 0.5 mm; for the experimental procedure, see Figure 1e,f).[6,59] The potential is held 250 mV after the oxidation peak potential of ferrocene during a time θ (similar to that of the previous technique) and gives an oxidation current, $i_{Fe} = Bn_{Fe}C_{Fe}D_{Fe}^{1/2}$ ($B = FS(\pi\theta)^{-1/2}$, S = electrode surface, n_{Fe} = 1). Similarly, the potential is held 250 mV after the reduction peak potential of R_1 of $PdCl_2(PPh_3)_2$ during the same time θ and gives a reduction current, $i_{Pd} = Bn_{Pd}C_{Pd}D_{Pd}^{1/2}$.[6,59] Consequently, $i_{Pd}/i_{Fe} = n_{Pd}C_{Pd}D_{Pd}^{1/2}/(C_{Fe}D_{Fe}^{1/2})$. Considering the two ratios, it emerges that

$$n_{Pd} = C_{Fe}[(i_{Pd}/i_{Fe})]^2/[C_{Pd}(i_{Pd}^{lim}/i_{Fe}^{lim})]$$

n_{Pd} = 2.04 ± 0.15 is easily determined from the known values of C_{Fe} and C_{Pd} and the measured values of i_{Pd}, i_{Fe}, i_{Pd}^{lim} and i_{Fe}^{lim}.[59] Comparison to ferrocene gives a more accurate result because the electrode surface or radius, whose values may not be known precisely, is eliminated in the expression of n_{Pd} (vide supra).

By this method, the reduction of $PdCl_2(PPh_3)_2$ is found to be an overall bielectronic irreversible process at 0.2 V s^{-1}, and the oxidation peak O_1 observed on the reverse scan does characterize a Pd(0) complex (Figure 6a, Scheme 25).

Scheme 25

$$PdCl_2(PPh_3)_2 + 2\,e \longrightarrow \text{" } Pd^0(PPh_3)_2 \text{"}$$

The number of electron(s) involved in the reduction of an organometallic complex is often determined in the literature by comparison of its reduction peak current (measured by cyclic voltammetry at a steady disk electrode) with the oxidation peak current of ferrocene at the same concentration (n_{Fe} = 1). This may lead to erroneous results. Indeed, $PdCl_2(PPh_3)_2$ and ferrocene at the same concentration of 2 mM in THF exhibit very similar reduction and oxidation peak currents, respectively, at a steady disk electrode. At first glance, one would have concluded that $n_{Pd(II)}$ = 1 with generation of a Pd(I) complex. This simple comparison delivers an erroneous value for $n_{Pd(II)}$ (found above to be 2) because on one hand the oxidation peak of ferrocene is reversible (with the known expression of the oxidation peak current, $i_{Fe}^p = \phi n_{Fe}FS(n_{Fe}F/(RT))^{1/2}D_{Fe}^{1/2}C_{Fe}v^{1/2}$, $\phi = 0.4463$)[6] whereas the reduction peak of $PdCl_2(PPh_3)_2$ is irreversible and consequently the factor ϕ is unknown. On the other hand, the diffusion coefficients of $PdCl_2(PPh_3)_2$ and ferrocene, involved in the expression of their respective peak currents as $D^{1/2}$, differ greatly ($D_{Fe} \approx 3D_{Pd}$).[59]

2.3.2. Generation of Anionic $Pd^0L_2X^-$ from $Pd^{II}X_2L_2$ (L = PPh_3) and Their Reactivity in Oxidative Addition to Aryl Halides

As reported above, the low-ligated complex $Pd^0(PPh_3)_2$ plays an important role as the active species in oxidative additions to aryl halides. It is however very often generated at very low concentration from nonreactive precursors such as $Pd^0(PPh_3)_3$ (Scheme 11) or Pd^0(dba)$(PPh_3)_2$ (Scheme 18). The overall bielectronic reduction of $PdX_2(PPh_3)_2$ (X = Cl, Br, I) should quantitatively afford $Pd^0(PPh_3)_2$ (Scheme 25). This has been checked in a first approach by performing double potential step chronoamperometry at a steady disk electrode (for an illustration of the technique, see Figure 1e,f). The potential is first held 250 mV after the reduction peak potential of $PdCl_2(PPh_3)_2$ at R_1 during a time θ, giving a reduction current $i_{Pd(II)}$. It is followed by a second potential step 250 mV after the oxidation peak potential at O_1 during the same time θ, giving an oxidation current $i_{Pd(0)}$. The ratio

$i_{Pd(0)}/i_{Pd(II)} = 0.295$ is constant for 1 ms < θ < 100 ms and close to the theoretical value of 0.293, which takes into account the diffusion.[6,58] This is indicative of a stoichiometric production of a Pd(0) complex in the overall bielectronic reduction of $PdCl_2(PPh_3)_2$ at scan rates higher than 0.1 V s^{-1}, whereas the electrogenerated Pd(0) is quantitatively oxidized at O_1 in an overall bielectronic process (Figure 6a).

When the cyclic voltammetry of $PdCl_2(PPh_3)_2$ (2 mM in THF) is performed at the scan rate of 0.2 V s^{-1} in the presence of PhI (20 mM), the oxidation peak O_1 of the electrogenerated Pd(0) is no longer observed on the reverse scan because of its oxidative addition to PhI (Figure 6b). The reaction is quite fast since it takes place within less than $\delta t = 10$ s, the time elapsed between the generation of Pd(0) at R_1 and its oxidation at O_1 ($\delta t = \Delta E/v$ with $\Delta E = (|E^{inv}| - |E^{p}_{R1}|) + (|E^{inv}| - |E^{p}_{O1}|)$, E^{inv} = inversion potential, v = scan rate). When the scan rate is increased, the time δt allotted for the oxidative addition decreases and some Pd(0) is recovered. In other words, by increasing the scan rate, that is, decreasing the time scale, the Pd(0) is more and more rapidly oxidized and has less and less time to react with PhI. In the present case, the Pd(0) is fully recovered, as indicated by its oxidation peak current at O_1, at the scan rate $v = 1000$ V s^{-1}. By means of fast cyclic voltammetry, it is thus possible to get kinetic data on the rate of the oxidative addition of PhI to the electrogenerated Pd(0).[57,58] This is illustrated in Figure 7a, which displays the evolution of the molar ratio x of the electrogenerated Pd(0) with log([PhI]/v) ($x = [Pd^0]/[Pd^0]_0 = i/i_0$, i = oxidation peak current of the Pd(0) electrogenerated from $PdBr_2(PPh_3)_2$ in the presence of excess PhI, i_0 = oxidation peak current of Pd(0) in the absence of PhI at the same scan rate v). The fact that a single curve is obtained whatever the PhI concentration is indicative of a first-order reaction for PhI: $\ln x = -k^{oa}[PhI]t$ (k^{oa} = rate constant of the oxidative addition). Since $t = \Delta E/v$, $\ln x = -k^{oa}[PhI]\Delta E/v$. The rate constant k^{oa} is determined from the value of $[PhI]/v_{1/2}$ corresponding to the half-reaction, as indicated in Figure 7a.[58]

A higher rate constant k^{oa}, determined for the Pd(0) complex generated by the reduction of $PdCl_2(PPh_3)_2$, suggests that the halide ions X^- delivered by the precursors $PdX_2(PPh_3)_2$ play a role in the oxidative addition process and that the electrogenerated Pd(0) complex is not the expected $Pd^0(PPh_3)_2$, as proposed in Scheme 25 but an anionic Pd(0) species ligated by halides. The decrease of the value of $\log(v_{1/2}/[PhI])$ (as representative of $\log k^{oa}$) with increasing concentration of Cl^- and increasing initial concentration of $PdCl_2(PPh_3)_2$ (Figure 7b) indicates that the chloride ions affect the rate of the oxidative addition by forming anionic Pd(0) complexes: a dimer $[Pd^0(PPh_3)_2(\mu\text{-}Cl)]_2^{2-}$ at low chloride concentrations ($[Cl^-] < 1$ mM), a dianionic $Pd^0(PPh_3)_2Cl_2^{2-}$ at high chloride concentrations ($[Cl^-] > 0.1$ M), and a monoanionic $Pd^0(PPh_3)_2Cl^-$ at medium chloride concentrations (Scheme 26).[58] All complexes are in equilibrium, and the dimer is the most reactive one. Only two anionic species $Pd^0(PPh_3)_2Br_n^{n-}$ ($n = 1$ or 2) are generated in the reduction of $PdBr_2(PPh_3)_2$ (Scheme 26).[58]

Further DFT calculations by Shaik et al. have supported the viability of monoanionic species $Pd^0(PPh_3)_2X^-$ (X = Cl, Br, I) in THF (Figure 8a).[60]

The formation of anionic Pd(0) species had been first proposed by Negishi et al. in the chemical reduction of $PdX_2(PPh_3)_2$ (X = Cl, Br, I) by an organolithium *n*BuLi in THF, as $[Pd^0(PPh_3)_2X^-,Li^+]_n$ (n = 1, 2, or aggregates?).[61] The reactivity of the latter in their oxidative addition to PhI could not be followed by ^{31}P NMR spectroscopy due to too fast reactions. Thanks to fast cyclic voltammetry, the existence of anionic Pd(0) species has been confirmed from a kinetic point of view, and they are now better characterized. Moreover, the reactivity of $Pd^0(PPh_3)_2X^-$ (X = Cl, Br) with PhI in THF is now well-characterized by the determination of their respective rate constants, k^{oa} (Table 3).

The chemical reduction of $PdCl_2(PPh_3)_2$ reported by Negishi et al.[61] has been mimicked by the electrochemical reduction of $PdCl_2(PPh_3)_2$ performed in the presence of the

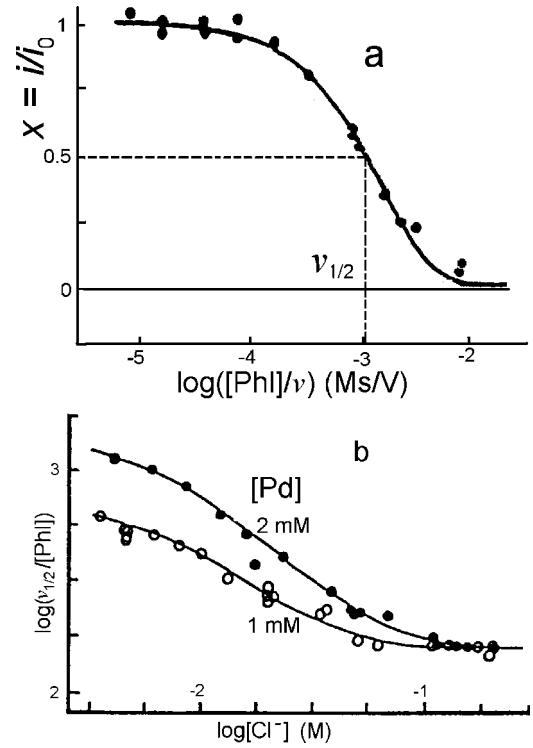

Figure 7. (a) Kinetics of the oxidative addition of PhI (1−10 equiv) to the Pd(0) complex generated in the electrochemical reduction of $PdBr_2(PPh_3)_2$ (2 mM) in THF, as monitored by fast cyclic voltammetry at steady gold disk electrodes (scan rate v in the range 0.1−10 V s^{-1}, d = 0.5 mm; in the range 20−1000 V s^{-1}, d = 0.125 mm). Plot of x against log([PhI]/v) ($x = [Pd^0]/[Pd^0]_0 = i/i_0$; i = oxidation peak current of Pd(0) at O_1 in the presence of PhI, i_0 = oxidation peak current of Pd(0) at O_1 in the absence of PhI at the same scan rate v) and for identical inversion of the potential scan (250 mV after the reduction peak potential of R_1). (b) Kinetics of the oxidative addition of PhI to the Pd(0) complex generated in the electrochemical reduction of $PdCl_2(PPh_3)_2$ (2 mM) in THF. Variation of $\log(v_{1/2}/[PhI])$ (as representative of $\log(k^{oa})$) versus chloride concentration and initial Pd(II) concentration.

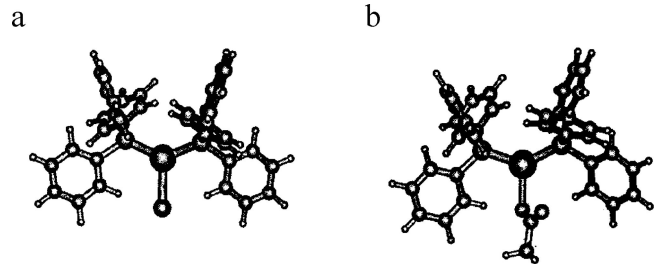

Figure 8. Optimized DFT structures: (a) for $Pd^0(PPh_3)_2Cl^-$ with Pd−Cl = 2.632 Å (similar complexes, $Pd^0(PPh_3)_2Br^-$ with Pd−Br = 2.792 Å and $Pd^0(PPh_3)_2I^-$ with Pd−I = 2.922 Å); (b) for $Pd^0(PPh_3)_2(OAc)^-$ with Pd−O = 2.369 Å.

Scheme 26

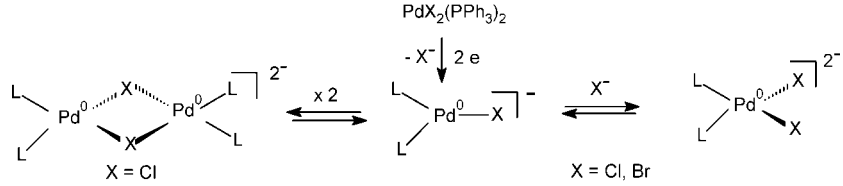

same cations, Li^+ or Zn^{2+}, as those that are delivered by chemical reductants. The oxidative addition of PhI is faster in the presence of cations (Table 3) (Amatore and Jutand).[62] Their interaction with the ligated chloride of $Pd^0(PPh_3)_2Cl^-$ by ion pairing generates a transient bent $Pd^0(PPh_3)_2$, which is more reactive than $Pd^0(PPh_3)_2Cl^-$ (Scheme 27).

Scheme 27

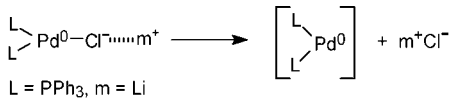

DFT calculations by Shaik et al. have established that the formation of tris-ligated anionic species $Pd^0L_2Cl^-$[60] favors the efficiency of a Pd-catalyzed cross-coupling reaction (HS^- as the nucleophile) because the Cl^- anion keeps a small P−Pd−P angle, which is required for a low activation barrier for the oxidative addition. In other words, δG^0 is minimized by stabilization of the transition state of the oxidative addition (Scheme 2).[4] The decreasing reactivity order of Pd(0) complexes in oxidative additions is given in Scheme 28.[4,60]

Scheme 28

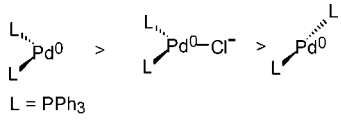

It is therefore established that the structure and reactivity of Pd(0) complexes in oxidative additions depend on the Pd(II) precursors, which deliver anions, and on the chemical reductants, which deliver cations.[3,62,63]

2.3.3. Generation of $Pd^0(NHC)_2$ from $Pd^{II}X_2(NHC)_2$ (NHC = N-Heterocyclic Carbenes) and Their Reactivity in Oxidative Addition to Aryl Halides

N-Heterocyclic carbenes (NHC) have been introduced as ligands in Pd complexes by Herrmann et al. to activate poorly reactive aryl bromides or chlorides in Heck reactions (Scheme 3).[64] NHCs are indeed strong σ-donor and weak π-acceptor ligands, which make Pd(0) complexes more electron-rich and consequently allow the activation of poorly reactive aryl halides in oxidative additions, the first step of Heck reactions. NHC and $Pd^0(NHC)_2$ may be isolated when the carbene has bulky substituents on the two nitrogen atoms (Chart 2).[65,66]

Chart 2

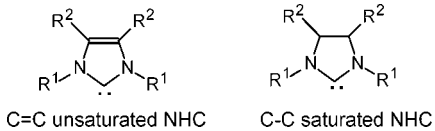

Herrmann et al. have introduced less stable C=C unsaturated NHCs via Pd(II) precursors such as $PdI_2(NHC)_2$ (R_1 = Me, R_2 = H, Chart 2).[64] A Heck reaction performed in the presence of the Pd(II) precursor was very slow. The reaction became faster after addition of hydrazine, a chemical reductant, which reduces the Pd(II) precursor into a Pd(0) complex active in the oxidative addition.[64] The oxidative addition of $Pd^0(NHC)_2$ to aryl halides has been reported and *trans*-$ArPdX(NHC)_2$ formed in the reaction have been isolated and characterized.[67–69]

Up to 2003, kinetics data on the oxidative addition were not available. In 2003, Roland, Jutand, et al. introduced a new C−C saturated NHC ligand (NHC_{Bn}) via $PdY_2(NHC_{Bn})_2$ (Y = I, Cl) (Scheme 29). They are efficient precursors for

Scheme 29

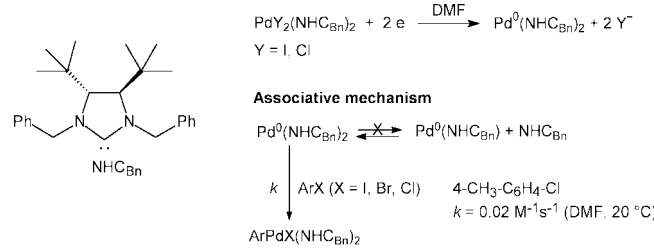

Heck reactions performed from aryl bromides at moderate temperatures.[70] Neither the carbene NHC_{Bn} nor the complex $Pd^0(NHC_{Bn})_2$ could be isolated because the two flexible benzyl groups are not bulky enough, as shown in the X-ray structure of the precursor $PdI_2(NHC_{Bn})_2$.[70] Cyclic voltammetry at a steady electrode has been used to generate the transient $Pd^0(NHC_{Bn})_2$ by reduction of $PdY_2(NHC_{Bn})_2$ (Y = I, Cl) in DMF.

The absolute number of electron(s) involved in the reduction of $PdI_2(NHC_{Bn})_2$ at R_1 (Figure 9a) has been determined (using the procedure described in section 2.3.1) and revealed an overall bielectronic reduction process (Scheme 29).[70] The electrogenerated $Pd^0(NHC_{Bn})_2$ is thus characterized by an oxidation peak observed on the reverse scan at O_1 (Figure 9a). The latter totally disappears in the presence of a stoichiometric amount of PhBr (3 mM) at the scan rate of 0.2 V s^{-1}, due to a fast oxidative addition, which takes place within less than δt = 11 s, the time elapsed between the generation of Pd(0) at R_1 and its oxidation at O_1 at that scan rate. At higher scan rate (10 V s^{-1}), $Pd^0(NHC_{Bn})_2$ has less time to react (δt = 0.25 s) and is partly recovered (dashed line in Figure 9a). Its reactivity with PhBr has been followed by fast cyclic voltammetry, and the rate constant *k* of the oxidative addition has been determined from the plot in Figure 9b (Table 4, Scheme 29).[70] The reaction rate is not affected by halide anions. Consequently, the same neutral $Pd^0(NHC_{Bn})_2$ is electrogenerated from $PdY_2(NHC_{Bn})_2$ (Y = I, Cl) (Scheme 29).

In 2006, Jutand et al. extended their former work of 2003 to the oxidative addition of the electrogenerated $Pd^0(NHC_{Bn})_2$

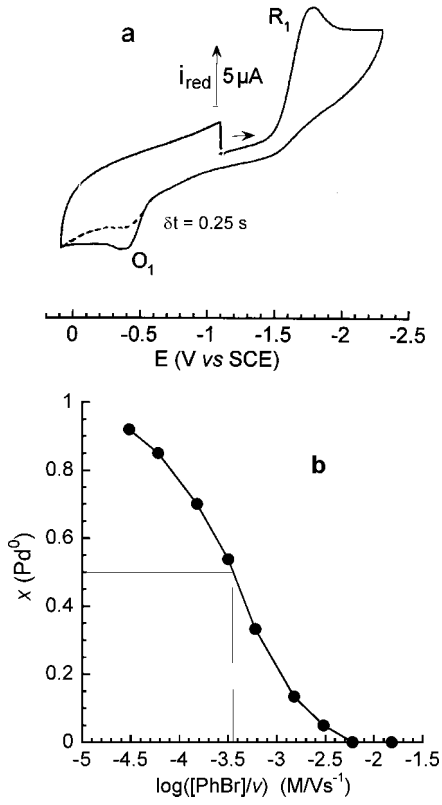

Figure 9. (a) Cyclic voltammetry of (—) $PdI_2(NHC_{Bn})_2$ (3 mM) in DMF (containing nBu_4NBF_4, 0.3 M) performed at a steady gold disk electrode (d = 0.5 mm) with a scan rate v = 10 V s^{-1}, at 20 °C and (– – –) in the presence of PhBr (3 mM) and (b) kinetics of the oxidative addition of PhBr (3 mM) to $Pd^0(NHC_{Bn})_2$ (3 mM) generated by the reduction of $PdI_2(NHC_{Bn})_2$ in DMF at 20 °C, plot of the molar fraction x of $Pd^0(NHC_{Bn})_2$ versus log([PhBr]/v) (x = i/i_0; i = oxidation peak current of the electrogenerated $Pd^0(NHC_{Bn})_2$ at O_1 in the presence of PhBr; i_0 = oxidation peak current of the electrogenerated $Pd^0(NHC_{Bn})_2$ at O_1 in the absence of PhBr, at a the same scan rate v determined as in panel a).

to aryl chlorides.[71] The oxidative additions take place at 20 °C in DMF (Table 4). As in all oxidative additions,[24] the following decreasing reactivity orders have been established: PhI > PhBr > PhCl; 4-CF_3-C_6H_4-Cl > C_6H_5-Cl > 4-CH_3-C_6H_4-Cl.

The electrochemical reduction of $PdI_2(NHC_{Bn})(PPh_3)$ generates the mixed complex $Pd^0(NHC_{Bn})(PPh_3)$, which is less reactive than $Pd^0(NHC_{Bn})_2$ with PhBr and PhI (Table 4).[70] The rate of its reaction with PhI is not affected upon addition of PPh_3. Consequently, $Pd^0(NHC_{Bn})(PPh_3)$ reacts with PhI in an associative mechanism and does not dissociate either to $Pd^0(NHC_{Bn})$ and *a posteriori* or to $Pd^0(PPh_3)$ since NHC_{Bn} is a better ligand for Pd(0) than PPh_3. Since $Pd^0(NHC_{Bn})_2$ is more reactive than $Pd^0(NHC_{Bn})(PPh_3)$, it emerges that $Pd^0(NHC_{Bn})_2$ also reacts via an associative mechanism without dissociation of NHC_{Bn} (Scheme 29). $Pd^0(NHC_{Bn})_2$ is more reactive than $Pd^0(NHC_{Bn})(PPh_3)$ because the carbene NHC_{Bn} is a stronger σ-electron donor than PPh_3.

In the late 2003, Caddick, Cloke, et al. reported kinetic data on the reactivity of an isolated $Pd^0(NHC_{Bu})_2$ in which NHC_{Bu} is a C=C unsaturated carbene, much more bulky and less electron-donating than NHC_{Bn} (Scheme 30).[69] $Pd^0(NHC_{Bu})_2$ reacts with 4-CH_3-C_6H_4-Cl in a quite slow first-order reaction, which has been followed by ^1H NMR spectroscopy.[69] Addition of the stable carbene NHC_{Bu} results in a slower oxidative addition. This establishes that

Scheme 30

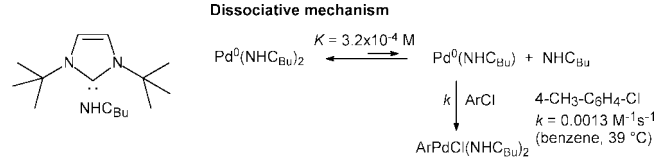

$Pd^0(NHC_{Bu})_2$ reacts via $Pd^0(NHC_{Bu})$ in a dissociative mechanism (Scheme 30).[69]The reaction from $Pd^0(NHC_{Bu})_2$ is quite slow because the reactive $Pd^0(NHC_{Bu})$ is generated at low concentration in its endergonic fast equilibrium with $Pd^0(NHC_{Bu})_2$ (see the value of K in Scheme 30);[69] $rate = k[Pd^0(NHC_{Bu})][ArCl] = kK[Pd^0(NHC_{Bu})_2][ArCl]/[NHC_{Bu}]$.

It emerges that the structure of the reactive species may be either a mono- or a bis-carbene Pd(0), such as $Pd^0(NHC_{Bu})$ (dissociative mechanism) or $Pd^0(NHC_{Bn})_2$ (associative mechanism). This is rationalized by steric factors. The stable carbene NHC_{Bu} is bulky and is therefore prone to dissociate from $Pd^0(NHC_{Bu})_2$. Conversely, the carbene NHC_{Bn} is less stable and less bulky than NHC_{Bu}. $Pd^0(NHC_{Bn})_2$ is less inclined to dissociate and reacts directly with the aryl halide.

Interestingly, comparison of the reactivity of 4-chlorotoluene with $Pd^0(NHC_{Bn})_2$ and $Pd^0(NHC_{Bu})_2$ (at the same concentration) shows that $Pd^0(NHC_{Bn})_2$, which reacts in the associative mechanism (Scheme 29), is more reactive than $Pd^0(NHC_{Bu})_2$, which reacts via $Pd^0(NHC_{Bu})$ in the dissociative mechanism (Scheme 30). Therefore, the involvement of a monoligated $Pd^0(NHC)$ as the active species is not a guarantee for a fast oxidative addition, because $Pd^0(NHC)$ is generated at low concentration in an endergonic equilibrium with the nonreactive $Pd^0(NHC)_2$.

Moreover, comparison of their respective rate constants k reveals that $Pd^0(NHC_{Bn})_2$ (k = 0.02 M^{-1} s^{-1} in DMF at 20 °C, Scheme 29)[71] is even more reactive than $Pd^0(NHC_{Bu})$ (k = 0.0013 M^{-1} s^{-1} in benzene at 39 °C, Scheme 30)[69] at identical concentrations of 4-chlorotoluene and Pd(0): $Pd^0(NHC_{Bn})_2 > Pd^0(NHC_{Bu}) \gg Pd^0(NHC_{Bu})_2$.

Therefore, the structure of the reactive Pd(0) in oxidative additions, that is, $Pd^0(NHC)_2$ versus $Pd^0(NHC)$, is governed by the bulk of the carbene ligand, but the reactivity is not necessarily controlled by the structure of the reactive species since a bis-ligated $Pd^0(NHC)_2$ (NHC = NHC_{Bn}) may be even more reactive than a monoligated $Pd^0(NHC')$ (NHC′ = NHC_{Bu}). Electronic factors must also be taken into consideration, C−C saturated carbenes (NHC_{Bn}) being stronger σ-donors than C=C unsaturated carbenes (NHC_{Bu}).

Such studies illustrate how electrochemistry via fast cyclic voltammetry performed at a steady disk electrode may be used to generate highly reactive Pd(0) complexes from stable Pd(II) precursors and to get kinetic data for their oxidative addition to aryl halides.

2.4. Characterization of Organometallic Complexes Generated in Situ in a Chemical Process from Precursors of Higher Oxidation State by Cyclic Voltammetry

2.4.1. Identification and Reactivity of the Active Pd(0) Complex Generated in Situ from $Pd(OAc)_2$ Associated with Phosphine Ligands

2.4.1.1. $Pd(OAc)_2$ Associated with Monophosphines. *2.4.1.1.1. Identification of the Pd(0) Complex Generated in*

Table 4. Rate Constants *k* of the Oxidative Addition of Aryl Halides to Pd(0) Complexes Electrogenerated from Pd(II) Precursors Ligated to *N*-Heterocyclic Carbenes in DMF at 20 °C (Scheme 29)

		k (M^{-1} s^{-1})				
Pd(II) precursor	reactive Pd(0)	PhI	PhBr	PhCl	4-CH_3−C_6H_4−Cl	4-CF_3−C_6H_4−Cl
$PdI_2(NHC_{Bn})_2$	$Pd^0(NHC_{Bn})_2$	≫1180	1180	0.13	0.02	0.35
$PdI_2(NHC_{Bn})(PPh_3)$	$Pd^0(NHC_{Bn})(PPh_3)$	830	2	*a*	*a*	*a*

[a] Not determined.

Situ from Pd(OAc)₂ + nPAr₃. The palladium(II) precursor $Pd(OAc)_2$ associated with *n* equiv PPh_3 ($n \geq 2$) is often used as catalyst. It was introduced by Dieck and Heck in 1974 in the so-called Heck reaction, arylation of an alkene in the presence of a base NEt_3 (Scheme 3).[72]

According to Heck, the first step of the catalytic reaction is an oxidative addition of the aryl halide to a Pd(0) complex generated in situ from $Pd(OAc)_2$ in a poorly defined chemical reduction by alkenes[73] or amines (used as base). In 1991, Jutand et al. discovered by means of cyclic voltammetry performed at a steady disk electrode that a Pd(0) complex is generated in situ in THF or DMF at room temperature upon mixing $Pd(OAc)_2$ and *n* equiv of PPh_3 ($n \geq 2$).[74] Indeed, the reduction peak current at R_1 characteristic of $Pd(OAc)_2(PPh_3)_2$ formed upon mixing $Pd(OAc)_2$ and *n* equiv of PPh_3 slowly decreases with time (Figure 10a). Concomitantly, an oxidation peak is observed at O_1 when the potential scan is first performed toward oxidation potentials (Figure 10b). Its oxidation peak current increases with time at the expense of the reduction peak current of $Pd(OAc)_2(PPh_3)_2$ and is no longer detected after addition of iodobenzene. Since peak currents are proportional to concentrations, it emerges that a Pd(0) complex is formed in situ from $Pd(OAc)_2(PPh_3)_2$ in a chemical reduction process. The phosphine oxide $Ph_3P(O)$ is also detected by cyclic voltammetry and ^{31}P NMR spectroscopy, suggesting a reduction of Pd(II) to Pd(0) by the phosphine.[74] By the same year, Hayashi et al. had come to the same conclusion.[75]

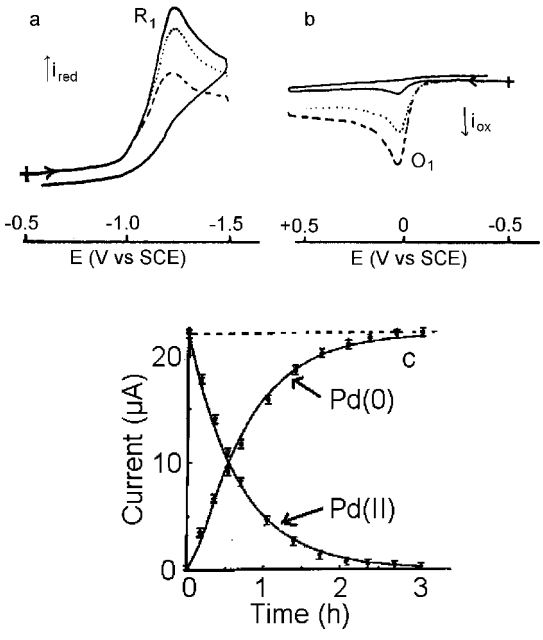

Figure 10. (a) Evolution with time of the reduction peak of $Pd(OAc)_2(PPh_3)_2$ generated in the reaction of $Pd(OAc)_2$ (2 mM) and PPh_3 (4 mM) at a steady gold disk electrode ($d = 0.5$ mm) and a scan rate of 0.2 V s^{-1} in DMF at 25 °C: (—) 4, (•••) 14, and (− − −) 33 min. (b) Evolution with time of the oxidation peak of the Pd(0) complex generated in situ from $Pd(OAc)_2(PPh_3)_2$: (—) 7, (•••) 17, and (− − −) 31 min. (c) Kinetics of the disappearance of $Pd(OAc)_2(PPh_3)_2$ generated from $Pd(OAc)_2$ (2 mM) and PPh_3 (20 mM) followed by chronoamperometry at a gold RDE ($d = 2$ mm, $\omega = 105$ rad s^{-1}) polarized at −1.30 V vs SCE and kinetics of the concomitant formation of $Pd^0(PPh_3)_3(OAc)^-$ generated in situ from $Pd(OAc)_2$ (2 mM) and PPh_3 (20 mM), followed by chronoamperometry at the same RDE polarized at +0.4 V vs SCE.

To determine the mechanism of the chemical reduction of Pd(II) to Pd(0) by the phosphine, the kinetics of formation of the Pd(0) complex has been followed by recording the increase with time of its oxidation plateau current measured at a rotating disk electrode polarized at a potential on the plateau of its oxidation wave (Figure 10c).[74] The kinetics of the disappearance of $Pd(OAc)_2(PPh_3)_2$ has been similarly followed by recording the decrease with time of its reduction plateau current measured at a rotating disk electrode polarized at a potential on the plateau of its reduction wave (Figure 10c).[74] The determination of reaction orders of 0 for PPh_3 and +1 for $Pd(OAc)_2(PPh_3)_2$ shows that the reduction process is intramolecular (reductive elimination), as illustrated in Scheme 31.[76] The rate constant of this rate-determining intramolecular reduction step has been determined (see k^{red} in Scheme 31).

Scheme 31

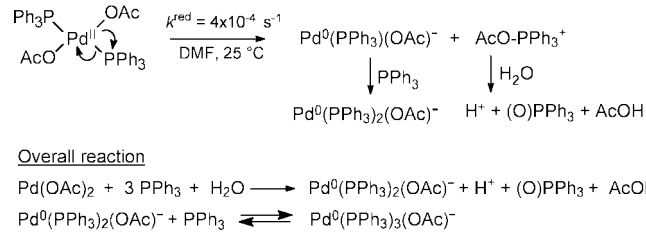

Further works by means of the same electrochemical techniques have established that the intramolecular reduction of Pd(II) to Pd(0) by phosphine ligands is quite general. It takes place from $Pd(OCOCF_3)_2$ associated with PPh_3[77] or from the cationic complex $Pd^{II}(PPh_3)_2^{2+}\cdot 2BF_4^-$ in the presence of water (via $Pd^{II}(OH)(H_2O)PPh_3)_2^+$).[78] Pd(0) complexes are formed in situ when $Pd(OAc)_2$ is associated with water-soluble phosphines TPPTS[79] and TPPTC,[80] with trialkylphosphines and triarylphosphines (4-Z-$C_6H_4)_3P$ (Z = EWG or EDG).[76] In the latter case, the formation of the Pd(0) complex follows a linear Hammett correlation with a positive slope ($\rho = +2.4$) in DMF at 25 °C.[76] The more electron-deficient the phosphine, the faster the reduction process is, in agreement with the intramolecular nucleophilic attack of the acetate onto the ligated phosphine proposed in Scheme 31. One major exception is P*o*-Tol_3, which cannot reduce $Pd(OAc)_2$ to a Pd(0) complex in DMF nor in THF (see section 2.4.2).

2.4.1.1.2. Structure and Reactivity of the Pd(0) Complex in Oxidative Addition to Iodobenzene. The oxidative addition of PhI to the Pd(0) complexes formed in situ from $Pd(OAc)_2$ and *n* equiv of PPh_3 ($n \geq 3$) has been followed by

chronoamperometry at a RDE, by recording the decrease with time of its oxidation plateau current at +0.2 V vs SCE. It emerges that the anionic $Pd^0(PPh_3)_2OAc^-$ is the reactive species (see k^{oa} in Table 3). Further DFT calculations by Shaik et al. support the viability of the anionic complex $Pd^0(PPh_3)_2(OAc)^-$ in THF (Figure 8b).[60]

The oxidative addition of PhI to $Pd^0(PPh_3)_2OAc^-$ delivers a new complex *trans*-PhPd(OAc)$(PPh_3)_2$, instead of the expected *trans*-PhPdI$(PPh_3)_2$, via an intermediate short-lived species evidenced by chronoamperometry at the rotating disk electrode polarized at +0.4 V vs SCE.[74,81] Indeed, at that potential, what is first observed is the decrease of the oxidation current of $Pd^0(PPh_3)_2OAc^-$ involved in a fast oxidative addition (decreasing part in Figure 11), unexpectedly followed by the increase of an oxidation current at longer times, characteristic of iodides, I^- (increasing part in Figure 11). The S-shaped curve suggests that iodides are released from an intermediate complex where the Pd(II) center is ligated by both OAc and I. A minimal structure for that intermediate could be an anionic pentacoordinated complex [PhPdI(OAc)$(PPh_3)_2^-$] on the way to PhPd(OAc)$(PPh_3)_2$ (right part of Scheme 32).[81] Due to its short lifetime ($t_{1/2}$ = ca. 40 s in DMF at 25 °C), this anionic 18-electron complex does not play any role in the further step of Heck reactions since it does not react with alkenes on the way to its fast evolution to PhPd(OAc)$(PPh_3)_2$.

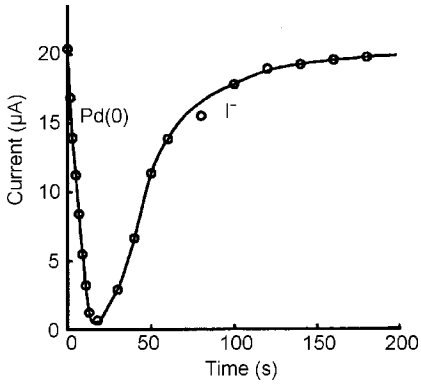

Figure 11. Kinetics of the oxidative addition of PhI (20 mM) to the anionic Pd(0) complex generated in situ from $Pd(OAc)_2$ (2 mM) and PPh_3 (20 mM) (decreasing part) followed by chronoamperometry at a gold rotating disk electrode (d = 2 mm, ω = 105 rad s^{-1}) polarized at +0.4 V vs SCE, in DMF at 25 °C and kinetics of the formation of iodide ions from the putative intermediate [$PhPd^{II}I(OAc)(PPh_3)_2^-$] formed in the faster oxidative addition (increasing part), on the way to the final complex PhPd(OAc)$(PPh_3)_2$ followed by chronoamperometry at the same gold RDE polarized at the same potential.

Scheme 32

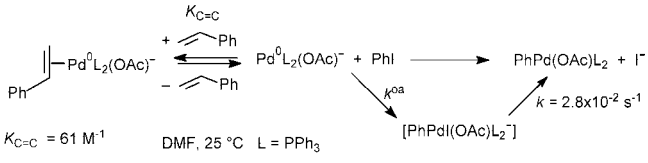

Factors Affecting the Rate of the Oxidative Addition. Amatore, Jutand et al. have reported that the oxidative addition of PhI to $Pd^0(PPh_3)_2(OAc)^-$ is slower when performed in the presence of a base such as NEt_3 (Table 3).[81,62] Protons, which are generated together with the Pd(0) complex by the hydrolysis of the phosphonium (Scheme 31), can interact with the acetate ligand of the anionic $Pd^0(PPh_3)_2(OAc)^-$ to form the more reactive bent $Pd^0(PPh_3)_2$ (Scheme 33). In the presence of NEt_3, the protons are neutralized, $Pd^0(PPh_3)_2(OAc)^-$ is more stable in relation to its decomposition by protons, and the oxidative addition is slower (Table 3).

Scheme 33

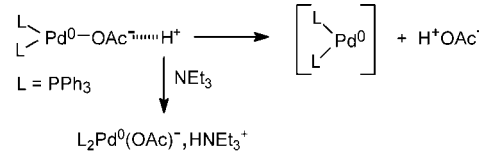

The oxidative addition is also slower when performed in the presence of alkenes (e.g., styrene), which are reagents in Heck reactions. The concentration of the reactive $Pd^0(PPh_3)_2(OAc)^-$ decreases by a partial complexation by the alkene, which generates a nonreactive complex (η^2-CH_2=CHR)$Pd^0(PPh_3)_2(OAc)^-$ (left part of Scheme 32).[49,51]

2.4.1.2. $Pd(OAc)_2$ Associated with a Bisphosphine. $Pd(OAc)_2$ associated with dppp (Ph_2P-$(CH_2)_3$-PPh_2) has been widely used as catalytic precursor in Heck reactions to investigate the factors that control the regioselectivity (see section 2.7.1.2).[82] Amatore, Jutand, et al. have observed that the reaction of $Pd(OAc)_2$ with dppp (1 equiv) does not generate a Pd(0) complex detectable by cyclic voltammetry performed first toward oxidation potentials (even at long times). This is a consequence of the reversibility of the reductive elimination, which takes place within Pd(OAc)(dppp) formed in the early stage (Scheme 34).[83] A second equivalent of dppp and water is required to shift the reversible reductive elimination to the final anionic $Pd^0(dppp)(OAc)^-$ characterized by its oxidation peak (−0.41 V vs SCE) (Scheme 34). The hemioxide dppp(O) is formed as well.[83] The formation in situ of $Pd^0(Binap)_2$ and the hemioxide Binap(O) from $Pd(OAc)_2$ and Binap (3 equiv) in the presence of water was reported earlier by Hayashi et al.[75]

The rate of formation of the Pd(0) complex from $Pd(OAc)_2$ and 2 dppp has been followed by recording the increase of its oxidation plateau current at a rotating disk electrode (k^{red} in Scheme 34).[83] The kinetics of the oxidative addition of PhI to $Pd^0(dppp)(OAc)^-$ has also been followed by the same technique. The reaction is quite complex and involves dimeric anionic Pd(0) complexes. The overall oxidative addition is slower (by a factor 300) than that performed from $Pd^0(PPh_3)_2(OAc)^-$ at the same concentrations of PhI.[83] The oxidative addition is slower in the presence of NEt_3 (see Scheme 33 for related effect with dppp).

2.4.2. Identification of the Active Pd(0) Complex Generated in Situ from P,C-Palladacyles

In contrast to PPh_3,[74] P*o*-Tol_3 cannot reduce $Pd(OAc)_2$ to a Pd(0) complex but a *P*,*C*-palladacycle is formed by cyclometalation: *trans*-di(μ-acetato)-bis[*o*-(di-*o*-tolylphosphino)benzyl]dipalladium (**5**) (Chart 3), as reported by Beller, Herrmann, et al.[84] Such a Pd(II) complex catalyzes Heck reactions involving aryl bromides and activated aryl chlorides.[84,85] In *P*,*C*-palladacycle-catalyzed C−N or C−C cross-coupling reactions, Louie and Hartwig have established that the true catalyst is a Pd(0) complex, formed in situ by reductive elimination within monomeric *P*,*C*-palladacycles whose acetate ligands have been substituted by N- or C-nucleophiles.[86]

Chart 3

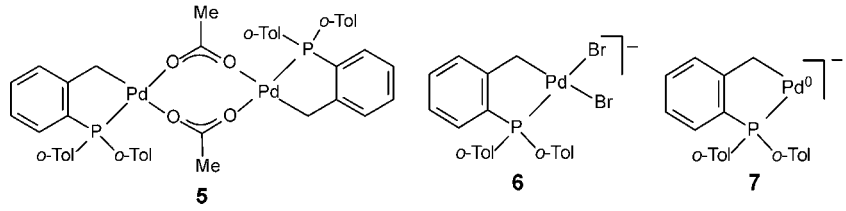

Scheme 34

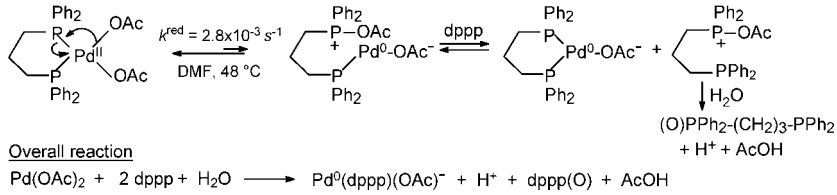

In Heck reactions, in the absence of clearly identified reductant and due to the recovery of the monomeric *P*,*C*-palladacycle **6** in a reaction performed from an aryl bromide, an oxidative addition of the Pd(II) palladacycle to aryl halides to deliver an aryl-Pd(IV) complex was first proposed by Herrmann et al.[84] The oxidative addition of aryl halides to Pd(II) complexes has been ruled out by DFT calculations.[87] An induction period observed in some Heck reactions (amine as base) has been rationalized by Beller and Riermeier, as a slowly occurring reduction of the palladacycle **5** to an active Pd(0) complex [Pd^0(P*o*-Tol_3)].[88] In 2001, even in the absence of any identified reductant, Böhm and Herrmann proposed a reduction in situ of the palladacycle **5** to an anionic Pd(0) complex **7**, still ligated to the benzyl moiety of the ligand and involved in a classical oxidative addition to aryl halides.[89]

In 2005, the electrochemical properties of the *P*,*C*-palladacycle **5** were investigated in DMF by d'Orlyé and Jutand to characterize the postulated complex **7**. The cyclic voltammogram of **5** performed at a steady disk electrode in DMF exhibits two successive reduction peaks at R_1 and R_2, which characterize the reduction of **5** and its monomeric forms, respectively (Figure 12a, Scheme 35).[90]

The electrogenerated Pd(0) complex, characterized by its oxidation peak O_1 at +0.2 V vs SCE, is observed on the reverse scan (Figure 12a). However, it is not the anionic Pd(0) complex **7** proposed by Böhm and Herrmann[89] but the known complex Pd^0(P*o*-$Tol_3)_2$ (**9**) formed upon fast protonation of **7** during the slow potential scan, followed by reductive elimination from complex **8** (Scheme 35).[90]

The reduction peak potential of the palladacycle **5** is quite negative (Scheme 35), and **5** could be reduced by, for example, zinc powder. Such a strong reducing agent is however never present in Heck reactions.

No Pd(0) complex is spontaneously generated from the palladacycle **5** at 25 °C even at 80 °C in the absence of any additives, since no oxidation peak is observed when the cyclic voltammetry of **5** is performed directly toward oxidation potentials in DMF (Figure 12b). In 2005, d'Orlyé and Jutand put as a hypothesis that a Pd(0) complex could be generated in situ from the palladacycle **5** in an endergonic reductive elimination between the acetate ligand and the *cis*-benzylic group attached to the Pd(II) center (Scheme 36).[90] This reaction must generate the monophosphine−Pd(0) complex **10** ligated by the new phosphine ligand **11** formed in the reductive elimination. The backward reaction in Scheme 36, an intramolecular oxidative addition of the Pd(0) to the C−O bond of the *o*-benzylic acetate in complex **10**, must be very fast because of its intramolecular character. This is why the equilibrium in Scheme 36 lies in favor of

Scheme 35

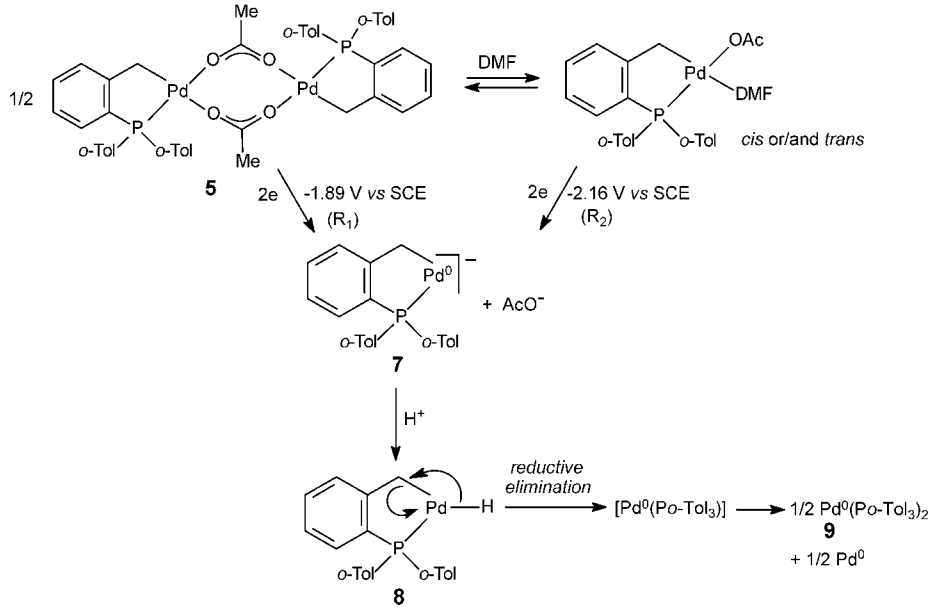

Scheme 36

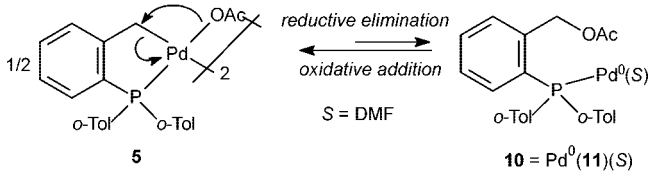

the palladacycle **5** and provides a very low thermodynamic concentration of the Pd(0) complex **10**.

To be able to detect a Pd(0) complex formed in situ by an oxidation peak observed in cyclic voltammetry performed toward oxidation potentials, the equilibrium in Scheme 36 must be shifted toward its right-hand side by trapping the Pd(0) complex **10** by additional ligands such as dba, P*o*-Tol_3, or AcO^-. Those additives have been selected because they cannot reduce the palladacycle **5** to a Pd(0) complex.

A Pd(0) complex is indeed generated in situ from the palladacycle **5** in DMF at 80 °C, after addition of P*o*-Tol_3 and dba in large excess, that is, in the absence of any reducing agents. This Pd(0) complex has been characterized by an oxidation peak (+0.19 V vs SCE), which disappears after addition of PhI, confirming the formation in situ of a Pd(0) from **5** or its monomeric form in DMF. The oxidation peak characterizes Pd^0(P*o*-Tol_3)$_2$ (**9**) formed from complex **10**, due to large excess of P*o*-Tol_3 (Scheme 37A).[90]

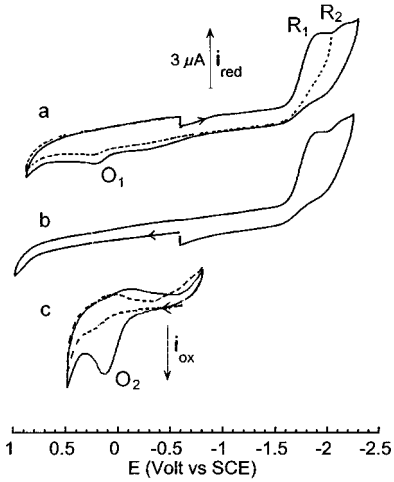

Figure 12. Cyclic voltammetry performed in DMF (containing nBu$_4$NBF$_4$, 0.3 M) at a steady gold disk electrode (d = 0.5 mm) at a scan rate of 0.5 V s^{-1}: (a) (—) reduction of the palladacycle (**5**, 2 mM) at 25 °C and (– – –) with the potential scan reversed after R_1; (b) Same as in panel a but oxidation first, at 25 °C; (c) (—) oxidation of the Pd(0) complex generated in situ from the palladacycle (**5**, 2 mM) in the presence of dba (18.9 mM), P*o*-Tol_3 (4 mM), and nBu$_4$NOAc (18.4 mM) at 80 °C and (– – –) after addition of PhI (74 mM) at 80 °C.

An anionic monopalladacycle **12** is formed upon addition of excess nBu$_4$NOAc to **5** in DMF (Scheme 37B). Acetate salts are often used as base in palladacycle-catalyzed Heck reactions.[84,85,88,89] After addition of a stoichiometric amount of P*o*-Tol_3 (P/Pd = 1) and excess dba to complex **12** in DMF, an oxidation peak O_2 is detected after 1 h at 80 °C, at a slightly less positive potential (+0.14 V vs SCE, Figure 12c) than that obtained in the absence of acetates (vide supra). The oxidation peak O_2 disappears after addition of excess PhI (Figure 12c), confirming that a Pd(0) complex has been generated in situ from the palladacycle **5** via the anionic complex **12**, in the absence of any reducing agent (Scheme 37B). The reversible reductive elimination has been shifted toward the formation of complex **14** by successive stabilization of the Pd(0) complex by acetate (complex **13**) and P*o*-Tol_3 (Scheme 37B).[90]

The reaction of Pd^0(dba)$_2$ with Ph_2P(*o*-benzyl acetate) (**15**, related to **11** but less bulky) gives a mononuclear *P*,*C*-palladacycle **16** formed by an intramolecular oxidative addition (Scheme 38).[90] This reaction definitively supports

Scheme 38

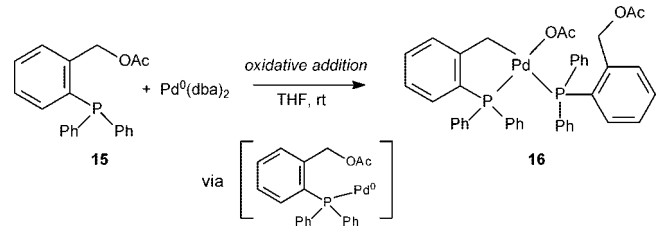

the idea that the formation of the Pd(0) complex **10** from the palladacycle **5** is reversible (Scheme 36).

Therefore, d'Orlyé and Jutand have established that the *P*,*C*-palladacycle **5** is a reservoir of a monophosphine−Pd(0) complex **10**, generated in situ by an intramolecular reduction. Such reaction is favored by acetate anions via the formation of an anionic monomeric *P*,*C*-palladacycle ligated by acetate (**12**). This explains why no induction period is observed in Heck reactions when NaOAc is used as base.[88]

Scheme 37

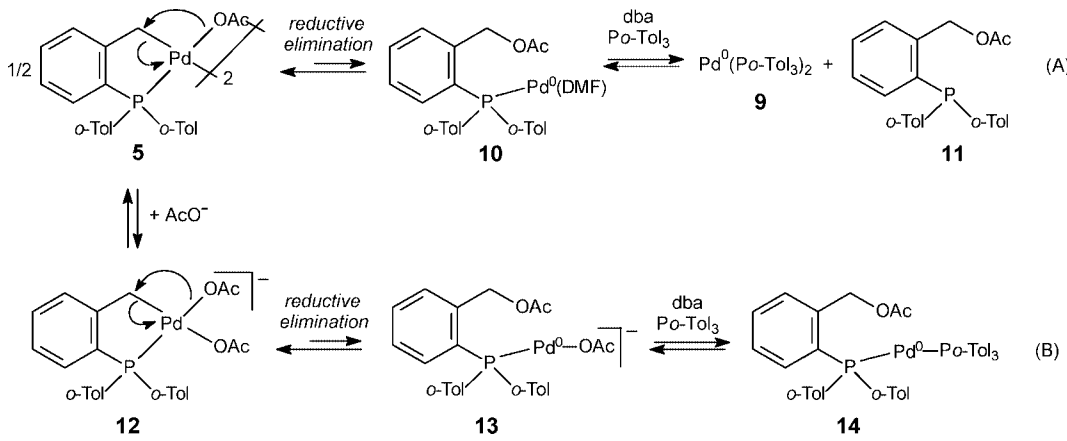

This is an illustration of the role of electrochemistry used as an analytical technique to detect and characterize organometallic species formed in situ from stable precursors ($Pd(OAc)_2$ associated with phosphines, P,C-palladacycles) by intramolecular chemical reductions.

2.5. Endergonic Dissociation in Organometallic Species. Determination of the Equilibrium Constant by Chronoamperometry at a Steady Disk Electrode

$ArPdXL_2$ complexes formed in oxidative addition of ArX to Pd(0) complexes are saturated 16-electron complexes (square-planar d^8 structure). Most of them undergo two kinds of reversible dissociations in a solvent (*S*) to deliver less strongly coordinated complexes more prone to react with nucleophiles (alkenes, alkynes, Rm, etc.): dissociation of one ligand L giving ArPdX*S*L or dissociation of one ligand X giving a cationic complex $ArPdSL_2^+$. Such dissociations are often endergonic so that the thermodynamic concentration of the dissociated complex is too low to be detected by usual techniques such as ^1H or ^{31}P NMR spectroscopy. Moreover, the equilibrium may be fast relative to the NMR time scale. Broad NMR signals are observed, and the equilibrium constant cannot be determined. Such problems may be solved by means of chronoamperometry performed at a steady disk electrode.

2.5.1. Dissociation of One Ligand L

The Stille reaction (Scheme 7) is much more efficient when the Pd(0) catalyst is ligated to $AsPh_3$ rather than to PPh_3.[91] Amatore, Jutand, et al. have established that *trans*-$PhPdI(AsPh_3)_2$ is formed in the oxidative addition of PhI to $Pd^0(AsPh_3)_2$ generated in situ from the precursor $\{Pd^0(dba)_2 + 2AsPh_3\}$ (see section 2.2.2).[43] The ^1H NMR spectrum of *trans*-$PhPdI(AsPh_3)_2$ in DMF-d_7 exhibits two broad signals for the protons of PhPd in the range 6.4−6.9 ppm, characteristic of a fast equilibrium between $PhPdI(AsPh_3)_2$, $PhPdI(DMF)(AsPh_3)$, and $AsPh_3$ (Scheme 39).[92] Indeed, addition

Scheme 39

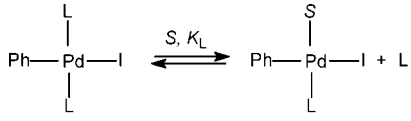

L = $AsPh_3$, S = DMF, 25 °C
$K_L = 3 \times 10^{-4}$ M

of $AsPh_3$ (6 equiv) results in the formation of $PhPdI(AsPh_3)_2$ characterized by three sets of well-resolved signals for PhPd. Due to broad NMR signals, the equilibrium constant K_L could not be determined by NMR at 22 °C.

The cyclic voltammogram of $PhPdI(AsPh_3)_2$ at a steady disk electrode in DMF exhibits two successive reduction peaks, R_1, reduction of $PhPdI(DMF)(AsPh_3)$, and R_2, reduction of $PhPdI(AsPh_3)_2$ (Figure 13a). Because the equilibrium in Scheme 39 may be shifted toward its right-hand side by the reduction of $PhPdI(DMF)(AsPh_3)$ at R_1 during the potential scan, the reduction peak current at R_1 is not proportional to the thermodynamic concentration of $PhPdI(DMF)(AsPh_3)$ but to a dynamic concentration (CE mechanism).[6]

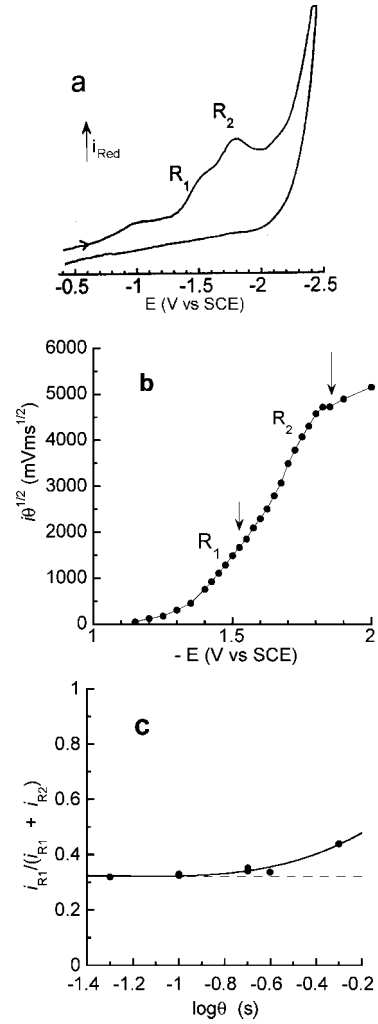

Figure 13. (a) Cyclic voltammetry of $PhPdI(AsPh_3)_2$ (2 mM) in DMF (containing nBu_4NBF_4, 0.3 M) at a steady gold disk electrode ($d = 0.5$ mm) with a scan rate of 0.2 V s^{-1} at 20 °C: R_1, reduction of $PhPdI(DMF)(AsPh_3)$; R_2, reduction of $PhPdI(AsPh_3)_2$. (b) Single potential step chronoamperometry performed at the same electrode. Plot of $i\theta^{1/2}$ against potentials for a step duration time $\theta = 0.2$ s. (c) Determination of the equilibrium constant K_L between $PhPdI(AsPh_3)_2$ and $PhPdI(DMF)(AsPh_3)$. Plot of $i_{R_1}/(i_{R_1} + i_{R_2})$ against log θ. i_{R_1} and $i_{R_1} + i_{R_2}$ are determined as indicated by the first and second arrow, respectively, in panel b.

By performing single potential step chronoamperometry at a steady disk electrode, that is, by holding the potential every 50 mV (from −1 to −2 V) during the same time θ and measuring the corresponding reduction currents i, one gets the normalized voltammogram, $i\theta^{1/2} = f(E)$, displayed in Figure 13b (the procedure is similar to that depicted in Figure 1e,f, but the single potential step is done in reduction). The reduction plateau currents i_{R_1} and $i_{R_1} + i_{R_2}$ are measured as indicated by the two arrows; ($i = FSnCD^{1/2}(\pi\theta)^{-1/2}$)[6] for different potential step durations θ. The plot of $i_{R_1}/(i_{R_1} + i_{R_2})$ against log θ delivers the curve displayed in Figure 13c. The current ratio decreases when θ decreases and becomes constant at short times ($\theta < 0.1$ s), showing that the equilibrium is frozen at these short times and is no longer shifted in the diffusion layer by the too fast reduction process at the electrode. The value of the plateau gives the relative thermodynamic concentrations of $PhPdI(DMF)(AsPh_3)$ and $PhPdI(AsPh_3)_2$ and the equilibrium constant K_L (Scheme 39).[42]

2.5.2. Dissociation of One Ligand X

Amatore, Jutand, et al. have shown that complexes *trans*-$PhPdX(PPh_3)_2$ (X = I, Br, Cl, OAc) display a dissociation of the ligand X in the dissociating solvent DMF (Scheme 40).

Scheme 40

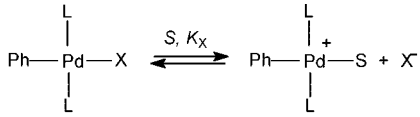

L = PPh_3, S = DMF, 20 °C

K_{OAc} = 133x10^{-5} M > K_I = 59x10^{-5} M > K_{Br} = 28x10^{-5} M > K_{Cl} = 5.3x10^{-5} M

The voltammogram of *trans*-$PhPdX(PPh_3)_2$ (X = I,[93] Br,[93] OAc[81]) exhibits in DMF two successive reduction peaks at low scan rates. *trans*-$PhPd(DMF)(PPh_3)_2^+$ is more easily reduced at R_1 (a one-electron transfer)[93] than the parent complex *trans*-$PhPdX(PPh_3)_2$ at R_2 (a two-electron transfer). Single potential step chronoamperometry at a steady disk electrode has been performed at various potentials and step durations θ.[93] Two normalized voltammograms for *trans*-$PhPdBr(PPh_3)_2$ are shown in Figure 14 for two different times

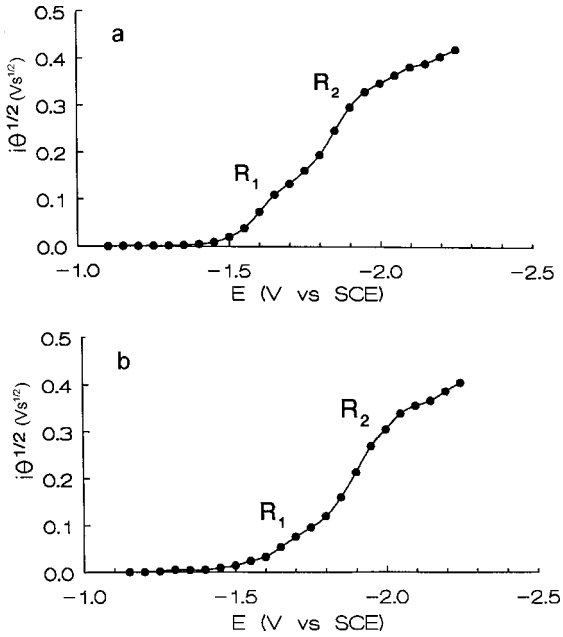

Figure 14. Single potential step chronoamperometric reduction of $PhPdBr(PPh_3)_2$ (2 mM) in DMF at 20 °C with variation of $i\theta^{1/2}$ against reduction potential for various step duration times θ: (a) θ = 200 ms at a steady gold disk electrode (d = 0.5 mm); (b) θ = 20 ms at a steady gold disk electrode (d = 0.125 mm).

θ. The reduction plateau current of *trans*-$PhPd(DMF)(PPh_3)_2^+$ at R_1 increases relative to that of *trans*-$PhPdBr(PPh_3)_2$ at R_2 when θ is increased, evidencing a shift of the equilibrium in Scheme 40 toward the cationic complex at long times, due to its continuous reduction and consequently consumption in the diffusion layer during the potential step (CE mechanism).[6] The plot of $i_{R_1}/(i_{R_1} + i_{R_2}/2)$ against log θ exhibits a plateau at short times θ (as in Figure 13c). The thermodynamic concentration of the cationic $PhPd(DMF)(PPh_3)_2^+$ in its equilibrium with $PhPdX(PPh_3)_2$ and the equilibrium constants K_X are determined from the plateau value.[93]

AcO^- is more easily dissociated from the parent complex than the halides, as expressed by their respective equilibrium constant K_X (Scheme 40).

2.6. Characterization of Ionic Organometallic Species and Their Rate of Formation by Conductivity Measurements

2.6.1. Ionic Species Generated in Oxidative Addition of Aryl Triflates to Pd(0) Complexes

The speculative cationic character of $ArPd(PPh_3)_n^+$ (n = 2 or 3) formed in the oxidative addition of aryl triflates to $Pd^0(PPh_3)_4$, was for the first time confirmed by conductivity measurements by Jutand and Mosleh in 1995.[30] The conductivity κ of a solution of $Pd^0(PPh_3)_4$ (2 mM) in DMF increased from a residual low conductivity κ_0 (2 μS cm^{-1}) to a final constant conductivity κ_{lim} (75 μS cm^{-1}) upon addition of excess 4-NO_2-C_6H_4-OTf (Figure 15a). This is

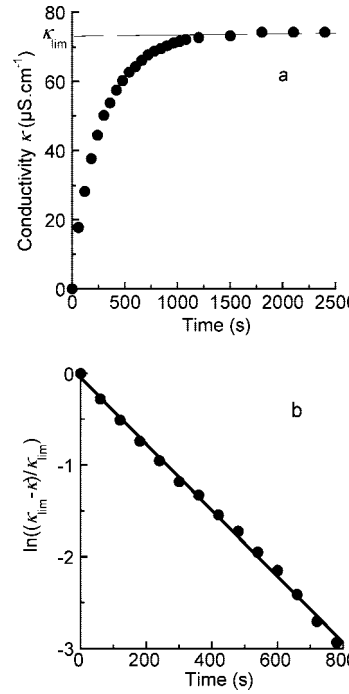

Figure 15. Kinetics of the formation of *trans*-4-NO_2-C_6H_4-$Pd(DMF)(PPh_3)_2^+ \cdot TfO^-$ in the oxidative addition of 4-NO_2-C_6H_4-OTf (10 mM) to $Pd^0(PPh_3)_4$ (2 mM) in DMF at 20 °C: (a) variation of the conductivity with time, $\kappa = \kappa_{exp} - \kappa_0$ (κ_{exp} = experimental conductivity at t; κ_0 = initial residual conductivity of 2 μS cm^{-1}); (b) variation of $\ln((\kappa_{lim} - \kappa)/\kappa_{lim})$ with time (κ = conductivity at t; κ_{lim} = final conductivity).

the first evidence of the formation of ionic species in an oxidative addition to aryl triflates. Moreover, the ionic species are rather stable, as attested by the constant limiting value κ_{lim} with time (Figure 15a).

Further characterization by ^1H and ^{31}P NMR spectroscopy, FAB, and ESI MS have shown that the cationic complexes contain only two phosphine ligands in a trans position (Scheme 41A).[30] The linear variation of the final conductivity κ_{lim} with palladium concentration indicates that free ions, $ArPd(DMF)(PPh_3)_2^+$ and TfO^-, are formed in DMF at 20 °C.[30,94]

$\Lambda_M = 35 \pm 2$ S cm^2 mol^{-1} for *trans*-4-NO_2-C_6H_4-Pd(DMF)$(PPh_3)_2^+ \cdot TfO^-$

$\Lambda_M = 57 \pm 2$ S cm^2 mol^{-1} for *trans*-4-NO_2-C_6H_4-Pd(DMF)$(PPh_3)_2^+ \cdot TfO^-$

In THF, free ions *trans*-ArPd(THF)$(PPh_3)_2^+$ and TfO^- are formed in equilibrium with the ion pairs, as attested by the variation of their conductivity with the square root of the palladium concentration.[30]

Since the conductivity κ of ArPd(DMF)$(PPh_3)_2^+ \cdot TfO^-$ is proportional to its concentration, the curve in Figure 15a characterizes the kinetics of the formation of the ionic species in the oxidative addition of the aryl triflate to $Pd^0(PPh_3)_4$ in DMF. The oxidative addition can thus be followed by conductivity measurements. The plot of $\ln((\kappa_{lim} - \kappa)/\kappa_{lim})$ with time is linear (Figure 15b). The reaction is first-order for ArOTf: $\ln((\kappa_{lim} - \kappa)/\kappa_{lim}) = -k_{app}[ArOTf]t$.[30] The rate constant for the formation of the cationic complex has been determined: $k_{app} = 0.35 \pm 0.02$ M^{-1} s^{-1} for 4-NO_2-C_6H_4-OTf in DMF at 20 °C. This rate constant is very similar to the rate constant of disappearance of $Pd^0(PPh_3)_3$, as independently determined by chronoamperometry at a RDE (see section 2.2.1.1): $k_{app} = 0.32 \pm 0.02$ M^{-1} s^{-1} (Scheme 41A).[30] The ionization of the intermediate neutral complex ArPd(OTf)L_2 (whenever formed) to ArPd(DMF)L_2^+ and TfO^- is thus faster than its formation in the oxidative addition. Therefore, the affinity of the anion TfO^- for the Pd(II) center is very weak in DMF.[30]

Scheme 41

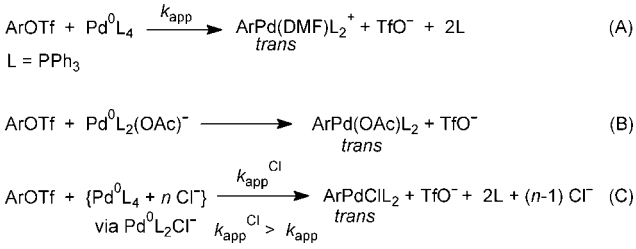

The oxidative addition of aryl triflates to the anionic $Pd^0(PPh_3)_2(OAc)^-$, generated from $Pd(OAc)_2$ and $3PPh_3$, leads to the major neutral *trans*-ArPd(OAc)$(PPh_3)_2$ in DMF (Scheme 41B)[95] in equilibrium with ArPd(DMF)$(PPh_3)_2^+$.

The oxidative addition of aryl triflates to the anionic $Pd^0(PPh_3)_2Cl^-$, generated by addition of chloride ions to $Pd^0(PPh_3)_4$ or by the electrochemical reduction of $PdCl_2(PPh_3)_2$, gives the neutral *trans*-ArPdCl$(PPh_3)_2$ in DMF (Scheme 41C).[30] Since chloride ions play an important role in the efficiency of palladium-catalyzed reactions performed from aryl triflates,[31,91,96] Jutand and Mosleh have investigated the influence of chloride ions on the kinetics of the oxidative addition of aryl triflates. The reactions have been followed by chronoamperometry at a RDE. The oxidative additions are faster in the presence of chloride ions (added as nBu_4NCl to $Pd^0(PPh_3)_4$ prior the addition of ArOTf)[30] due to the formation of anionic $Pd^0(PPh_3)_2Cl^-$ (Scheme 41C).

Consequently, the chloride ions play a dual role in the oxidative addition of aryl triflates to $Pd^0(PPh_3)_4$: acceleration of the oxidative addition and formation of neutral *trans*-ArPdCl$(PPh_3)_2$ (Scheme 41C).[30]

The oxidative addition of aryl iodides to (P^N^P)Pd^0(dba) complexes has been followed by conductivity measurements

Scheme 42

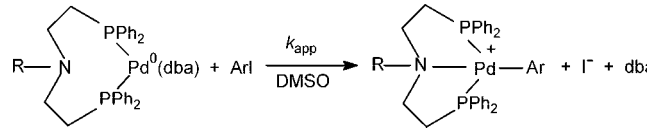

in DMSO by Hii et al. (Scheme 42).[97] The cationic character found for ArPd(P^N^P)$^+$ complexes indicates that the P^N^P ligands behave as tridentate ligands for the Pd(II) center with release of the iodide ion. The influence of the substituent R on the nitrogen atom of the ligand and on the aryl group of ArI on the rate of the oxidative addition has been monitored by conductivity measurements (Scheme 42).[97]

2.6.2. Ionic Species Generated in Oxidative Addition of Vinyl Triflates to Pd(0) Complexes

Jutand and Negri have established that the oxidative addition of vinyl triflates to $Pd^0(PPh_3)_4$ in DMF gives free ionic species *trans*-(η^1-vinyl)Pd^{II}(DMF)$(PPh_3)_2^+$ and TfO^-, characterized by conductivity measurements (Figure 16), ^{1}H

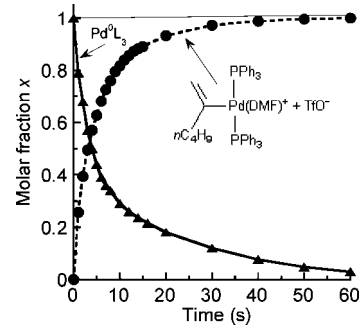

Figure 16. Oxidative addition of CH_2=C(nBu)-OTf (2 mM) to $Pd^0(PPh_3)_4$ (2 mM) in DMF at 10 °C: (– – –) Kinetics of the formation of CH_2=C(nBu)-Pd(DMF)$(PPh_3)_2^+ \cdot TfO^-$, variation of the molar fraction of the ionic species with time, as determined by conductivity measurements; (—) variation of the molar fraction of $Pd^0(PPh_3)_3$ with time, as determined by chronoamperometry at a RDE ($d = 2$ mm, $\omega = 105$ rad s^{-1}).

and ^{31}P NMR, and ESI MS (Scheme 43).[38] The rate of formation of the ionic species is the same as the rate of the oxidative addition of the vinylic triflate to $Pd^0(PPh_3)_4$, determined by chronoamperometry at a RDE (Figure 16) (see section 2.2.1.2), attesting to a fast ionization step.[38]

Cationic *trans*-(η^1-vinyl)Pd(DMF)$(PPh_3)_2^+$ are less stable than *trans*-ArPd(DMF)$(PPh_3)_2^+$. Indeed, a slow degradation gives the phosphonium salt vinyl-PPh_3^+ and a Pd(0) complex, which is detected when the oxidative addition is performed under stoichiometric conditions (Scheme 43). In the presence of excess vinyl triflate, a catalytic reaction takes place that transforms the PPh_3 ligands to vinyl-PPh_3^+ and destroys the catalyst and cationic complex (Scheme 43).

Scheme 43

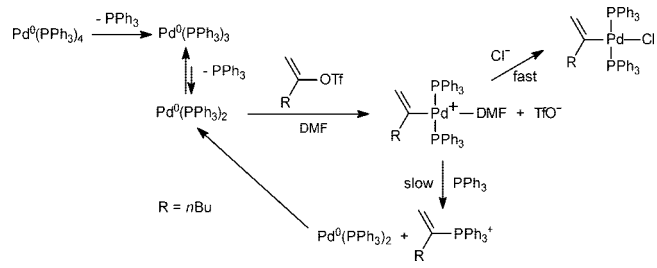

Fortunately, the cationic complex can be stabilized upon addition of chloride ions by formation of more stable neutral *trans*-(η^1-vinyl)PdCl(PPh_3)$_2$ (Scheme 43).[38] These results rationalize the beneficial effect of chlorides ions in Pd-catalyzed reactions involving vinyl triflates.[31,96]

2.6.3. Ionic Species Generated in the Reversible Oxidative Addition of Carboxylic Acids to Pd(0) Complexes

Some palladium-catalyzed reactions are initiated by the reaction of a carboxylic acid AH with Pd^0L_n complexes: isomerization of alkynes to 1,3-dienes, cycloisomerization of enynes,[98] hydrocarboxylation of alkynes,[99] and hydrocarbonylation of aryl halides.[100] The reaction of a carboxylic acid AH (acetic or formic acid) with Pd^0L_n was supposed to generate a hydrido-palladium(II), $HPd^{II}AL_{n'}$.[101] In 1998, Trost proposed the formation of cationic $HPdL_{n'}^+$ "undoubtedly formed to some extent, albeit in an unfavorable equilibrium".[102]

Amatore, Jutand, et al. have followed the reaction of $Pd^0(PPh_3)_4$ with acetic or formic acid by conductivity measurements in DMF at 25 °C.[103] The conductivity κ increases after addition of n equiv of acetic acid of $Pd^0(PPh_3)_4$ to reach a limiting value (κ_{equil} in Figure 17a), which increases

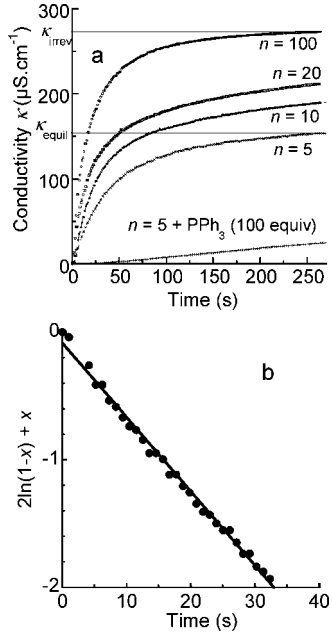

Figure 17. (a) Conductivity in DMF of HPd(DMF)-$(PPh_3)_2^+ \cdot AcO^-$ generated in the reaction of $Pd^0(PPh_3)_4$ (2 mM) with n equiv of acetic acid and in the presence of 100 equiv of PPh_3 (n = 5) at 25 °C and (b) kinetics of the oxidative addition of acetic acid (0.2 M) to $Pd^0(PPh_3)_4$ (2 mM) in DMF at 25 °C (uppermost curve in panel a), plot of 2 ln(1 − x) + x vs time (x = κ/κ_{irrev}; κ = conductivity at t; κ_{irrev} = final conductivity under conditions where the reaction is made irreversible), 2 ln(1 − x) + x = $-k_+$[AH]t (Scheme 44).

when n is increased up to 100 (κ_{irrev} in Figure 17a). The conductivity is lower in the presence of excess PPh_3 (Figure 17a).

Therefore, the reaction of $Pd^0(PPh_3)_4$ with acetic acid (via $Pd^0(PPh_3)_2$) gives ionic species that are in equilibrium with Pd(0) complexes and acetic acid because the ionic species concentration increases with the acetic acid concentration. PPh_3 is involved in the backward reaction of this equilibrium

Scheme 44

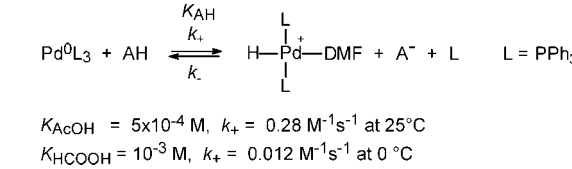

(Scheme 44). The structure of the cationic complex *trans*-$HPd^{II}(DMF)(PPh_3)_2^+$ has been established by ^1H and ^{31}P NMR spectroscopy (Scheme 44).[103] The very negative ^1H NMR shift confirms the hydride character for the H ligated to the Pd(II) center. The same cationic complex, *trans*-$HPd(DMF)(PPh_3)_2^+$, is formed in a reversible reaction, either from acetic acid or from formic acid (Scheme 44).[103]

The equilibrium constants have been determined using conductivity data (Figure 17a for AcOH, Scheme 44). The forward rate constants k_+ (Figure 17b, Scheme 44) have been determined using the conductivity data obtained when the reactions are made irreversible (e.g., the uppermost curve of Figure 17a for HOAc). A first-order reaction found for the carboxylic acids (k_{obs} = k_+[AH]) is indicative of a rate-determining oxidative addition of the carboxylic acid to $Pd^0(PPh_3)_2$, followed by a faster ionization of the intermediate neutral complex $HPdA(PPh_3)_2$.[103] This rules out a protonation of $Pd^0(PPh_3)_2$, which would have displayed a reaction order of 1/2 for CH_3CO_2H and HCO_2H.

2.6.4. Ionic Species Generated in Reversible Oxidative Addition of Allylic Carboxylates or Carbonates to Pd(0) Complexes

2.6.4.1. Allylic Carboxylates. Nucleophilic substitutions on allylic carboxylates are catalyzed by palladium complexes (Tsuji−Trost reaction) (Scheme 45).[104,105]

Scheme 45

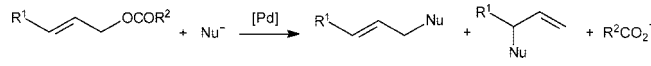

The catalytic cycle starts with a reaction of the allylic carboxylate with a low-ligated Pd^0L_2, which is supposed to proceed in two successive steps: a reversible complexation of the C=C bond of the allylic carboxylate to Pd^0L_2 to generate $Pd^0(\eta^2$-$R^1CH{=}CH$-CH_2-$OCOR^2)L_2$, followed by an oxidative addition step (also called ionization step), which delivers a cationic complex (η^3-R^1CH-CH-CH_2)$Pd^{II}L_2^+$ with the leaving group $R^2CO_2^-$ as the counteranion.[104,105] A few results from literature suggested that the oxidative addition step was reversible. Indeed, in the absence of nucleophile, isomerization of the C=C bond of allylic acetates had been observed and isomerization at the allylic position in substituted cyclic allylic acetates as well.[106] Before 1999, the cationic character of (η^3-allyl)PdL_2^+ complexes associated with a carboxylate counteranion had never been established. This problem has been clarified thanks to conductivity measurements performed on reactions of allylic carboxylates with different precursors {$Pd^0(dba)_2$ + 2 L or 1 L_2} (L = monophosphine PPh_3[107] or L_2 = bisphosphine dppb, dppf, or diop[108].[109–112]

As illustrated in Figure 18a, the conductivity κ of a solution of $Pd^0(dba)(PPh_3)_2$ (generated from $Pd^0(dba)_2$ and PPh_3 (2 equiv) in DMF increases with time after addition of excess $CH_2{=}CH$-CH_2-OAc, to reach a plateau (κ_{equil}) whose value increases upon successive additions of the allyl acetate.[109]

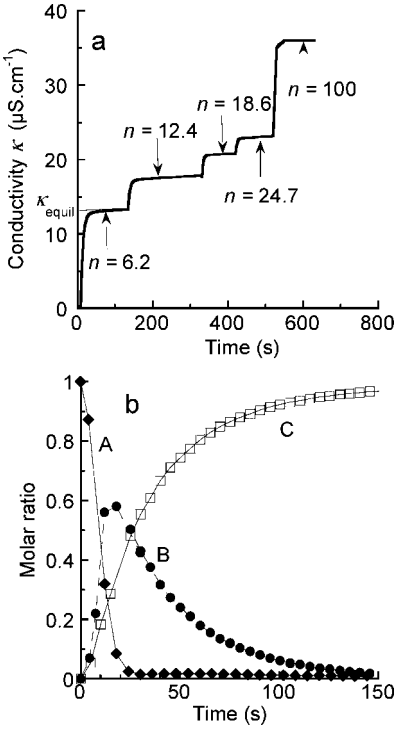

Figure 18. (a) Conductivity in DMF of (η^3-CH_2−CH-CH_2)$Pd(PPh_3)_2^+ \cdot AcO^-$ formed in the reaction of $Pd^0(PPh_3)_2$ (generated from $Pd^0(dba)_2$ (2 mM) + PPh_3 (4 mM)) with CH_2═CH-CH_2-OAc added successively at 20 °C (n = cumulative equivalents of CH_2═CH-CH_2-OAc) and (b) kinetics of the reaction of CH_2═CH-CH_2-OAc (10 mM) with Pd^0(dppb) formed from $Pd^0(dba)_2$ (2 mM) and dppb (2 mM) in DMF at 25 °C: (A, ◆) molar ratio of Pd^0(dba)(dppb) versus time as determined by UV spectroscopy at 425 mm; (B ●) molar ratio of the neutral intermediate complex Pd^0(η^2-CH_2═CH-CH_2-OAc)(dppb) versus time, as determined from curves A and C (B = 1 − (A + C)); (C, □) molar ratio of the ionic complex (η^3-CH_2-CH-CH_2)$Pd(dppb)^+ \cdot AcO^-$ versus time, as determined by conductivity measurements.

This establishes that ionic species are formed in equilibrium with the starting reagents. The conductivity κ_{equil} decreases upon addition of dba, attesting that dba is involved in the reverse reaction of the equilibrium (Scheme 46). No conductivity is observed in THF but the reaction takes place, leading to ion pairs [(η^3-CH_2-CH-CH_2)$Pd(PPh_3)_2^+ AcO^-$], as monitored by ^{31}P NMR spectroscopy.[109]

Scheme 46

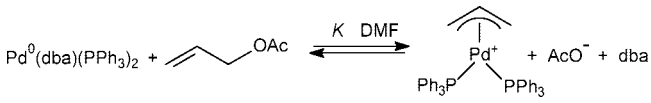

The complex (η^3-CH_2−CH-CH_2)$Pd(PPh_3)_2^+ \cdot AcO^-$ has been characterized in situ in DMF by a ^{31}P NMR singlet by comparison with an authentic sample, (η^3-CH_2−CH-CH_2)$Pd(PPh_3)_2^+ \cdot BF_4^-$. The reversibility of the equilibrium in Scheme 46 has been established independently by reacting (η^3-CH_2-CH-CH_2)$Pd(PPh_3)_2^+ \cdot BF_4^-$ with $n$$Bu_4$NOAc (1 equiv) in the presence of dba (2 equiv). $Pd^0(dba)(PPh_3)_2$ and CH_2═CH-CH_2-OAc formed in the backward reaction have been characterized by ^{31}P NMR and ^1H NMR, respectively.[109] The presence of both broad and thin signals on the same ^1H NMR spectrum indicates that different equilibria are operating at different equilibration rates. This suggests that the reaction proceeds in at least two steps via the literature-postulated intermediate Pd^0(η^2-CH_2═CH-CH_2-OAc)L_2, which however cannot be characterized when L = PPh_3 (Scheme 47). The equilibrium constant of the overall equilibrium, $K = K_{dba}K_1K_2$, has been determined (Scheme 47, L = PPh_3).[109]

Scheme 47

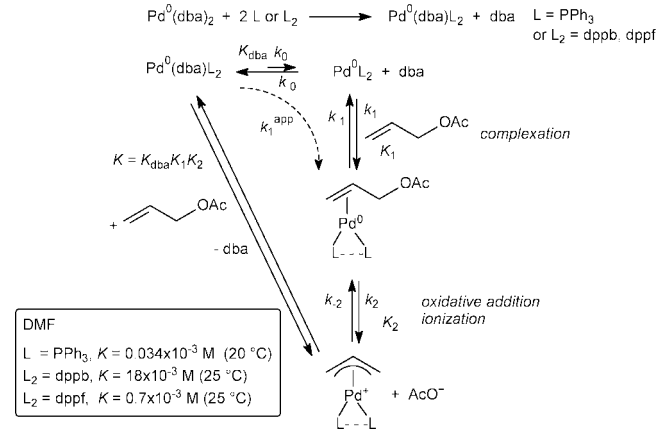

Clear-cut formation of a neutral intermediate Pd^0(η^2-CH_2═CH-CH_2-OAc)L_2 has been evidenced for bidentate ligands L_2 = dppb and dppf.[110] The reaction of CH_2═CH-CH_2-OAc with Pd^0(dppb) generated from $Pd^0(dba)_2$ and dppb (1 equiv) in DMF has been followed by conductivity measurements. Ionic species are formed in equilibrium with the starting reagents, whereas dba is involved in the backward reaction. The equilibrium constant K of the overall equilibrium has been determined using conductivity data (Scheme 47). The kinetics of formation of the ionic species (η^3-CH_2-CH-CH_2)$Pd(dppb)^+$ and AcO^-, generated in the reaction of CH_2═CH-CH_2-OAc (10 mM) and Pd^0(dba)(dppb) (2 mM) has been followed by conductivity measurements in DMF (curve C in Figure 18b), whereas the disappearance of Pd^0(dba)(dppb) was monitored by UV spectroscopy at 385 nm (curve A in Figure 18b). The rate of disappearance of Pd^0(dba)(dppb) is faster ($t_{1/2}$ = 8 s) than the rate of formation of the cationic complex (η^3-CH_2-CH-CH_2)$Pd(dppb)^+$ ($t_{1/2}$ = 25 s) whose kinetic curve C is S-shaped at short times (S-shaped curve being even more amplified for dppf).[110] Consequently, an intermediate neutral complex Pd^0(η^2-CH_2═CH-CH_2-OAc)(dppb) is first generated and gives the cationic complex (η^3-CH_2-CH-CH_2)$Pd(dppb)^+$ in a slower reaction (Scheme 47). The neutral complex Pd^0(η^2-CH_2═CH-CH_2-OAc)(dppb) whose evolution with time is deduced from the kinetic curves A and C (curve B in Figure 18b) cannot

Scheme 48

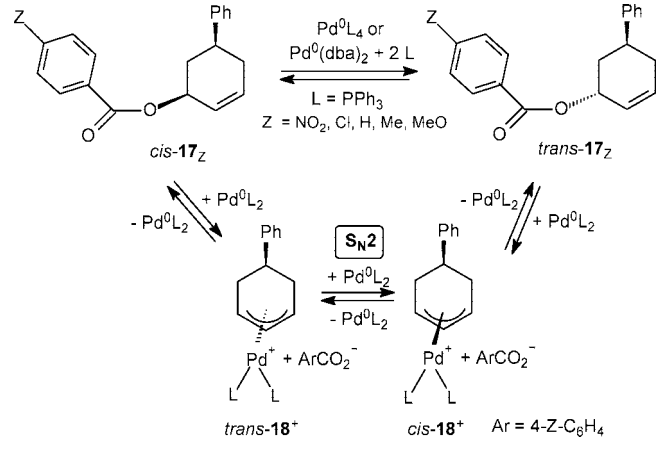

Scheme 49

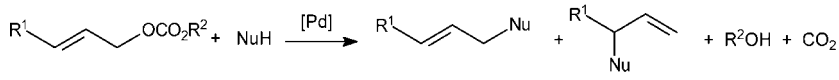

be characterized by usual spectroscopy due to its too short lifetime, but this is the first kinetic evidence of its formation.[110]

Therefore, the complexation and oxidative addition/ionization steps proceed successively with different time scales, depending on the allyl acetate concentration. The oxidative addition/ionization is slower (rds) than the overall complexation step from $Pd^0(dba)L_2$ under usual concentrations in catalytic reactions (DMF, 25 °C). Indeed, $k_1^{app}[CH_2{=}CH\text{-}CH_2\text{-}OAc] > k_2$ as soon as $[CH_2{=}CH\text{-}CH_2\text{-}OAc] > 1$ mM (L_2 = dppb) and > 3 mM (L_2 = dppf) (Scheme 47).[110]

The influence of leaving groups $R^2CO_2^-$ on the reaction of allylic carboxylates with Pd(0) complexes ligated by PPh_3, dppb, or dppf has been investigated via the determination of the equilibrium constants $K = K_{dba}K_1K_2$ and the rate constants of the complexation and ionization steps (when not too fast).[112] The ionization step is faster than the complexation step for good leaving groups (carbonate, trifluoroacetate), whereas the ionization step may be rate-determining for poor leaving groups (acetate, benzoates).[112]

The reversible reaction of *cis*-5-phenylcyclohex-2-enyl-4-Z-benzoate, *cis*-**17**$_Z$, with $Pd^0(PPh_3)_2$ generated from two precursors, $Pd^0(PPh_3)_4$ or $\{Pd^0(dba)_2 + 2\ PPh_3\}$, proceeds with isomerization at the allylic position to give *trans*-**17**$_Z$ (Scheme 48).[113] The rate of the isomerization *cis*-**17**$_Z$/*trans*-**17**$_Z$ depends on the Pd(0) precursors ($Pd^0(PPh_3)_4$ > $\{Pd^0(dba)_2 + 2\ PPh_3\}$) for a given Z, in agreement with a S_N2 mechanism induced by $Pd^0(PPh_3)_2$ for the isomerization of the cationic *trans*-**18**$^+$/*cis*-**18**$^+$ (Scheme 48). Indeed, $Pd^0(PPh_3)_4$ delivers a higher concentration of $Pd^0(PPh_3)_2$ than $\{Pd^0(dba)_2 + 2\ PPh_3\}$ in their respective equilibrium (see section 2.2.2). This is a kinetic confirmation for the S_N2 mechanism established by Bäckvall et al. for the isomerization of related cationic complexes.[114,115] For the same precursor, the rate of the isomerization *cis*-**17**$_Z$/*trans*-**17**$_Z$ is affected by the leaving group (decreasing rate, 4-NO_2-C_6H_4-CO_2^- > 4-Cl-C_6H_4-CO_2^- > C_6H_5-CO_2^- > 4-Me-C_6H_4-CO_2^- > 4-MeO-C_6H_4-CO_2^-). The equilibrium constants between *cis*-**17**$_Z$ and the cationic **18**$^+$ decrease in the same trend.[113] The better the leaving group, the higher the concentration of the cationic complex and the faster the isomerization of *cis*-**17**$_Z$ to *trans*-**17**$_Z$ is.

2.6.4.2. Allylic Carbonates. The palladium-catalyzed reaction of allylic carbonates can be performed from neutral pronucleophile NuH (Scheme 49) because the anion EtO-CO_2^-, formed in the reaction of the allylic carbonates with Pd(0) complexes, can deliver CO_2 and the basic EtO^- is able to deprotonate NuH.[116]

The reaction of $Pd^0(PPh_3)_2$, generated from $\{Pd^0(dba)_2 + 2PPh_3\}$, with the cyclic allylic carbonate *cis*-**19** (Scheme 50) has been followed by conductivity measurements in DMF at 20 °C (Figure 19a).[117] The conductivity κ increases with time to reach a limiting value, which increases when the allylic carbonate concentration is increased and decreases after addition of dba (Figure 19a). From these experiments, it is established that ionic species are formed in equilibrium with the allylic carbonate and the Pd(0) complex whereas dba is involved in the backward reaction. The protons of the anion $EtOCO_2^-$ have been characterized by ^1H NMR spectroscopy. They remain unchanged after 1 h, which is

Scheme 50

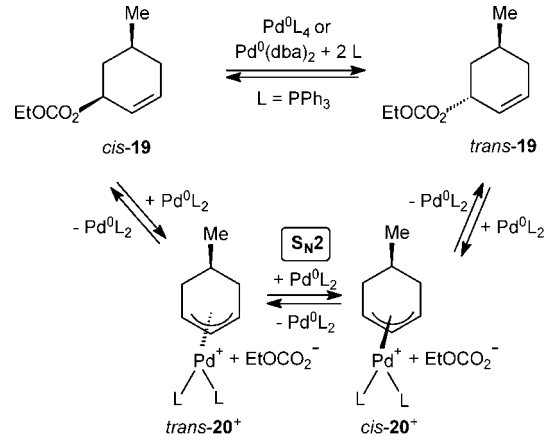

indicative of an unexpected relative stability of the ethyl carbonate anion in relation to its decarboxylation.[117] Consequently, the cyclic allylic carbonate *cis*-**19** reacts with the Pd(0) complex through an overall reversible reaction with formation of cationic complex **20**$^+$ with $EtOCO_2^-$ as the counteranion (Scheme 50).

Isomerization of *cis*-**19** to *trans*-**19** takes place. Its rate is affected by the Pd(0) precursors ($Pd^0(PPh_3)_4$ > $\{Pd^0(dba)_2$

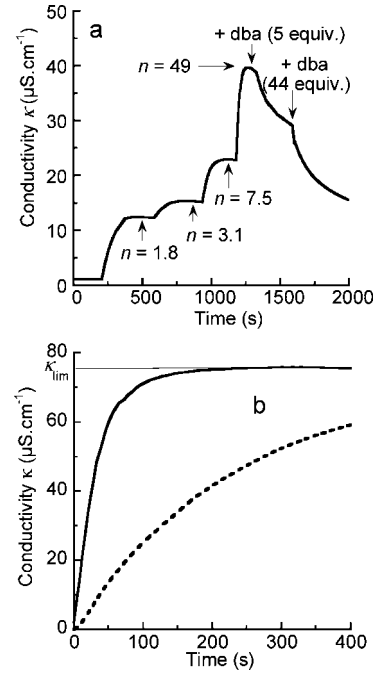

Figure 19. (a) Conductivity of the cationic complex (η^3-allyl)$Pd(PPh_3)_2^+ \cdot EtOCO_2^-$, **20**$^+$, generated in the reaction of $Pd^0(PPh_3)_2$ formed from $Pd^0(dba)_2$ (2 mM) and PPh_3 (4 mM), with the cyclic allylic carbonate *cis*-**19**, added successively ($0 < t < 1250$ s) (n = cumulative equivalents), followed by successive additions of dba, in DMF at 20 °C and (b) Kinetics of (—) the reaction of $CH_2{=}CH\text{-}SnBu_3$ (20 mM) with $PhPdI(AsPh_3)_2$ (2 mM) in DMF at 25 °C, followed by conductivity measurements of I^- and Bu_3Sn^+ formed together with $PhCH{=}CH_2$ as a coproduct, $\kappa = \kappa_{exp} - \kappa_0$ (κ_{exp} = experimental conductivity at t; κ_0 = initial residual conductivity of 3 μS cm^{-1}) and κ_{lim} = conductivity of an authentic sample of $ISnBu_3$ (2 mM) in DMF; (– – –) same kinetics but in the presence of $AsPh_3$ (5 equiv).

+ 2PPh$_3$}) and thus proceeds via the isomerization of the cationic complexes *trans*-**20**$^+$ to *cis*-**20**$^+$ by a S_N2 mechanism induced by $Pd^0(PPh_3)_2$, followed by the nucleophilic attack of the ethyl carbonate ion (Scheme 50).[117] Consequently, the loss of stereospecificity in nucleophilic substitutions on the cyclic allylic carbonate *cis*-**19**, reported by Moreno-Mañas et al.,[118] is due to the isomerization of the cationic complexes **20**$^+$.

Thanks to conductivity measurements, it is now well established that the reaction of allylic carboxylates or carbonates with Pd^0L_2 complexes (L = monophosphine or L_2 = bisphosphine) is a reversible reaction that gives cationic complexes (η^3-allyl)PdL_2^+ with carboxylates or carbonates as the counteranions via the ionization of intermediate neutral complexes Pd^0(η^2-allylic carboxylate)L_2, which may be rate-determining. Consequently, the carboxylate or carbonate anions are not "innocent" leaving groups since they can react in competition with nucleophiles with the cationic complexes (η^3-allyl)PdL_2^+ to give back the allylic carboxylates or carbonates and a Pd(0) complex. Moreover, the reaction proceeds by isomerization at the allylic position in cyclic allylic carboxylates or carbonates via a S_N2 mechanism induced by Pd^0L_2 complexes. A change of the Pd(0) precursor may thus affect the stereospecificity of catalytic nucleophilic allylic substitutions.

The results reported above show that conductivity measurements can be efficiently used to characterize ionic organometallic complexes formed in elemental steps of catalytic reactions, to determine the rate or equilibrium constant or both for their formation and consequently to get deeper insights into the mechanism of palladium-catalyzed reactions[119] (for an unusual use of conductivity measurements to investigate the mechanism of a Pd-catalyzed Stille reaction, see section 2.7.3).[92]

2.7. Mechanism of Palladium-Catalyzed Reactions: Catalytic Cycles

The mechanisms of palladium-catalyzed reactions are presented herein. In all catalytic cycles, one or several steps (as indicated by bold characters) have been characterized by electrochemical techniques, as illustrated above. The mechanism of the first step of most catalytic cycles, that is, the oxidative addition of aryl halides to Pd(0) complexes, has been fully investigated by electrochemical techniques. The mechanism of some further steps has been established using electrochemical techniques or classical techniques such as ^{1}H or ^{31}P NMR spectroscopy or both.

2.7.1. Palladium-Catalyzed Heck Reactions

The Pd-catalyzed Heck reaction is one of the most efficient routes for the vinylation of aryl halides or triflates.[10,12,13,15,82,120–123] Its mechanism strongly depends on the precursors of the active Pd(0) complex, the ligands, the bases, and temperature.

2.7.1.1. Precursor $Pd(OAc)_2$ Associated with a Monophosphine Ligand, L = PPh_3. The mechanism of Heck reactions using the precursor $Pd(OAc)_2$ associated with PPh_3 (Scheme 51) is displayed in Scheme 52.

Scheme 51

Heck reaction

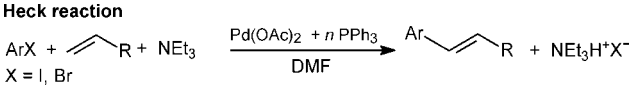

Electrochemical techniques have been used as follows:[3,62,76,77,81,93]
(i) To determine the mechanism of formation in situ of the anionic $Pd^0(PPh_3)_2(OAc)^-$ from the precursor {$Pd(OAc)_2$ + 3PPh$_3$} and to characterize its reactivity in oxidative addition to PhI by the determination of the rate constant k^{oa} (see section 2.4.1.1 and Table 3).
(ii) To characterize the complex *trans*-PhPd(OAc)$(PPh_3)_2$ formed in the oxidative addition and to get evidence of its equilibrium with the cationic complex *trans*-PhPd(DMF)-$(PPh_3)_2^+$ with the determination of the equilibrium constant K_{OAc} (see sections 2.4.1.1 and 2.5.2).
(iii) To compare the reactivity of *trans*-PhPdX$(PPh_3)_2$ (X = I, OAc, BF_4) with styrene by monitoring the kinetics of formation of (*E*)-stilbene by cyclic voltammetry (increase of the reduction peak current of (*E*)-stilbene with time). The following reactivity order is observed in DMF at 25 °C:[81] *trans*-PhPd(OAc)L_2 > *trans*-PhPd(DMF)L_2^+ ≫ *trans*-PhPdIL_2 (L = PPh_3). In contrast to *trans*-PhPdIL_2, which does not react with styrene at 25 °C unless AcO^- is added (i.e., with formation of *trans*-PhPd(OAc)L_2, see $K_{I/OAc}$ in Scheme 53),[81] *trans*-PhPd(OAc)L_2 reacts with styrene because the bidentate character of the ligand OAc assists an easier dissociation of PPh_3 than in *trans*-PhPdIL_2. The formation of (*E*)-stilbene is indeed inhibited by excess L = PPh_3, which is indicative of a prior dissociation of one ligand L to allow alkene coordination (Scheme 53A). The cationic complex *trans*-PhPd(DMF)L_2^+ is less reactive than *trans*-PhPd(OAc)L_2 because its trans geometry imposes a trans coordination of the alkene relative to the Ph ligand. An endergonic trans/cis isomerization is thus required before the alkene insertion (Scheme 53B). The determination of the apparent rate constant of the carbopalladation, k^{cb}, establishes that the carbopalladation is rate-determining for identical concentration of PhI and styrene (Scheme 52).
(iv) To evidence the unexpected multiple role of the base (NEt_3): a decelerating effect on the rate of the oxidative addition by stabilization of the anionic $Pd^0L_2(OAc)^-$ vis a vis its decomposition to the more reactive bent complex Pd^0L_2 by protons (see section 2.4.1.1 and Table 3) and an accelerating effect on the rate of the carbopalladation step by increasing the concentration of the more reactive *trans*-PhPd(OAc)L_2 via the quenching of protons which could favor its dissociation to the less reactive *trans*-PhPd(DMF)L_2^+ (Scheme 52).[62,81]
(v)To evidence a second unexpected role of alkenes, CH_2=CHR, a decelerating effect on the rate of the oxidative addition by formation of nonreactive Pd^0(η^2-CH_2=CHR)$L_2(OAc)^-$ (for determination of $K_{C=C}$, see section 2.4.1.1).

Therefore, electrochemical techniques have been successfully used (i) to rationalize the beneficial role of acetate ions delivered by the precursor $Pd(OAc)_2$, which are ligands of all Pd(0) and Pd(II) complexes involved in the catalytic cycle, and (ii) to reveal the unexpected common dual effect of the base and the alkene, which both decelerate the fast oxidative addition performed from PhI and accelerate the rate-determining carbopalladation performed from styrene, making the rate of these two steps closer to each other and the catalytic reaction more efficient.

2.7.1.2. Precursor $Pd(OAc)_2$ Associated with a Bisphosphine Ligand, dppp. The mechanism of Heck reactions using the precursor $Pd(OAc)_2$ associated with the bidentate ligand dppp (Scheme 54) is displayed in Scheme 55.

Electrochemical techniques have been used as follows:[83]

Scheme 52

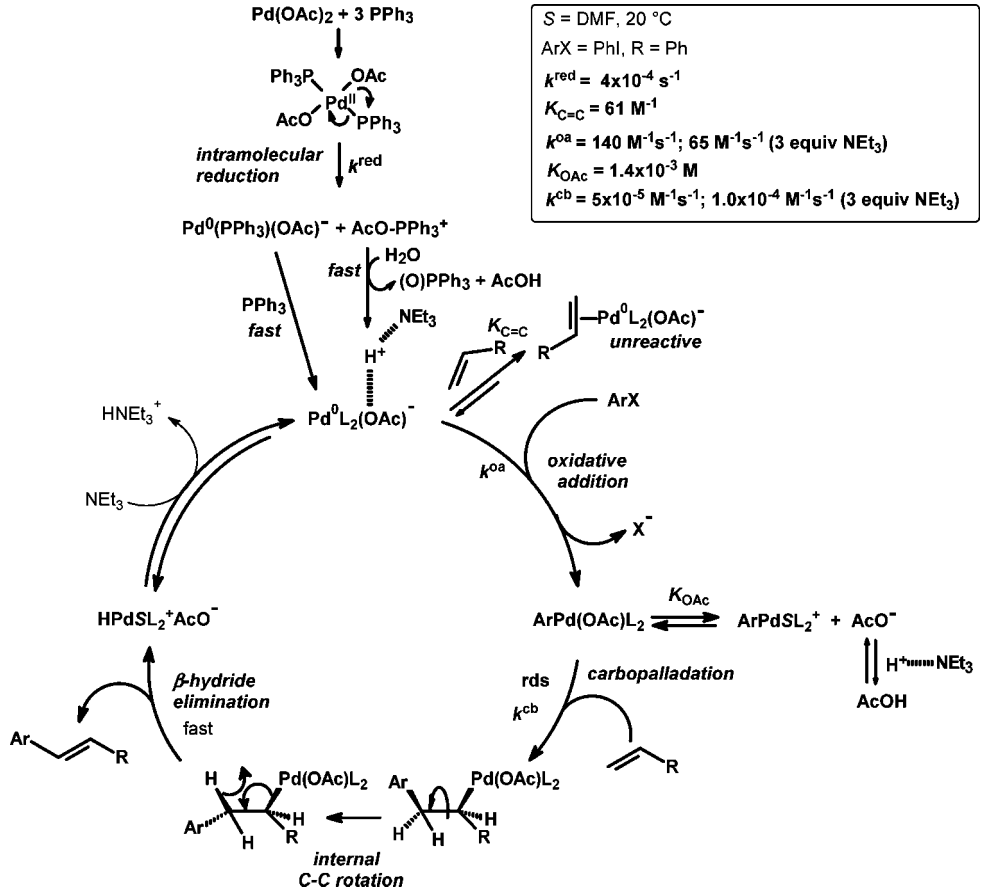

Scheme 53

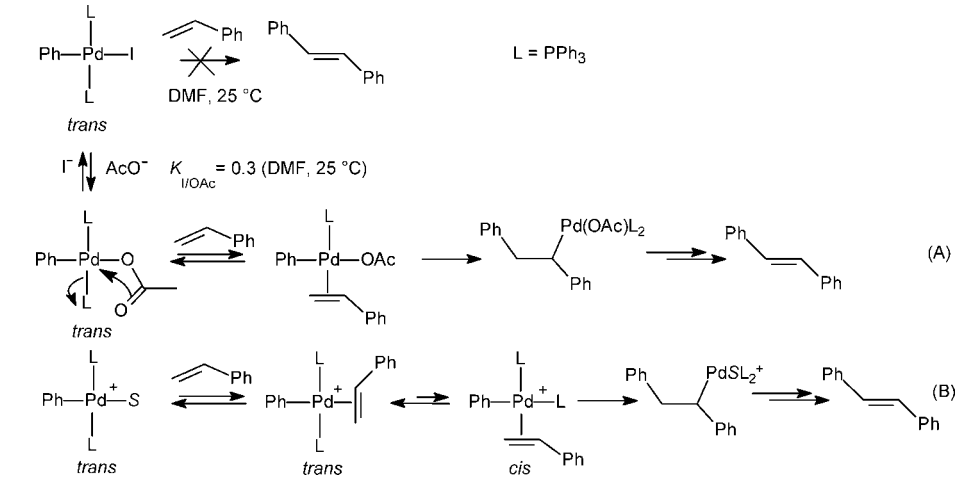

Scheme 54

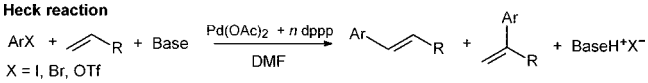

(i) To establish the mechanism of formation in situ of the anionic $Pd^0(dppp)(OAc)^-$ from the precursor {$Pd(OAc)_2$ + 2dppp} (see section 2.4.1.2) and to characterize its reactivity in oxidative addition to PhI.

(ii) To characterize the cationic complex $PhPd(dppp)(dppp(O))^+$ formed in the oxidative addition in which the hemioxide dppp(O) behaves as a monodentate ligand (Scheme 55). Such complex is quite unreactive with usual alkenes.[124,125] However, PhPdI(dppp) and PhPd(OAc)(dppp) are formed, respectively, upon addition of a large amount of I^- or AcO^-, which are present in catalytic Heck reactions performed from aryl iodides and when acetate salts are used as base (Scheme 55).[83]

(iii) To characterize the cationic complex $PhPd(DMF)(dppp)^+$ present at very low thermodynamic concentration in its equilibrium with PhPdI(dppp) or PhPd(OAc)(dppp) by cyclic voltammetry.[124] Such cationic complex $PhPd(DMF)(dppp)^+$ plays a crucial role in Heck reactions, as the reactive species with alkenes. The kinetics of the reaction of PhPdX(dppp) (X = I, OAc) with alkenes CH_2=CHR (R = Ph, O*i*Bu, CO_2Et) has been monitored by ^{31}P NMR spectroscopy by Amatore, Jutand, et al. The reaction exclusively proceeds from the cationic complex $PhPd(DMF)(dppp)^+$ (X = I, R = Ph, O*i*Bu; X = OAc,

Scheme 55

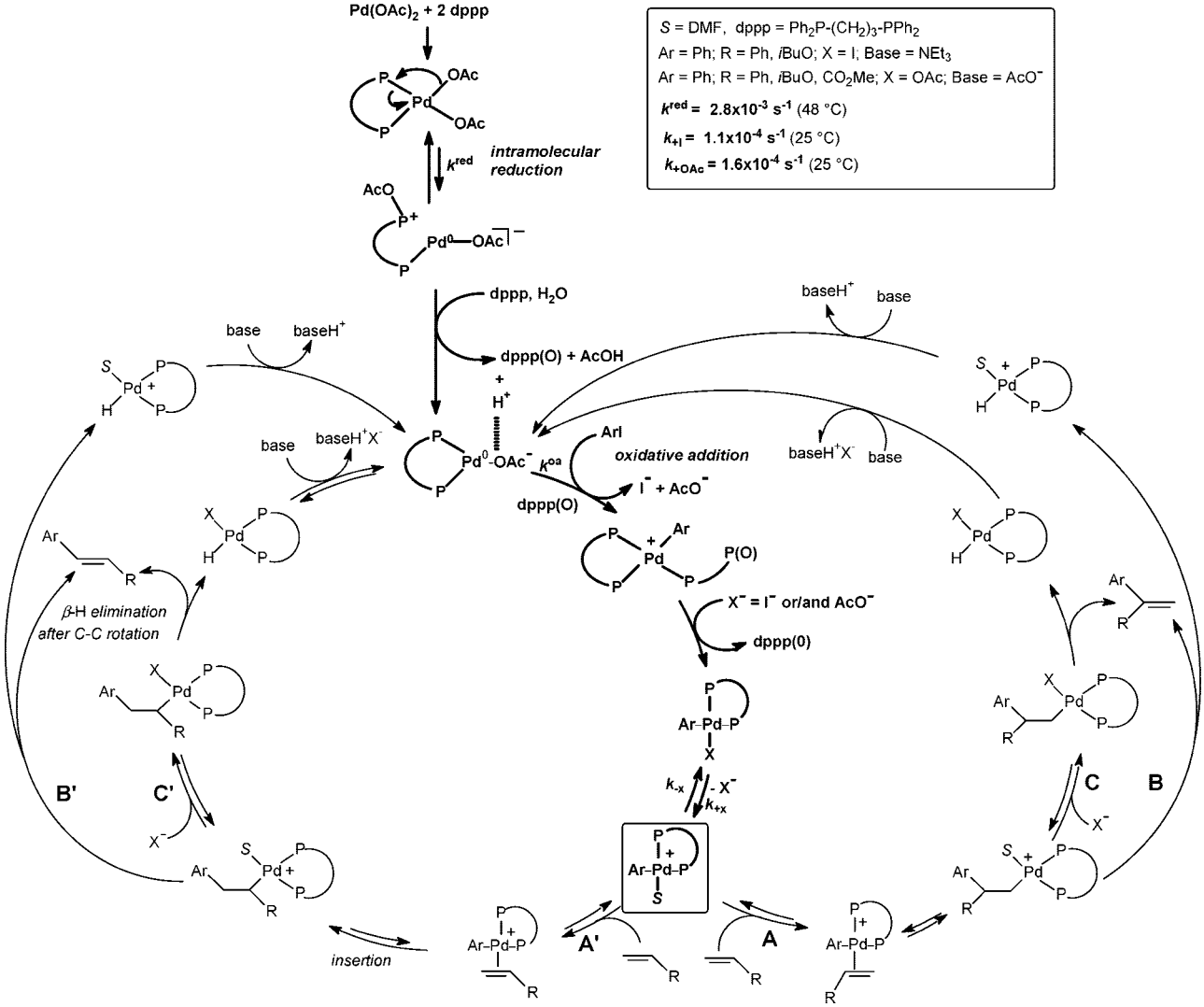

R = Ph, O*i*Bu, CO_2Et),[124,125] in contradiction with postulated mechanisms involving the reaction of PhPd(DMF)(dppp)$^+$ or PhPdI(dppp).[82] Only the reaction of PdPhI(dppp) with CH_2═$CHCO_2Et$ involves both neutral and cationic complexes reacting in parallel.[124] The regioselectivity of the reaction, that is, formation of the branched or linear alkenes, is now rationalized by a new mechanism depicted in Scheme 55.[125] The anions I^- or AcO^- can react with the cationic complexes alkyl-Pd*S*(dppp)$^+$ formed in the reversible insertion of the alkene into the Ph−Pd bond of the cationic complex PhPd*S*-(dppp)$^+$. At low concentration of X^- (e.g., in the presence of a halide scavenger such as Ag^+) or at high ionic strength[126] (which disfavored the reaction of X^- with the cationic complexes alkyl-Pd*S*(dppp)$^+$), the reaction gives the branched product from the cationic ArCH(R)-CH_2−Pd*S*(dppp)$^+$ (path A + B) because the formation of ArCH(R)-CH_2−Pd*S*(dppp)$^+$ in path A is favored (complexation of the alkene to ArPd*S*(dppp)$^+$ sterically favored, as generally accepted).[82] At high X^- concentrations or at low ionic strength, the cationic complexes ArCH(R)-CH_2-Pd*S*(dppp)$^+$ or ArCH_2-CH(R)-PdX(dppp)$^+$ can be quenched as the neutral ArCH(R)-CH_2-Pd-X(dppp) (path A + C) or ArCH_2-CH(R)-PdX(dppp) (path A′ + C′), respectively. Since all steps are equilibrium, the path A + C (which might have delivered the branched product) can be shifted toward the path A′ + C′, which delivers the linear product. The driving force would be the formation of ArCH_2-CH(R)-PdX(dppp), which is more stable than ArCH(R)-CH_2-Pd-X(dppp) (C−Pd bond more stable for the more substituted carbon). Such a new mechanism rationalizes the effect of halides (released from ArX) and ionic strength on the regioselectivity of the reaction.[126]

2.7.2. Palladium-Catalyzed Cross-Coupling of Aryl Halides with Nonstabilized Nucleophiles

The mechanism of Pd-catalyzed cross-coupling reactions of aryl halides with nonstabilized nucleophiles—organolithium,[17] Grignard,[17] and organozinc reagents[18](Schemes 6 and 56)[10,63]—is displayed in Scheme 57.

Scheme 56

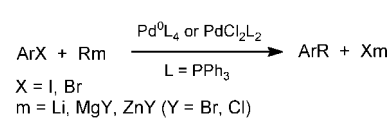

Electrochemical techniques have been used by Amatore, Jutand et al.:[3,57–59,62]

(i) To generate the anionic $Pd^0(PPh_3)_2Cl^-$ from the precursor $PdCl_2(PPh_3)_2$ and to characterize its reactivity in oxidative addition to PhI by the determination of the rate constant k^{oa}

Scheme 57

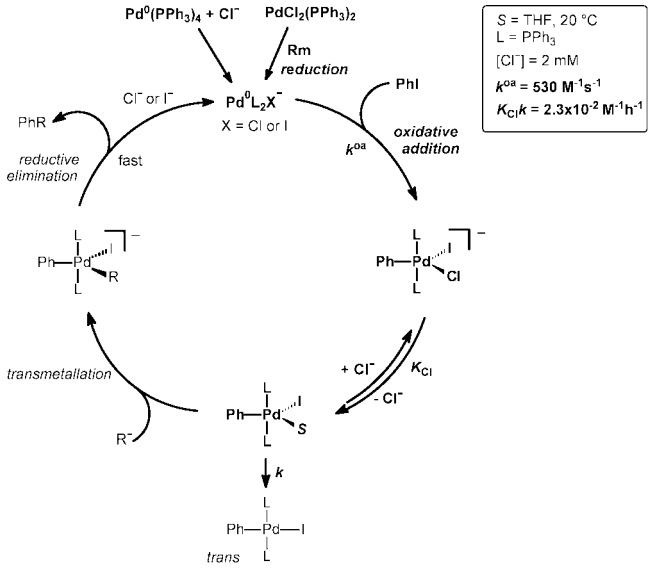

(see section 2.3.2 and Table 3). This electrochemical reduction mimics the chemical reduction by the nucleophile Rm in solvents where ion pairs [Cl^-m^+] are not formed.

(ii) To characterize the influence of cations Li^+ or Zn^{2+} on the rate of the oxidative addition (Table 3). Those cations may be delivered in the chemical reduction of $PdCl_2(PPh_3)_2$ by the nucleophile Rm. In THF, where ion pairs may be formed, the presence of cations make the oxidative addition faster by interaction with the anionic $Pd^0(PPh_3)_2Cl^-$, which generates a more reactive bent $Pd^0(PPh_3)_2$ (Schemes 27 and 28).

(iii) To detect the anionic intermediate [$PhPdI(Cl)(PPh_3)_2^-$] first formed in the oxidative addition (Figure 6b and Scheme 57) on the way to *trans*-$PhPdI(PPh_3)_2$, via an equilibrium involving chloride ions and the neutral complex $PhPdIS(PPh_3)_2$ (see $K_{Cl}k$ in Scheme 57).[58] Such a neutral complex $PhPdIS(PPh_3)_2$ is supposed to react with the nucleophile R^- to generate a transient anionic complex [$PhPdIR(PPh_3)_2^-$] in which the two ligands Ph and R sit in an adjacent position required for the reductive elimination (Scheme 57).[58]

In nonpolar solvents, anionic $Pd^0L_2Cl^-$ complexes are probably not formed due to ion pairing between Cl^- and the cations delivered by the nucleophile. Consequently the formation of anionic complexes [$PhPdI(Cl)L_2^-$] must be also bypassed.[62] *trans*-$PhPdIL_2$ is thus formed and reacts with the nucleophile.[17] The cross-coupling product is however delivered in a slower reaction due to nonfavored isomerization of *trans*-$PhPdNuL_2$ to *cis*-$PhPdNuL_2$ before the reductive elimination step, which delivers PhNu.[17,62]

2.7.3. Palladium-Catalyzed Stille Reactions

As reported by Farina et al.[91] the Stille reaction[127,128] is much more efficient when $AsPh_3$ is used rather than PPh_3 associated with $Pd^0(dba)_2$ in THF (Scheme 58). According

Scheme 58

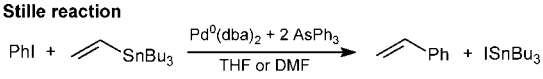

to Farina, the higher efficiency of $AsPh_3$ comes from an easier dissociation of $AsPh_3$ from $PhPdI(AsPh_3)_2$, which allows coordination of the vinyl stannane via its C=C bond.[91,127]

Scheme 59

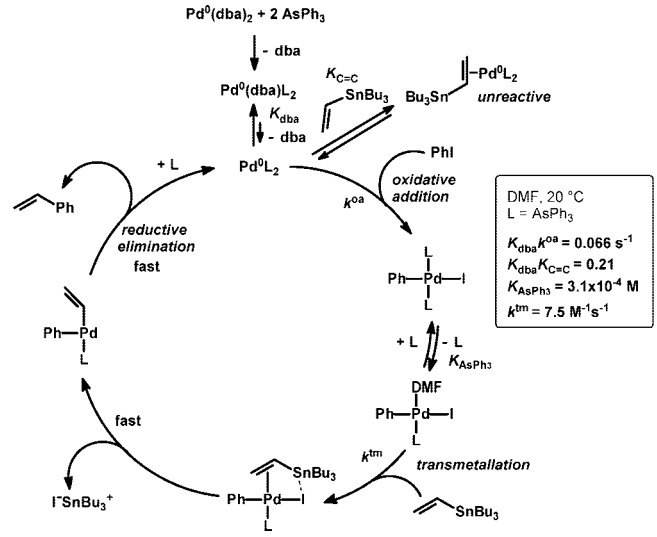

The mechanism of this Stille reaction has been established by Amatore, Jutand, et al. in DMF (Scheme 59). >Electrochemical techniques have been used for the following:[43,92]

(i) To investigate the mechanism of the oxidative addition of PhI: characterization of $Pd^0(AsPh_3)_2$ generated as the minor but reactive complex from the major but nonreactive $Pd^0(dba)(AsPh_3)_2$, formed by reacting $Pd^0(dba)_2$ and $AsPh_3$ (2 equiv.) with the determination of $K_{dba}k^{oa}$ (see section 2.2.2 and Scheme 59); characterization of the nonreactive $Pd^0(\eta^2\text{-}CH_2{=}CH\text{-}SnBu_3)(AsPh_3)$ generated in the presence of $CH_2{=}CH\text{-}SnBu_3$ with the determination of $K_{dba}K_{C=C}$ (see section 2.2.3 and Scheme 59).[43]

(ii) To characterize the complex $PhPdI(DMF)(AsPh_3)$ formed by endergonic dissociation of $AsPh_3$ from $PhPdI(AsPh_3)_2$ with the determination of the equilibrium constant K_{AsPh3} (see section 2.5.1).

(iii) To discriminate between an associative[129] or dissociative[91] mechanism for the reaction of $CH_2{=}CH\text{-}SnBu_3$ with $PhPdI(AsPh_3)_2$ in the rate-determining transmetalation (Scheme 59). Taking the opportunity that $ISnBu_3$, which is formed at the same rate as the coupling product $PhCH{=}CH_2$, is fully dissociated into the free ions I^- and Bu_3Sn^+ in DMF, the kinetics of formation of the ionic species I^- and Bu_3Sn^+, that is, the kinetics of the transmetalation has been investigated by conductivity measurements (Figure 19b).[92] From the retarding effect of $AsPh_3$ (added in low excess) on the rate of the transmetalation (Figure 19b), it is definitively established that the transmetalation proceeds by reaction of $CH_2{=}CH\text{-}SnBu_3$ with $PhPdI(DMF)(AsPh_3)$ generated by dissociation of $AsPh_3$ from $PhPdI(AsPh_3)_2$ (Scheme 59). The rate constant of the transmetalation step, k^{tm}, has been determined, as well as K_{AsPh3}[92] whose value is similar to that found independently by means of single potential step chronoamperometry at a steady electrode (see section 2.5.1).[43]

The catalytic reaction involving $AsPh_3$ is indeed more efficient than that involving PPh_3 because the dissociation of PPh_3 from $PhPdIL_2$ is less favored, as confirmed by a slower transmetalation step from $PhPdI(PPh_3)_2$ evidenced by conductivity measurements.[92] The dissociative mechanism in DMF was recently supported by DFT calculations by Alvarez, de Lera, et al.[130] and Espinet et al.[131]

Moreover, the common decelerating effect of dba and $CH_2{=}CH\text{-}SnBu_3$ on the rate of the oxidative addition of PhI (see section 2.2.3)[43] favors the efficiency of the catalytic

reaction by making the rate of the fast oxidative addition of PhI closer to the rate of the slower transmetalation by CH_2=CH-$SnBu_3$.[51]

This illustrates how conductivity measurements can be used to investigate the kinetics of formation of an ionic coproduct (e.g., I^-, Bu_3Sn^+) and to get deeper insight into the mechanism of a catalytic reaction that does not involve any ionic palladium complexes.[119]

2.7.4. Palladium-Catalyzed Copper-Free Sonogashira Reactions

In contrast to Stille reactions, which are more efficient when $AsPh_3$ is used as ligand instead of PPh_3, Jutand et al. have reported that the cross-coupling of a terminal alkyne with PhI in the presence of a base also serving as solvent is more efficient with PPh_3 as ligand (see table in Scheme 60).[132] Such Pd-catalyzed reactions, independently discovered by Cassar[14] and Heck[15] (Scheme 4), have been supplanted by the so-called Sonogashira reaction,[16] which involves a Cu(I) salt as cocatalyst (Scheme 5). The Cu-free reaction is very sensitive to the base, usually an amine used also as solvent, as pioneered by Linstrumelle et al.[133] ($Pd^0(PPh_3)_4$ as precursor) and also observed by Jutand et al. (Scheme 60).[132]

Scheme 60

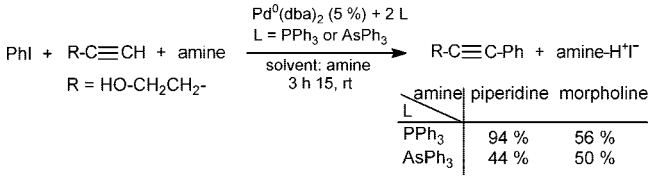

The mechanism of the reaction of Scheme 60 is displayed in Scheme 61.[132] Electrochemical techniques have been used for the following:

(i)To investigate the mechanism of the very first steps of the catalytic cycle, that is, to characterize Pd^0L_2 generated as the minor but reactive complex in oxidative addition to PhI, from the major but nonreactive $Pd^0(dba)L_2$ (L = PPh_3 or $AsPh_3$) or Pd^0L_3 (L = PPh_3) with the determination of $K_L k^{oa}$ and $K_{dba}k^{oa}$ (see sections 2.2.1 and 2.2.2 and Scheme 61). As far as PPh_3 is concerned, one concludes that the oxidative addition is not the rate-determining step of the catalytic reaction since the oxidative addition follows the reactivity order $Pd^0(PPh_3)_4$ > {$Pd^0(dba)_2$ + 2 PPh_3} whereas a reverse order is found for the catalytic reaction.[132,133]

(ii)To highlight the multiple roles of amines used as base and solvent, which moreover accelerates the oxidative addition of PhI by formation of Pd^0L(amine) (L = PPh_3, amine = piperidine, morpholine) with the determination of $k'^{oa}K_L K_{amine}$ (Scheme 61).[132]

The further steps of the catalytic cycle have been investigated by ^1H and ^{31}P NMR spectroscopy. A second unexpected effect of the amine has been discovered by Jutand et al.: the reversible substitution of one ligand L by the amine in $PhPdIL_2$ formed in the oxidative addition (X-ray structure for PhPdI(morpholine)($AsPh_3$)).[132] The substitution of $AsPh_3$ is more favored than that of PPh_3 (see $K_{L/amine}$ in Scheme 61).[132,134]

Two mechanisms are proposed for the Pd-catalyzed Cu-free Sonogashira reactions, performed from PhI and HO-CH_2CH_2-C≡CH (Scheme 61), depending on the amine and ligand: path A when the alkyne is a better ligand than the amine for the Pd(II) center in $PhPdIL_2$ (L = PPh_3, amine = piperidine or morpholine) or path B when the amine is a better ligand than the alkyne for the Pd(II) center in $PhPdIL_2$ (L = $AsPh_3$, amine = piperidine). This explains why the catalytic reaction in Scheme 60 is more efficient when using PPh_3 rather than $AsPh_3$, when piperidine is the solvent and the base (path A more efficient than path B).

Consequently, the amine does not react as a simple base in Cu-free Sonogashira reactions, but is also involved as ligand for Pd(0) and aryl-Pd(II) complexes.[132,134]

2.7.5. Palladium-Catalyzed Homocoupling of Arylboronic Acids

The Pd-catalyzed homocoupling of arylboronic acids (Scheme 62)[135,136] can be a side-reaction in Miyaura−Suzuki reactions when they are accidentally performed in air (Scheme 8).[137]

Electrochemical techniques have been used by Amatore, Jutand, et al. to investigate the rate and mechanism of the two first steps of the homocoupling reaction of Scheme 62.[138] Taking the opportunity that the peroxo complex (μ^2-O_2)$Pd(PPh_3)_2$ (formed by reaction of O_2 with $Pd^0(PPh_3)_2$) exhibits an oxidation peak, the kinetics of its reaction with $ArB(OH)_2$ has been followed by recording the decay with times of its oxidation plateau current at a rotating disk electrode. A second-order reaction found for $ArB(OH)_2$ characterizes the reversible formation of an intermediate complex that involves an interaction of one oxygen of $O_2Pd(PPh_3)_2$ with the boron atom of $ArB(OH)_2$ (Figure 20 and Scheme 63).[138] Such intermediate complexes have been characterized by ^{31}P NMR and supported by DFT calculations (Figure 20).[138] The reaction of a second molecule of

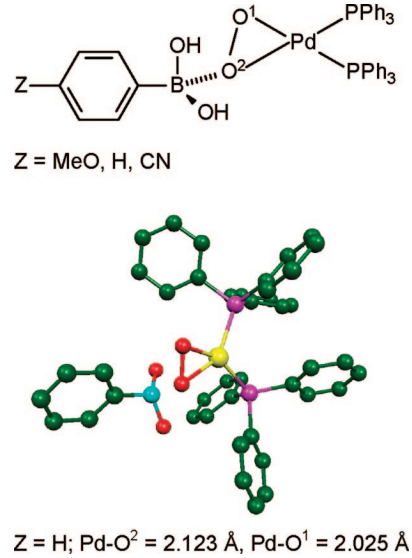

Figure 20. Optimized DFT structure (Z = H).

$ArB(OH)_2$ with the intermediate complex shifts the equilibrium toward the formation of the final complex *trans*-$ArPd(OH)(PPh_3)_2$ (Scheme 63).

The mechanism of the further step, a transmetalation on *trans*-$ArPd(OH)(PPh_3)_2$ by $ArB(OH)_2$, has been established by ^{31}P and ^1H NMR spectroscopy with formation of rather stable *trans*-$ArPdAr(PPh_3)_2$ when one aryl group is substituted by an EWG (path A in Scheme 63). All complexes observed at long times have a trans geometry.[138] Consequently, path B occurring at shorter times and involving only cis complexes cannot be excluded (Scheme 63).

Scheme 61

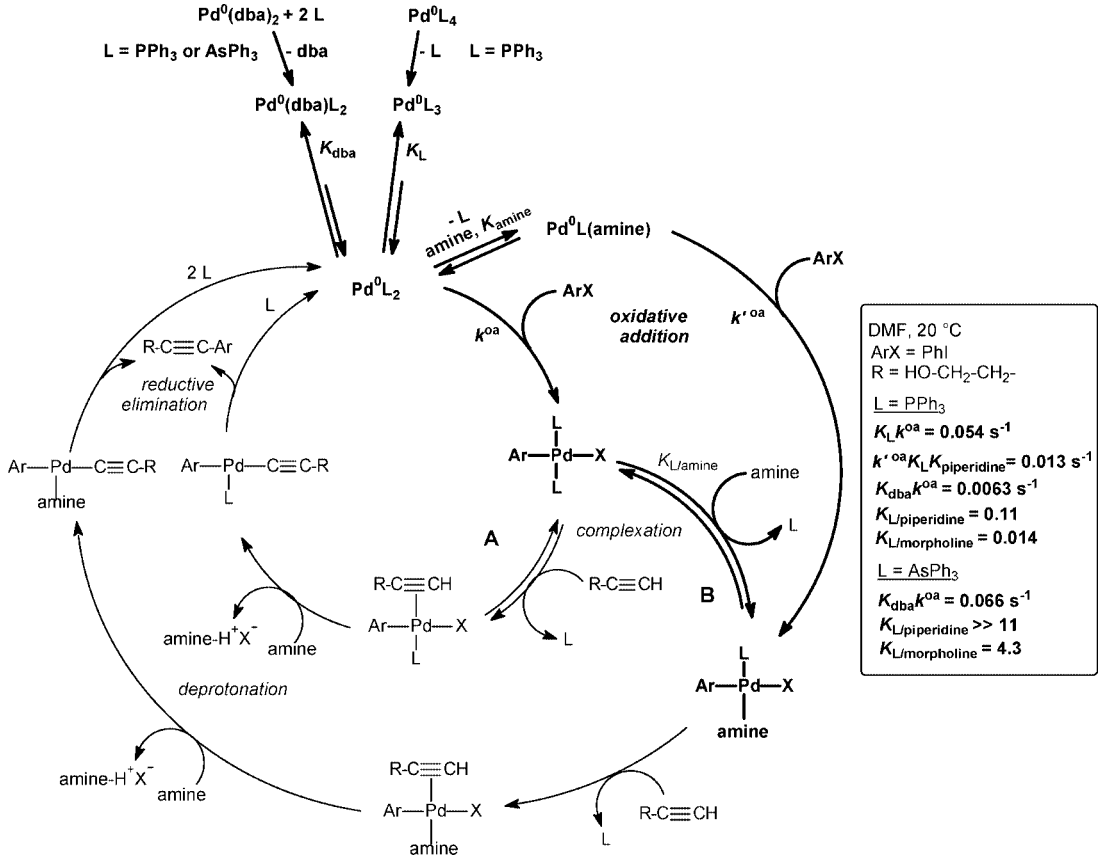

Scheme 62

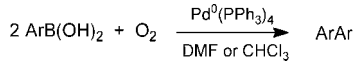

2.7.6. Palladium-Catalyzed C−S Cross-Coupling Reactions

The Pd-catalyzed cross-coupling of PhI and a thiol (RSH) derived from a cysteine has been optimized by Moreau and Campagne (Scheme 64).[139,140]

Scheme 63

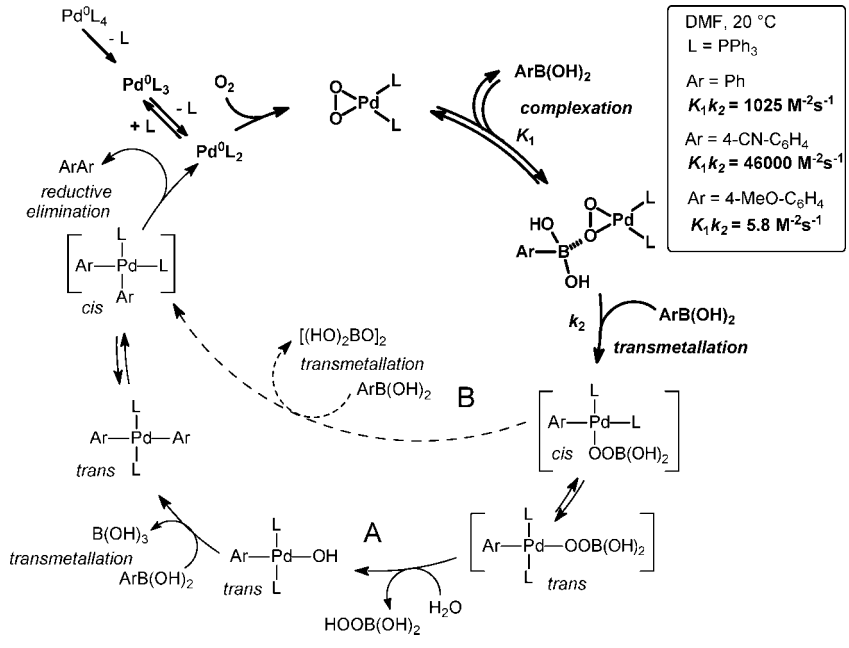

Scheme 64

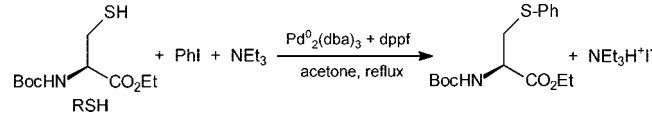

The mechanism of the reaction has been established by Jutand, Campagne, et al. (Scheme 65).[141] The mechanism of each step of the catalytic cycle has been investigated separately, one step after the other, but in the context of the

Scheme 65

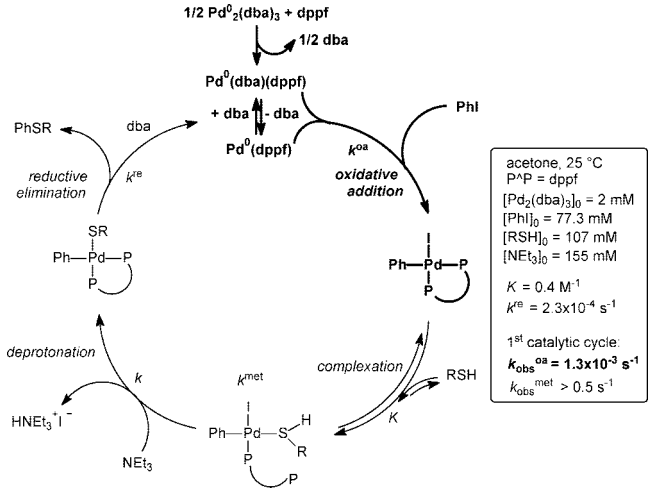

real catalytic reaction—same Pd(0) precursor ($Pd_2(dba)_3$), same ligand (dppf), same reagents, same base (NEt_3), and same solvent (acetone), using the initial concentrations of each components to determine the rate-determining step. The reactions have been performed at 25 °C.

Electrochemical techniques have been used to investigate the mechanism of the very first steps of the catalytic cycle, that is, to characterize the species Pd^0(dppf) and Pd^0(dba)(dppf) generated in acetone from $Pd^0{}_2(dba)_3$ and dppf (dppf/Pd = 1), which both react in parallel with PhI. The observed overall rate constant k_{obs}^{oa} (s^{-1}) has been determined in acetone for the initial concentrations of PhI and $Pd^0{}_2(dba)_3$ used in the catalytic reaction (Scheme 65).[141]

The mechanism of the further steps of the catalytic cycle has been investigated by ^1H and ^{31}P NMR spectroscopy. An alternative mechanism is proposed to the classical transmetalation of PhPdI(dppf) by RS^-. The thiol RSH is reversibly ligated to the Pd(II) center in PhPdI(dppf) after decoordination of one P of the ligand. The equilibrium constant K has been determined by ^{31}P NMR (Scheme 65). The more acidic ligated thiol is deprotonated by NEt_3 to give PhPd(SR)(dppf), which undergoes a reductive elimination leading to the coupling product PhSR and Pd^0(dba)(dppf) (Scheme 65). All complexes Pd^0(dba)(dppf), PhPdI(dppf), PhPdI(K^1-dppf)(SRH), and PhPd(SR)(dppf) have been characterized by ^{31}P NMR. The rate constant of the reductive elimination, k^{re}, has been determined by ^{31}P NMR. A minimum value for the observed rate constant k_{obs}^{met} of the fast formation of PhPd(SR)(dppf) from PhPdI(dppf) has been estimated by ^{31}P NMR as well, for the initial concentrations of NEt_3 and RSH used in the catalytic reaction (Scheme 65).[141]

From the values of the observed rate constants (k_{obs}^{oa}, k_{obs}^{met}) and the rate constant k^{re} (all expressed in s^{-1}) determined for each step investigated independently from each other, it emerges that the reductive elimination is rate-determining before 80% conversion, whereas the oxidative addition becomes rate-determining beyond 80% conversion because of the decrease of the PhI concentration as the catalytic reaction proceeds ($k_{obs}^{oa} = k^{oa}$[PhI]). This inversion of the rate-determining step has been confirmed by a simulation of the kinetics of the catalytic reaction, using the initial concentrations of reagents and catalyst and the rate constants determined above. Figure 21 displays a zoom on the concentration profiles of the catalytic species in the course of the catalytic

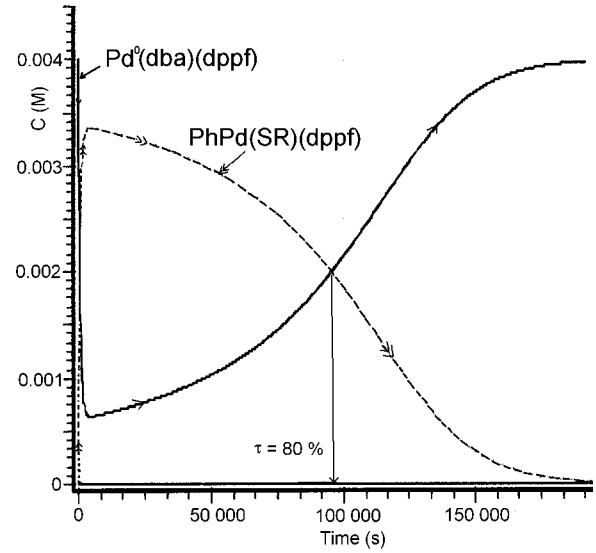

Figure 21. Simulation by AnaCin2000 program of the concentration profiles of the catalytic species in the reaction of Scheme 64, using the initial concentrations of PhI, NEt_3, RSH, and Pd(0) of the catalytic reaction and the rate constants determined in acetone at 25 °C. (—>—) Pd^0(dba)(dppf); (—≫—) PhPd(SR)(dppf). τ = conversion.

reaction. Only two complexes are observed in appreciable concentration: Pd^0(dba)(dppf) whose concentration fast decreases at the beginning of the catalytic reaction due to a fast oxidative addition and PhPd(SR)(dppf), which accumulates before 80% conversion because it is involved in the rate-determining reductive elimination. Beyond 80% conversion, Pd^0(dba)(dppf) accumulates because it is involved in the rate-determining oxidative addition. The other complexes of the catalytic cycle are not detectable because they are present at low steady-state concentrations, in agreement with the mechanism proposed in Scheme 65.

This is the first work reported in the literature where all steps of a catalytic cycle have been described, including the characterization of all catalytic organometallic species and their rate constants or equilibrium constant as well. Interestingly, it is established that the rate-determining step of a catalytic cycle may change in the course of a catalytic reaction due to decreasing reagent concentrations.[141]

3. Transition-Metal Catalyzed Electrosynthesis: The Electron as Reagent

Some organic reactions are reductions or oxidations that can be accomplished via a chemical or electrochemical process.[142,143] Problems arise when the reactions require powerful chemical reductants or oxidants or proceed at very high potentials.

An inorganic mediator may be used whose reduction (or oxidation) generates an active species able to reduce (or oxidize) the substrate by an outer-sphere mechanism without formation of any organometallic species.[144,145] This homogeneous redox process gives back the initial form of the mediator, which is subsequently transformed into its active form at the cathode (or anode). The electrons are not transferred directly from the electrode to the substrate but via the mediator, which is used in a catalytic amount. These mediated electrosyntheses consume a stoichiometric amount of electrons. Even if the mediator is a transition metal salt or complex, the catalytic reaction does not involve any

intermediate organometallic species. Such reactions will be not reported herein (for reviews, see refs 144 and 145).

Another more versatile alternative consists in the use of a transition metal that can activate the organic substrate and provide an organometallic species that is more easily reduced (or oxidized) than the organic substrate. Such reactions involve a double activation: chemical activation of the substrate by a transition metal catalyst, followed by activation by electron transfer of the organometallic species formed in the chemical activation. A chemical activation of the organic substrate by a transition metal may also be advantageously used when the direct electrochemical reduction (or oxidation) of the substrate does not generate the expected species due to an undesired bond breaking induced by the direct electron transfer.

Some transition metal-catalyzed reactions do not require any activation of intermediate organometallic species by electron transfer, but electrons may be required to recycle the active catalyst (which initiates the catalytic cycle) from a nonreactive one generated in every catalytic cycle.

In all those transition metal-catalyzed electrosyntheses, the electrons play the role of a reagent (reductant or oxidant) and must be used in stoichiometric amounts. In addition, the electrons may be used at the very beginning of the electrolyses to generate the active form of the catalyst from a nonreactive precursor.

Two simultaneous electrochemical reactions take place in all electrosyntheses, one at the cathode and another one at the anode. Those two reactions can be carried out in a one-compartment cell (undivided cell) or in a two-compartment cell separated by a frit or a membrane (divided cell). The former is used when a sacrificial metallic anode is required whose oxidation releases cations, which may have a beneficial effect for the reaction taking place at the cathode.[146]

The following section reports transition metal-catalyzed electrosyntheses that proceed via organometallic intermediates.[144,146–148] Their mechanisms (when known) are included. They have been of course investigated by means of electrochemical techniques, as developed in section 2 for catalytic reactions that do not involve any electron transfer at an electrode.

3.1. Transition Metal-Catalyzed Electrosyntheses Involving One-Electron Activation of Organometallic Intermediates

3.1.1. Nickel-Catalyzed Electroreductive Carboxylation of Aryl Halides

The direct electrochemical reduction of aryl halides in the presence of carbon dioxide should generate aromatic carboxylic acids via the carboxylation of electrogenerated aryl anions (Scheme 66).

Scheme 66

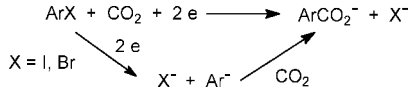

Such electroreductive carboxylations often proceed with poor yields and cannot be performed with most aryl bromides or chlorides, which exhibit very negative reduction potentials in usual solvents (acetonitrile, THF, DMF), that is, potentials that are even more negative than that of CO_2 whose reduction becomes the major process.[142,143] This problem may be solved by introduction of cations (Mg^{2+}, Zn^{2+}), which facilitate the electrochemical reduction of aryl halides by complexation of the halides. The cations may be supplied by the oxidation of a sacrificial metallic anode (Zn or Mg via $M \rightarrow M^{2+} + 2e^-$) in an undivided cell, as pioneered by Périchon et al.[149]

A more versatile alternative is to use a transition metal complex that catalyzes the electrocarboxylation process, such as $NiCl_2$(dppe) (dppe = PPh_2-$(CH_2)_2$-PPh_2), a Ni(II) complex ligated by bisphosphine ligand (Scheme 67), as reported by

Scheme 67

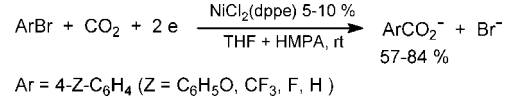

Fauvarque, Périchon, et al.[150,151] The electrolyses are carried out at less negative potentials than those of the aryl halides.[151]

The mechanism has been investigated by Amatore and Jutand by means of electrochemical techniques (Scheme 68,

Scheme 68

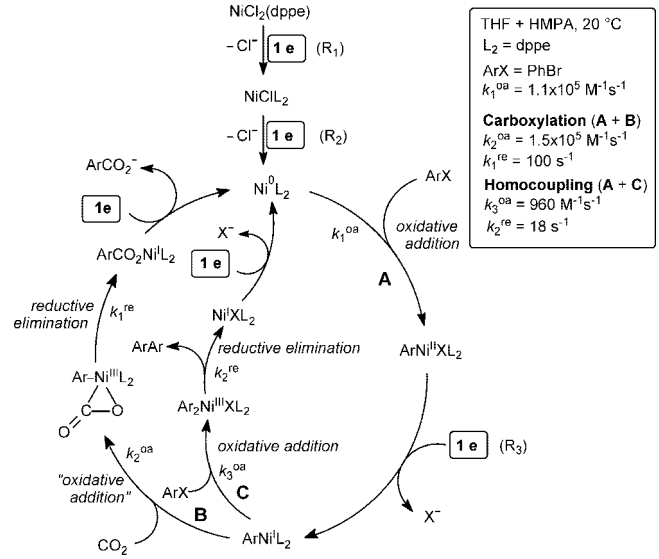

paths A + B).[152,153] $NiCl_2$(dppe) is reduced in two successive one-electron steps (R_1 and R_2) at the beginning of the electrolysis to a low-ligated complex Ni^0(dppe), which undergoes a fast oxidative addition to ArBr to give $ArNi^{II}Br$(dppe). The rate constant (k_1^{oa}) of the oxidative addition has been determined by fast cyclic voltammetry at a steady disk electrode. The reduction of $ArNi^{II}Br$(dppe) takes place at a less negative potential (R_3) than that of ArBr and involves one electron to give $ArNi^{I}$(dppe). The latter reacts with CO_2 (k_2^{oa}) leading to $ArNi^{III}(\mu^2$-$CO_2)$(dppe). A reductive elimination (k_1^{re}) affords a Ni(I) carboxylate $ArCO_2Ni^IL_2$. The electrolysis is carried out at the reduction potential of $ArNi^{II}Br$(dppe) (R_3). At that potential $ArCO_2Ni^IL_2$ is reduced back to the active Ni^0(dppe) by a one-electron transfer, which also releases the aromatic carboxylic acid. The evolution of the catalytic reduction plateau current of $PhNi^{II}Br$(dppe) (measured at a rotating disk electrode) with CO_2 and ArBr concentrations allows the determination of the rate constants k_2^{oa} and k_1^{re}. From the values of k_1^{oa}, k_2^{oa}, and k_1^{re} determined for PhBr, it emerges that the reductive elimination is rate-determining for CO_2

and PhBr concentrations used in catalytic reactions ($\gg 10^{-3}$ M) (Scheme 68).[152,153]

The electrolysis consumes two electrons per mole, one for the activation of $ArNi^{II}Br(dppe)$ and the second one for the recycling of the Ni(0) catalyst. As a consequence of the one-electron transfer, the carboxylation takes place within the coordination sphere of the nickel and not from an aryl anion, Ar^- (Scheme 68).

3.1.2. Nickel-Catalyzed Electroreductive Carboxylation of α-Methylbenzyl Halides: Electrosynthesis of Anti-inflammatory Agents

Aryl-2 propionic acids (naproxen, ibuprofen, fenoprofen) are anti-inflammatory agents (Scheme 69). The direct

Scheme 69

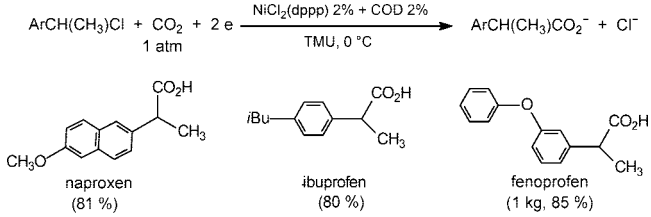

electrochemical reduction of $ArCH(CH_3)Cl$ in the presence of CO_2 generates aryl-2 propionic acids via the carboxylation of the anion $ArCH(CH_3)^-$. However, the reactions require very negative reduction potentials (Fauvarque et al.)[154] or the presence of cations (Zn^{2+} or Mg^{2+}) generated at a sacrificial Zn or Mg anode, which catalyze the electrochemical reduction process (Périchon et al.).[146,149]

The electrosyntheses of aryl-2 propionic acids are catalyzed by $NiCl_2(dppp)$ (dppp = Ph_2P-$(CH_2)_3$-PPh_2) associated with the coligand COD (1,5-cyclooctadiene), as reported by Fauvarque et al. (Scheme 69).[154–158]

The electrosynthesis of fenoprofen has been scaled up to 1 kg in a Grignard type reactor, an undivided cell equipped with a graphite woven cathode and a titanium anode. Lithium oxalate is oxidized to CO_2 at the anode. The electrosynthesis has been performed in the nontoxic solvent TMU (tetramethylurea) with 2% of the nickel catalyst.[158] CO_2 is bubbled into the reactor at atmospheric pressure and at 0 °C to increase its solubility. Zinc powder, which is oxidized at the titanium anode, may be used as an alternative to lithium oxalate or sacrificial anode.[157]

The mechanism of the reaction is similar to that involving aryl halides (Scheme 68, A + B). $ArCH(CH_3)NiCl(dppp)$ formed in the oxidative addition is more easily reduced than $ArCH(CH_3)Cl$. Its activation by one-electron reduction gives $ArCH(CH_3)Ni(dppp)$. The reaction proceeds via the carboxylation of $ArCH(CH_3)Ni^{I}(dppp)$ and not from the anion $ArCH(CH_3)^-$. This suggests a possible asymmetric electrosynthesis, using a nickel catalyst ligated by a chiral bidentate ligand. However, the asymmetric electrosynthesis of biologically active chiral aryl-2 propionic acids is still a challenge.

3.1.3. Nickel-Catalyzed Electroreductive Homocoupling of Aryl Halides

The complex $NiCl_2(dppe)$ is also a good catalyst for the electrosynthesis of biaryls via the electroreductive homocoupling of aryl bromides (Scheme 70).[159]

Scheme 70

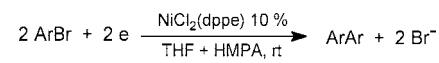

The mechanism of the homocoupling is depicted in Scheme 68 (paths A + C).[159,160] The catalytic cycles of the nickel-catalyzed carboxylation and homocoupling have in common the same key complex, $ArNi^{I}(dppe)$. The two catalytic cycles are indeed branched at the level of $ArNi^{I}(dppe)$, which may either react with CO_2, leading to the carboxylation process, or undergo a second oxidative addition to ArBr (k_3^{oa}) leading to a Ni(III) complex, $Ar_2Ni^{III}Br(dppe)$ whose reductive elimination (k_2^{re}) gives the biaryl and a Ni(I) complex. The latter is recycled back to the initial Ni(0) by a one-electron reduction. The evolution of the catalytic reduction plateau current of $PhNi^{II}Br(dppe)$ (measured at a rotating disk electrode), with PhBr concentrations allows the determination of the rate constants k_3^{oa} and k_2^{re} (Scheme 68, path C). It emerges that the rate-determining step of the catalytic cycle is the second oxidative addition (k_3^{oa}) at low PhBr concentrations whereas the reductive elimination (k_2^{re}) is rate-determining at high PhBr concentrations ($C > 0.02$ M). When the electrolysis is performed from PhBr and CO_2, the carboxylic acid $PhCO_2H$ is formed without any PhPh. This indicates that the carboxylation is more efficient than the homocoupling. Comparison of the two rate constants k_2^{oa} and k_3^{oa} confirms that PhNi(dppe) is indeed ca. 100 times more reactive with CO_2 than with PhBr at identical concentrations (Scheme 68).[159,161]

The electroreductive homocoupling of aryl halides is also efficiently catalyzed by Ni(II) complexes ligated to 2,2′-bypiridyl (bpy) (Scheme 71). The electrolyses are performed

Scheme 71

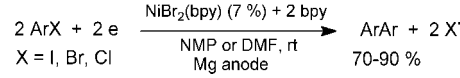

at room temperature in an undivided cell equipped with a sacrificial Mg anode.[147,162,163] The electrolyses have also been performed in protic solvents, alcohols (Troupel et al.)[164] or water (Troupel et al.),[165] or in ionic liquids (Fe anode, Barhdadi et al.,[166] Jouikov et al.[167]). The homocoupling has been extended to substituted-2-bromopyridines (Zn or Fe anode) by Navarro et al.[168,169]

The mechanism investigated by Devaud et al. may proceed by two paths.[170] A mechanism involving paths A + C in Scheme 72 is reminiscent of that established for $NiCl_2(dppe)$ catalyst, that is, oxidative addition of the electrogenerated $Ni^0(bpy)$ to ArX. The $ArNi^{II}X(bpy)$ formed in the oxidative addition is activated by a one-electron reduction giving $ArNi^{I}(bpy)$, which undergoes an oxidative addition to ArX to generate $Ar_2Ni^{III}X(bpy)$. A reductive elimination gives the biaryl and $Ni^{I}X(bpy)$, which is recycled to the active $Ni^0(bpy)$ complex by a one-electron reduction at the cathode. Such a mechanism requires the activation of an organometallic intermediate, $ArNi^{II}X(bpy)$, by electron transfer, and the electrolyses must be conducted at the reduction potential of this intermediate (R_2).[170]

A second competitive mechanism is also proposed (Scheme 72, paths A + B) in which $ArNi^{II}X(bpy)$ undergoes a ligand scrambling, which gives $ArNi^{II}Ar(bpy)$ and $Ni^{II}X_2(bpy)$. A reductive elimination from $ArNi^{II}Ar(bpy)$ gives the biaryl and $Ni^0(bpy)$, whereas $Ni^{II}X_2(bpy)$ is recycled back to $Ni^0(bpy)$ by reduction at the cathode.[170] According to this

Scheme 72

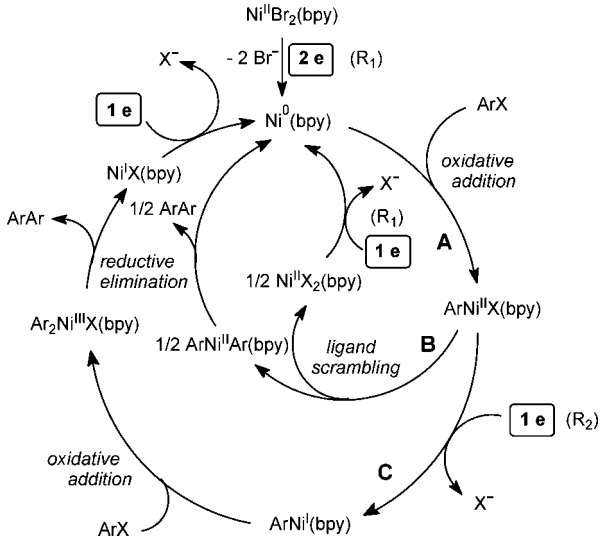

mechanism, the activation of an organonickel intermediate by electron transfer is not required and the electrolyses can be conducted at the reduction potential of the $Ni^{II}X_2(bpy)$ precursor (R_1). From an experimental point of view, it may be difficult to discriminate between the two mechanisms since the reduction potential of $ArNi^{II}X(bpy)$ and $Ni^{II}X_2(bpy)$ may be close to each other.[170] $NiBr_2$ associated with 2,2′-dipyridylamine (1:1) is much more efficient than $NiBr_2(bpy)$ for the electroreductive homocoupling of aryl bromides in ethanol (Fe anode), as reported by Troupel et al.[171]

The electroreductive homocoupling of vinyl bromides or chlorides is efficiently catalyzed by $NiBr_2(bpy)$, leading to 1,3-dienes (Scheme 73; Labbé et al.,[172] Condon, Durandetti

Scheme 73

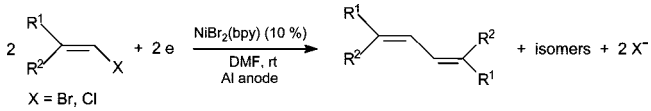

et al.[173]). The electrolyses are carried out in an undivided cell equipped with a sacrificial Al anode in DMF.

The mechanism has been investigated by Labbé et al.[172] The vinyl halide undergoes a first oxidative addition to the electrogenerated $Ni^0(bpy)$, leading to vinyl-$Ni^{II}X(bpy)$. The monoelectronic activation of the latter gives vinyl-$Ni^{I}(bpy)$ whose oxidative addition to the vinyl halide generates $(vinyl)_2Ni^{III}Br(bpy)$. The 1,3-diene is formed by reductive elimination leading to $Ni^{I}(bpy)$ as well, which is recycled to $Ni^0(bpy)$ by a one-electron reduction at the cathode. The catalytic cycle is thus very similar to that proposed for the Ni/bpy catalyzed homocoupling of aryl halides (Scheme 72, paths A + C).

3.1.4. Nickel-Catalyzed Electroreductive Polymerization of Organic Dihalides

The complex $NiCl_2(dppe)$ catalyzes the electrosynthesis of poly(1,4-phenylene) from 1,4-dibromobenzene (Scheme 74)[174,175] or from 4,4′-dibromobiphenyl.[176] Similarly, $NiBr_2(bpy)$ catalyzes the electroreductive polymerization of 3-substituted 2,5-dihalothiophenes (Scheme 75),[177] as well as 2,5-dibromofurane.[178]

The electrosynthesis of poly-*p*-xylene (PPX) has been performed by the direct electrochemical reduction of 4-$BrCH_2$-

Scheme 74

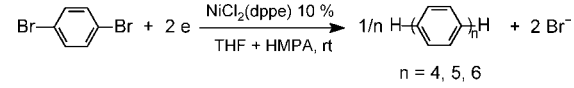

Scheme 75

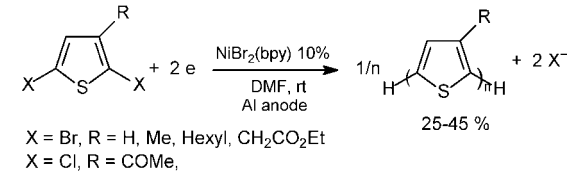

C_6H_4-CH_2Br (1,4-bis(bromomethyl)benzene), which is a lachrymatory reagent (Utley et al.).[179] The electrosynthesis could not be performed from the cheaper and less lachrymatory 1,4-bis(chloromethyl)benzene whose reduction potential is much more negative. The electroreductive polymerization of 1,4-bis(chloromethyl)benzene has been efficiently catalyzed by $NiCl_2(P\hat{}P)$ (P^P = dppe, dppp) (Scheme 76)

Scheme 76

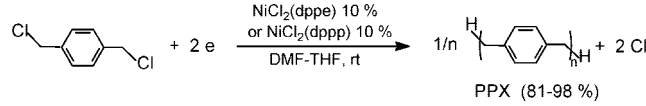

via the formation of 4-$ClCH_2$-C_6H_4-$CH_2NiCl(P\hat{}P)$, which are both more easily reduced than 4-$ClCH_2$-C_6H_4-CH_2Cl.[180] The mechanism is similar to that reported for the Ni-catalyzed electroreductive homocoupling of aryl halides (Scheme 68, paths A + C), involving monoelectronic transfers.

The complex $NiI_2(dppe)$ catalyzes the electroreductive polymerization of diodoacetylene to polyynes (Scheme 77).[181]

Scheme 77

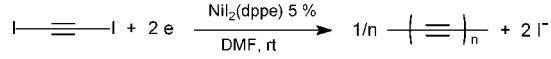

3.1.5. Nickel-Catalyzed Electroreductive Heterocoupling of Organic Halides

The electroreductive heterocoupling of aryl halides and α-bromo- or chloroesters catalyzed by $NiBr_2(bpy)$ gives $ArCH(R)CO_2Et$ (Scheme 78), as reported by Sibille et al.[182]

Scheme 78

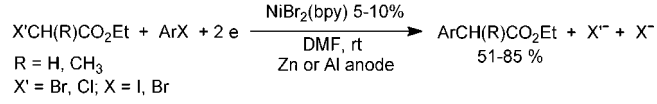

and Durandetti et al.[183,184] The electrosyntheses are performed in an undivided cell equipped with a sacrificial Zn or Al anode and require to be carried out upon continuous slow addition of the α-haloester[182–184] to avoid its competitive oxidative addition to the electrogenerated $Ni^0(bpy)$, reaction, which is faster than the oxidative addition to the aryl halide.[172]

The electroreductive heterocoupling has been performed from α-chloroketones (45−80% yield) by the same group.[183,184] 2-Bromothiophene and 3-bromothiophene undergo the electroreductive coupling with α-choroesters and benzyl or vinyl halides.[185]

The Ni-catalyzed electroreductive heterocoupling of two aryl bromides with an α-chloropropionic imide bearing a chiral auxiliary gives, after hydrolysis, two 2-aryl propionic acids, (*S*)-naproxen, and (*S*)-flurbiprofen (anti-inflammatory agents) with good diastereomeric and enantiomeric excess (Scheme 79).[186]

Scheme 79

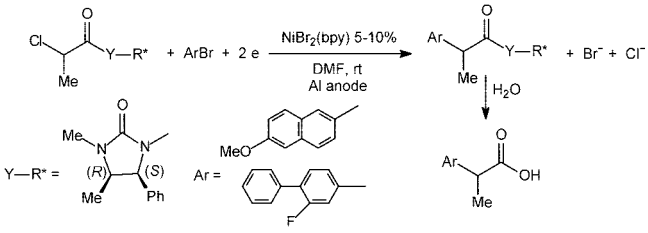

3.1.6. Cobalt-Catalyzed Electroreductive Heterocoupling of Aryl Halides and Vinylic or Allylic Acetates

The electroreductive heterocoupling of aryl halides and vinylic acetates is catalyzed by $CoBr_2$ associated with excess bpy, as reported by Gosmini et al. (Scheme 80).[187] The

Scheme 80

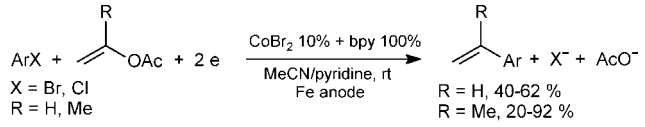

electrolyses are performed in an undivided cell equipped with a sacrificial Fe anode.

The mechanism has been investigated by Buriez, Labbé, et al. (Scheme 81, the bpy ligands are voluntarily omitted).[188,189] In the main paths A + B, the oxidative addition of ArX to

Scheme 81

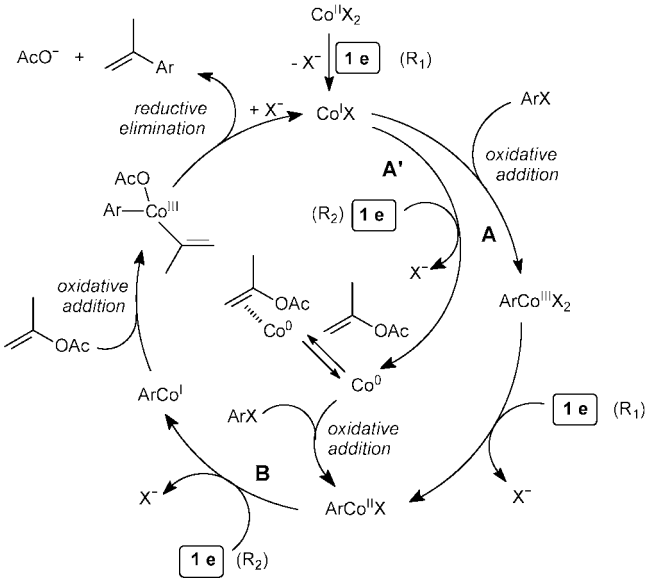

an electrogenerated $Co^{I}X$ gives $ArCo^{III}X_2$, which is reduced in two successive one-electron steps (R_1 and R_2) to $ArCo^{I}$. $ArCo^{I}$ undergoes an oxidative addition to the vinylic acetate to form $ArCo^{III}(OAc)(\eta^1$-vinyl). A reductive elimination generates the coupling product and $Co^{I}X$. In an alternative path, A′ + B (Scheme 81), the common complex $ArCo^{II}X$ is formed by oxidative addition of ArX to electrogenerated Co(0), which is stabilized by complexation to the C=C bond of the vinylic acetate. $Co^{I}X$ and $ArCo^{II}X$ are reduced at the same potential (R_2), which is more negative than the common reduction potential of $Co^{II}X_2$ and $ArCo^{III}X_2$ (R_1). The electrolyses are efficient if they are performed at the reduction potential of $ArCo^{II}X$ (R_2) and in the presence of cations Fe^{2+} released in the oxidation of the sacrificial Fe anode. The latter play a key role by trapping the acetate ions responsible for the catalyst poisoning.[188,189]

The electroreductive heterocoupling of aryl halides and allyl acetate or carbonate is catalyzed by $CoBr_2$, as reported by Gosmini et al. (Scheme 82).[190] The pyridine serves as

Scheme 82

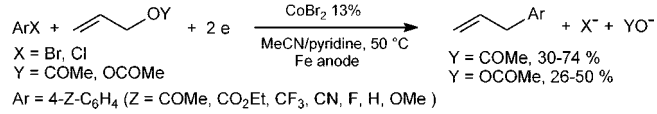

ligand for Co complexes. The electrolyses are performed in an undivided cell equipped with a sacrificial Fe anode. A tentative mechanism is proposed by Buriez, Labbé, et al., which involves the monoelectronic reduction of $ArCo^{III}X_2$ to $ArCo^{II}X$ as a key step.[191]

3.1.7. Cobalt-Catalyzed Electroreductive Hydroalkylation of Electron-Deficient Alkenes

Cobalt(I) in vitamin B_{12} or Co(III) in a vitamine B_{12} model compound catalyzes the intramolecular and intermolecular electroreductive hydroalkylation of electron-deficient alkenes, as reported by Scheffold et al.[192,193] (Scheme 83). The electrolyses are performed in a divided cell at a Hg-pool cathode at a constant potential. A mechanism is proposed for the intramolecular version performed from cyclohexenones substituted in the α-position by an alkyl chain bearing a terminal C−Br bond (R−Br), leading to bicyclic ketones (Scheme 83). A Co(I) complex activates the R−Br bond to generate $R-Co^{III}-Br$ complexes, which are reduced by transfer of one electron to yield Co^{II} intermediate. One Co(III) complex has been isolated ($n = 4$, Scheme 83). Its electrochemical reduction performed at the potential of its second reduction peak in the presence of protons generates the decalone ($n = 4$).[192]

3.2. Transition Metal-Catalyzed Electrosyntheses Involving a Two-Electron Activation of Organometallic Intermediates

3.2.1. Palladium-Catalyzed Electroreductive Carboxylation of Aryl Halides or Triflates

3.2.1.1. Palladium-Catalyzed Electroreductive Carboxylation of Aryl Halides. The palladium-catalyzed electroreductive carboxylation of aryl halides has been reported by Torii et al. (Scheme 84).[194]

A preliminary mechanistic approach had shown that the isolated $PhPdBr(PPh_3)_2$, formed in the oxidative addition of PhBr to $Pd^0(PPh_3)_4$, was reduced at less negative potential than the parent PhBr and that its reduction in the presence of CO_2 generated the desired carboxylic acid $PhCO_2H$.[194] The mechanism of the electroreductive carboxylation step has been then more deeply investigated by Amatore, Jutand, et al. using electrochemical techniques.[195] Complexes $ArPdX(Cl)(PPh_3)_2^-$ or $ArPdX(PPh_3)_2$ (X = I, Br), generated in the oxidative addition of ArX to electrogenerated

Scheme 83

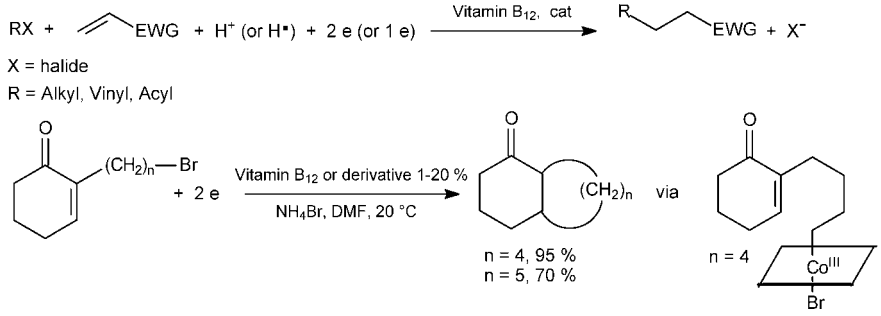

Scheme 84

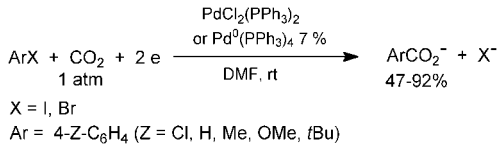

$Pd^0(PPh_3)_2Cl^-$ or $Pd^0(PPh_3)_4$, respectively, are reduced at less negative potentials than the parent ArX (Scheme 85).[58,195] Their reduction is an overall two-electron step, which generates the anionic $ArPd^0(PPh_3)_2^-$ in equilibrium with $Pd^0(PPh_3)_2$ and the anion Ar^- (Scheme 85, paths A + B or A′ + B).[195] The carboxylation proceeds from Ar^-, that is, outside the coordination sphere of the palladium, from the same Ar^- that would have been formed by the putative direct electrochemical reduction of ArX. Importantly, Ar^- is generated in the reduction of $ArPdX(Cl)(PPh_3)_2^-$ or $ArPdX(PPh_3)_2$ at a less negative potential than the reduction potential of ArX. Therefore, aryl halides (such as 4-MeO-C_6H_4-Br), which are reduced at very negative potentials (beyond that of CO_2), can successfully be transformed into the corresponding carboxylic acids via the reduction of aryl−Pd(II) complexes.[195]

Interestingly, two different kinds of activation of $ArMXL_2$ complexes can take place, a one-electron transfer for Ni complexes ligated by the bisphosphine dppe (Scheme 68)[152] versus an overall two-electron transfer for Pd complexes ligated by the monophosphine PPh_3 (Scheme 85),[195] affecting the mechanism of the carboxylation step: within the Ni coordination sphere in the former case versus outside the coordination sphere in the Pd case.

3.2.1.2. Palladium-Catalyzed Electroreductive Carboxylation of Aryl Triflates. Aryl triflates, easily synthesized from available phenols, are often used as an alternative to aryl halides.[31] However, even if aryl triflates can be reduced at a cathode in DMF, their reduction in the presence of CO_2 does not generate the desired aromatic carboxylic acids as the major product but the corresponding phenols (Scheme 86), as reported by Jutand et al.[196]

The electrochemical reduction of an aryl triflate first generates a radical anion $ArOTf^{\bullet -}$ whose major evolution is not the cleavage of the Ar−O bond, which would eventually generate the aryl anion Ar^- prone to react with CO_2, but the cleavage of the O−S bond leading to the undesired phenoxide after a second electron transfer (Scheme 86).[196] This problem has been solved by Jutand et al., by using a palladium catalyst, which favors the cleavage of the Ar−O bond (Scheme 87).[196,197]

Whereas the direct electrochemical reduction of 1-naphthyl triflate in the presence of CO_2 leads, after hydrolysis, to only 13% of the 1-naphthyl carboxylic acid (Scheme 86), addition of 10% of $PdCl_2(PPh_3)_2$ results in the formation of the desired carboxylic acid in 83% yield (Scheme 87). The electrolysis is carried out at a less negative potential than that of 1-naphthyl triflate, under atmospheric pressure of CO_2. The reaction has been extended to various aryl triflates. It is regiospecific and exhibits good compatibility with substituents Z on the aryl group (Scheme 87).[196,197]

A more sophisticated molecule, 1,3,5-tris(4-carboxyphenyl)benzene, has been synthesized via the Pd-catalyzed electrochemical process (Scheme 88).[196]

The mechanism of the Pd-catalyzed electroreductive carboxylation of aryl triflates is close to that of the Pd-catalyzed electroreductive carboxylation of aryl halides

Scheme 85

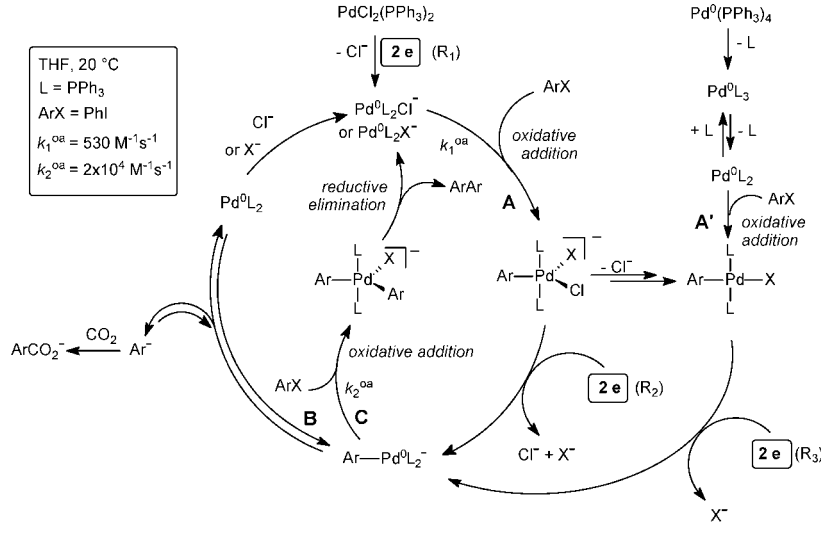

Scheme 86

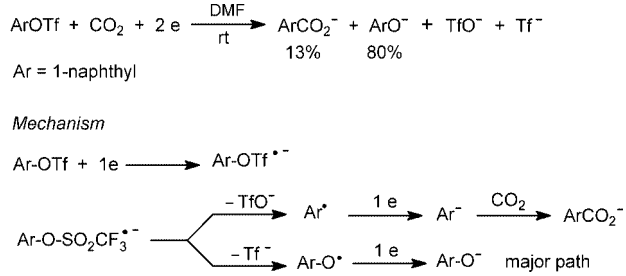

Scheme 87

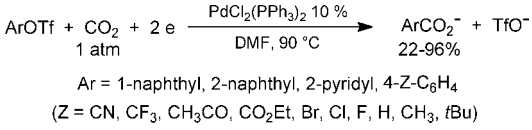

Scheme 88

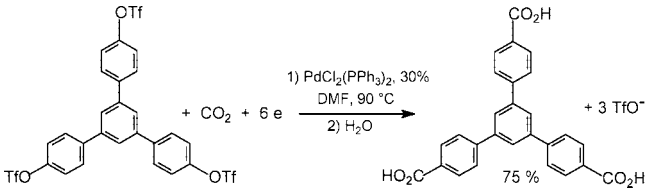

except that it involves neutral aryl−Pd(II) complexes (Scheme 89, A + B).[196]

The precursor $PdCl_2(PPh_3)_2$ is reduced to the anionic $Pd^0(PPh_3)_2Cl^-$ at the very beginning of the electrolysis (R_1) (see section 2.3.2).[58] Its oxidative addition to ArOTf generates a neutral complex $ArPdCl(PPh_3)_2$, due to the low affinity of the triflate anion for the Pd(II) center (Scheme 41 in section 2.6.1).[30] $ArPdCl(PPh_3)_2$ is activated by an overall two-electron step (R_2), which proceeds at a less negative potential than the reduction potential of ArOTf.[196] The reduction peak potentials of $ArPdCl(PPh_3)_2$ have been determined by cyclic voltammetry to fix the potential of the electrolyses. The reduction of $ArPdCl(PPh_3)_2$ generates the anionic $ArPd^0(PPh_3)_2^-$ in equilibrium with the anion Ar^- and $Pd^0(PPh_3)_2$,[195] which re-enters the catalytic cycle by coordination of a chloride ion (Scheme 89, paths A + B).

Scheme 90

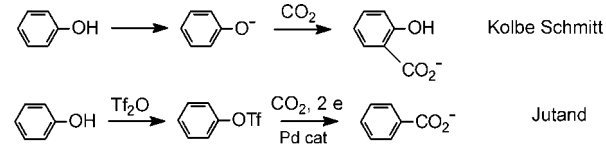

The carboxylation proceeds from the anion Ar^-.

The chemical and electrochemical activations are both crucial. The palladium (via the activation of the Ar−O bond by oxidative addition) catalyzes the reduction of ArOTf to the desired Ar^- and bypasses the undesired formation of ArO^- that would be obtained in the direct electrochemical reduction of ArOTf. Interestingly, the chloride ions delivered by the precursor $PdCl_2(PPh_3)_2$ have a positive effect by forming neutral $ArPdCl(PPh_3)_2$ instead of cationic $ArPd(DMF)(PPh_3)_2^+$ (Scheme 41 in section 2.6.1).[30] Indeed, the electrochemical reduction of cationic $ArPd(DMF)(PPh_3)_2^+$ is monoelectronic and leads to $ArPd^I(PPh_3)_2$ with subsequent formation of biaryl.[93]

The carboxylation of aryl triflates is in a sense more challenging than that of aryl halides since the direct electrochemical reduction of aryl halides (whenever possible) always generates the desired anion Ar^- (Scheme 66). Moreover, this process is an inversion of reactivity induced by electron transfer. Aryl triflates can now react with an electrophile (CO_2) whereas they are usually known to react with nucleophiles in cross-coupling reactions, in the presence of the same $PdCl_2(PPh_3)_2$ catalyst.[31]

Since aryl triflates are synthesized from phenols, their palladium-catalyzed electroreductive carboxylation can be compared with the direct carboxylation of phenoxides (Kolbe Schmitt reaction), which leads to carboxylic acids without alteration of the phenol function (Scheme 90, upper reaction). The palladium-catalyzed electroreductive carboxylation is thus the only way to generate aromatic carboxylic acids from phenols via their triflate derivatives with cleavage of the aromatic C−O bond (Scheme 90, bottom reaction).[196,197]

Scheme 89

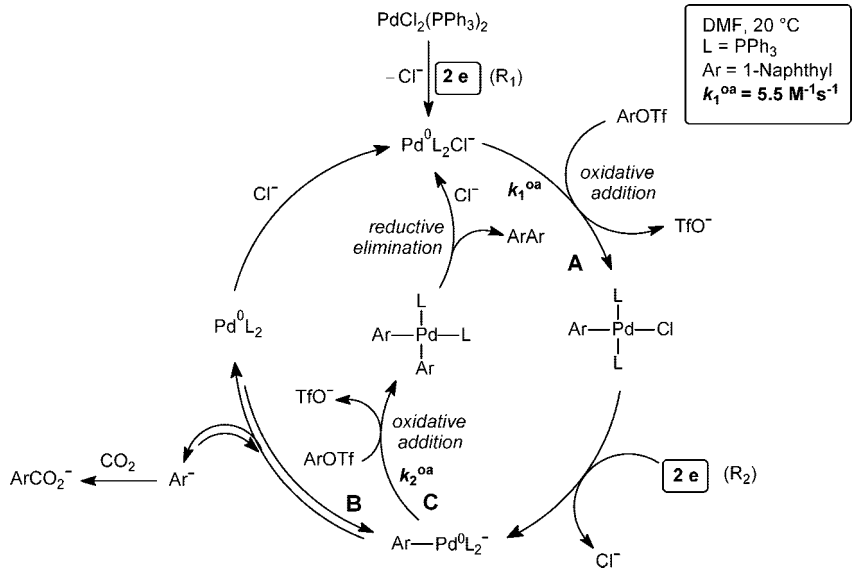

Scheme 91

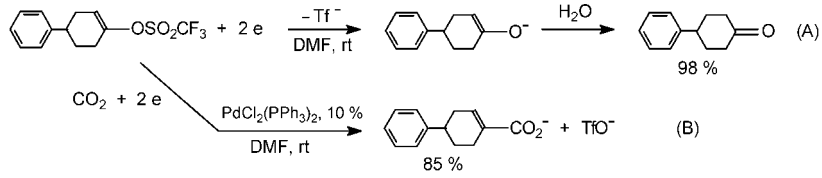

Scheme 92

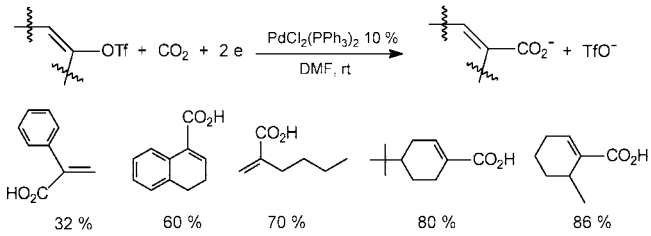

3.2.2. Palladium-Catalyzed Electroreductive Carboxylation of Vinyl Triflates

Jutand and Negri have reported that the direct electrochemical reduction of a vinyl triflate gives the corresponding ketone after consumption of two electrons per mole via the cleavage of its O−S bond (Scheme 91A).[198] The same reaction performed in the presence of CO_2 with $PdCl_2(PPh_3)_2$ as catalyst and carried out at a less negative potential gives the α,β-unsaturated carboxylic acid (Scheme 91B).[198]The Pd-catalyzed electroreductive carboxylation of vinyl triflates has been successfully developed (Scheme 92).[196,198] The reactions are stereospecific. The electrolyses are performed at room temperature and are faster than the carboxylation of aryl triflates (see section 3.2.1.2) because the oxidative additions of vinyl triflates[196] to $Pd^0(PPh_3)_2Cl^-$ are faster than those of aryl triflates.[30] As for aryl triflates, the cleavage of the vinylic C−O bond of vinyl-OSO_2CF_3 by the electrogenerated $Pd^0(PPh_3)_2Cl^-$ catalyst is favored versus the O−S bond cleavage. The vinyl-$PdCl(PPh_3)_2$ complexes formed in the oxidative addition, whose reduction potentials have been determined by cyclic voltammetry, are more easily reduced than the parent vinyl-OTf. The electrolyses are carried out at the reduction potentials of vinyl-$PdCl(PPh_3)_2$, avoiding the direct reduction of vinyl-OTf to the undesired ketones.[196] Even if not established, the carboxylation might proceed from a vinylic anion by analogy to the carboxylation of aryl triflates.

Most α,β-unsaturated carboxylic acids are not obtained in the absence of any catalyst, as reported by Tokuda et al.[199] Indeed, the direct electrochemical reduction of alkyl-substituted vinyl triflates, performed in the presence of CO_2 and Mg^{2+} cations released by a sacrificial Mg anode, affords the β-keto carboxylic acids by carboxylation of the enolate generated by the cleavage of the O−S bond (Scheme 93). Moreover, this reduction process may be induced by $CO_2^{\bullet-}$,

Scheme 93

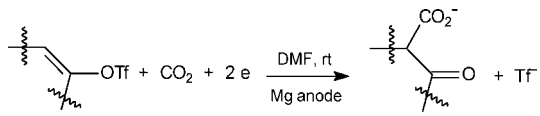

the reduced form of CO_2, which is more easily reduced than alkyl-substituted vinyl triflates in DMF.[196,200] Consequently, the activation of alkyl-substituted vinylic triflates by the Pd(0) catalyst is quite helpful, in the sense that the palladium catalyzes their reduction and moreover favors the desired cleavage of the vinylic C−O bond.

More easily reduced phenyl-substituted vinyl triflates are converted to α,β-unsaturated carboxylic acids in the presence of Mg^{2+} by cleavage of the vinylic C−O bond.[200] Their reduction potentials are nevertheless still very negative. The palladium catalyst makes their reduction proceed at less negative potentials via the formation of electroactive vinyl−Pd(II) complexes.

The palladium-catalyzed electroreductive carboxylation of vinyl triflates is an alternative route to Mg^{2+}-catalyzed,[146,149,201] Ni-catalyzed,[202] or Pd-catalyzed[194] electroreductive carboxylation of vinyl halides. Vinyl triflates are synthesized from alkynes or ketones, which can be therefore transformed into α,β-unsaturated carboxylic acids in the presence of CO_2, an electron source, and a Pd catalyst via the vinyl triflates (Scheme 94).[196,198] When vinyl triflates are generated from

Scheme 94

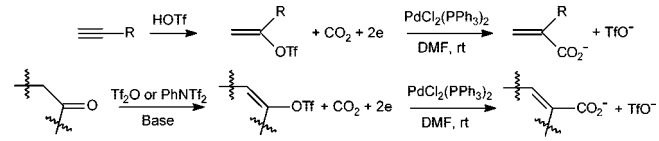

terminal alkynes, the Pd-catalyzed stereospecific carboxylation affords the α,β-unsaturated carboxylic acids exclusively with the carboxyl group at the more substituted position (Scheme 94).[196,198] The Ni-catalyzed electroreductive hydrocarboxylation of terminal alkynes has been reported by Duñach et al., but the reaction is not as regioselective and affords a mixture of two α,β-unsaturated carboxylic acids in favor of the branched ones (see section 3.3.1.1).

3.2.3. Palladium-Catalyzed Electroreductive Homocoupling of Aryl Halides or Triflates

3.2.3.1. Palladium-Catalyzed Electroreductive Homocoupling of Aryl Halides. The palladium-catalyzed electroreductive homocoupling of aryl halides has been reported by Torii et al. (Scheme 95).[203]The mechanism has been

Scheme 95

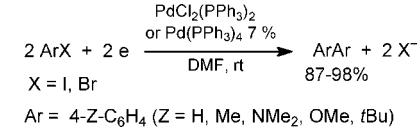

established by Amatore, Jutand, et al. by means of electrochemical techniques (Scheme 85, paths A (or A′) + C).[204] ArX undergoes an oxidative addition to the anionic $ArPd^0(PPh_3)_2^-$ leading to the anionic $ArPdAr(X)(PPh_3)_2^-$, which gives the biaryl and a Pd(0) complex by reductive elimination. Therefore, two oxidative additions are involved, separated by a two-electron reduction process. The second oxidative addition (k_2^{oa}) is faster than the first one (k_1^{oa}) by a factor 40 when ArX = PhI (Scheme 85).[204]

Scheme 96

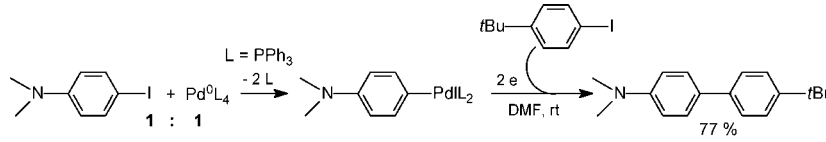

Torii et al. have explored the challenging Pd-catalyzed electroreductive heterocoupling of two different aryl halides ArX and Ar′X′ to generate dissymmetrical biaryls Ar−Ar′.[203] They have established that a reaction performed step by step, using a stoichiometric amount of a Pd(0) complex, leads to the major formation of the dissymmetrical biaryl (Scheme 96). $ArPdXL_2$ formed in the stoichiometric oxidative addition of the aryl halide ArX to $Pd^0(PPh_3)_2$ must be reduced before reacting with the second aryl halide Ar′X′, in agreement with the mechanism proposed by Amatore, Jutand, et al. for the Pd-catalyzed homocoupling of aryl halides: two oxidative additions of aryl halides, separated by a two-electron reduction (Scheme 85, A′ + C).[204] The mechanism of the heterocoupling of two different aryl halides has been further investigated. The first oxidative addition of Pd(0) to aryl halides follows the decreasing reactivity orders[24,26] ArI > ArBr > ArCl; 4-EWG-C_6H_4-X > 4-EDG-C_6H_4-X. If at similar concentrations ArX is more reactive than Ar′X′ in the first oxidative addition, the electrogenerated anionic $ArPd^0L_2^-$ will be first obtained and will react with either ArX or Ar′X′ in the second oxidative addition. Such reaction is about 40 times faster than the first oxidative addition (for the same ArX) but is less sensitive to electronic factors (nevertheless with the same reactivity order).[204] Therefore, the more reactive aryl halide ArX in oxidative additions will favor the formation of ArAr first. ArAr′ will be formed when the concentration of ArX becomes much lower than that of Ar′X′ to allow competition in the second oxidative addition. From this mechanism, one can predict that a Pd-catalyzed electroreductive heterocoupling performed on a stoichiometric mixture of ArI (4-*t*Bu-C_6H_4-I) and Ar′I (4-Me_2N-C_6H_4−I) will lead to a mixture of ArAr, ArAr′ and Ar′Ar′, which has been observed experimentally: 21%, 45%, and 24% yield, respectively.[204] Such a problem may be bypassed if the electrolyses are performed (i) in a two-step batch procedure, each batch involving a stoichiometric amount of palladium as in Scheme 96, or (ii) by a slow introduction of the most reactive aryl halide during the electrolyses, so as to compensate its intrinsic higher reactivity in oxidative addition by a lower concentration.

3.2.3.2. Palladium-Catalyzed Electroreductive Homocoupling of Aryl Triflates. Symmetrical biaryls are synthesized from aryl triflates in the presence of $PdCl_2(PPh_3)_2$ by electroreductive homocoupling (Scheme 97).[95,197] The

Scheme 97

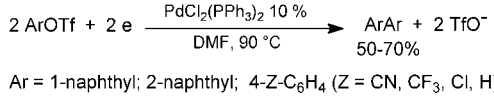

reactions are regiospecific. The electrolyses are performed at the reduction potential of the intermediate complexes $ArPdCl(PPh_3)_2$.[95] The formation of ArAr is a minor side reaction when the electrolyses are performed in the presence of CO_2. This indicates that both reactions, carboxylation and homocoupling, proceed via a common intermediate, the anionic $ArPd^0(PPh_3)_2^-$.[95,204] The mechanism of the homocoupling is displayed in Scheme 89 (paths A + C). In the homocoupling reaction, the aryl triflate is activated twice, in its oxidative addition to the electrogenerated $Pd^0(PPh_3)_2Cl^-$ and in its oxidative addition to the electrogenerated $ArPd^0(PPh_3)_2^-$. Interestingly, the Ar−O bond is selectively cleaved in both oxidative additions.

Scheme 98

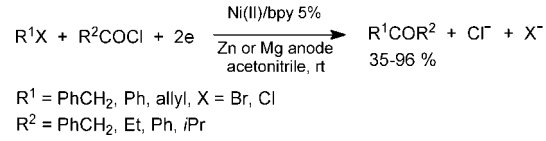

Scheme 99

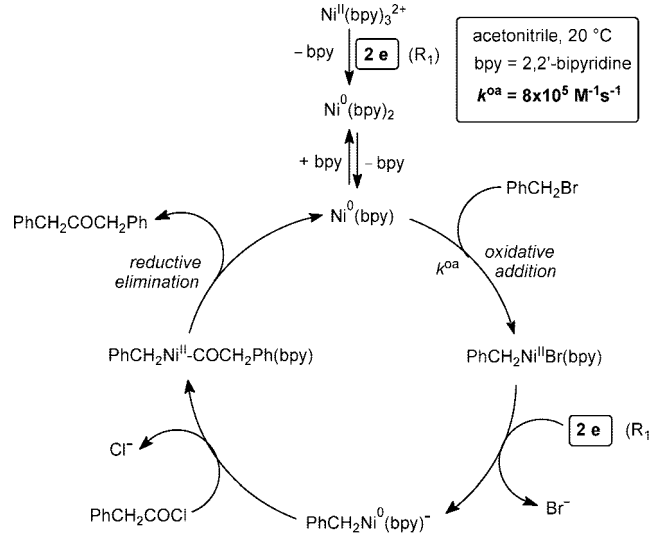

3.2.4. Nickel-Catalyzed Electroreductive Heterocoupling of Organic Halides: Electrosynthesis of Ketones

The reductive heterocoupling of alkyl, benzyl, or aryl halides and acyl chlorides gives ketones in the presence of a Ni(II) catalyst ligated by the bpy ligand, either $NiBr_2(bpy)$ or a cationic complex $Ni(bpy)_3(BF_4)_2$ (Scheme 98).[205]The electrolyses are performed at the reduction potential of the Ni(II) precursor, that is, at a less negative potential than those of the two organic halides. The mechanism of the heterocoupling between $PhCH_2COCl$ and $PhCH_2Br$ catalyzed by $Ni(bpy)_3(BF_4)_2$ has been investigated by Amatore, Jutand, et al. (Scheme 99).[206] A $Ni^0(bpy)$ complex is generated at the beginning of the electrolysis by an overall bielectronic reduction of the precursor $Ni^{II}(bpy)_3^{2+}$ (R_1). The rate constant of its oxidative addition (k^{oa}) to $PhCH_2Br$ giving $PhCH_2Ni^{II}Br(bpy)$ has been determined by fast cyclic voltammetry at a steady disk electrode and is ten times higher than that of $PhCH_2COCl$. The overall two-electron reduction of $PhCH_2Ni^{II}Br(bpy)$ (at the same or at less negative potential than that of $Ni^{II}(bpy)_3^{2+}$ at R_1) generates an anionic complex $PhCH_2Ni^0(bpy)^-$, which does not undergo a second oxidative addition to $PhCH_2Br$ but reacts with $PhCH_2COCl$ (nucleophilic substitution) to give a ketone after reductive elimina-

tion from $PhCH_2Ni^{II}$-$COCH_2Ph(bpy)$.[206] The reductive heterocoupling requires a double activation, chemical activation of the benzylic bromide by a Ni(0) complex followed by activation of the resulting $PhCH_2NiBr(bpy)$ by a two-electron transfer.

3.2.5. Transition Metal-Catalyzed Electrosyntheses of Substituted Cyclopropanes

Substituted cyclopropanes are formed in the $NiBr_2$-catalyzed electroreductive coupling of *gem*-dibromo compounds (CH_2Br_2, CH_3CHBr_2) and electron-deficient alkenes, as reported by Léonel et al. (Scheme 100).[207]When the

Scheme 100

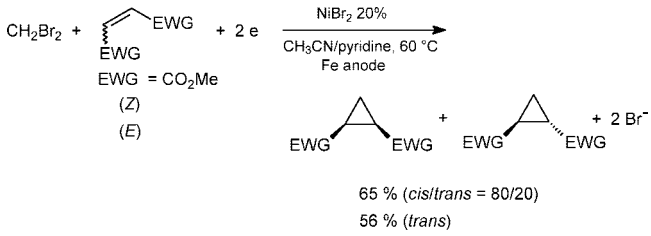

electron-deficient alkene is more easily reduced than the *gem*-dihalide compound ($RCHX_2$), its direct reduction in the presence of $RCHX_2$ leads to substituted cyclopropanes with a stereochemistry opposite to that obtained in the Ni-catalyzed reactions.[208] This points out a change of the mechanism: an ionic mechanism in the noncatalyzed reaction[208] versus a mechanism involving the formation of a Ni-carbene in the catalyzed reaction.[207] A nickel catalyst is thus required when the alkene is less easily reduced than the *gem*-dihalide compound. An electrogenerated Ni(0) must activate $RCHX_2$ by oxidative addition to give RCH(X)−NiX whose further two-electron reduction generates a nickel−carbene [RCH═Ni] prone to react with the alkene to form the substituted cyclopropane together with the active Ni(0).

Electroreductive cyclopropanations of electron-deficient alkenes are also catalyzed by CuBr (Scheme 101), as reported

Scheme 101

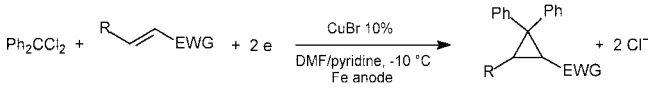

by Paugam et al.[209] Trichloroalkyl derivatives lead to substituted chlorocyclopropanes.[210]

3.3. Transition Metal-Catalyzed Electrosyntheses via Electrochemical Recycling of the Catalyst

Some transition metal-catalyzed reactions may involve organometallic species (generated by chemical activation of an organic substrate by the transition metal), which do not require any subsequent activation by electron transfer. However, the catalytic cycle may generate an inactive catalyst,which must be reduced or oxidized back to its active form. As a consequence, a stoichiometric amount of electrons is required to achieve a catalytic electrosynthesis by recycling the active catalyst at every catalytic cycle. This may be achieved by a direct or mediated electrochemical process.

3.3.1. Direct Electrochemical Recycling of the Catalyst

3.3.1.1. Nickel-Catalyzed Electroreductive Hydrocarboxylation of Alkynes. The electroreductive hydrocarboxylation of alkynes catalyzed by $Ni(bpy)_3(BF_4)_2$ has been reported by Duňach, Périchon et al.[211–214] The reactions performed in an undivided cell equipped with a sacrificial Mg anode afford a mixture of two α,β-unsaturated acids (Scheme 102). The major branched α,β-unsaturated acid is

Scheme 102

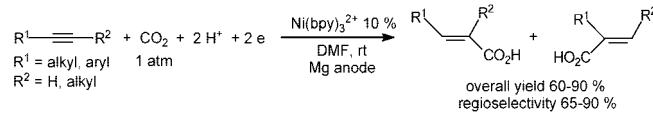

obtained from terminal alkynes.[211,212]A mechanism is proposed by the same group (Scheme 103).[214] The electrochemical reduction of the Ni(II) precursor generates a Ni(0) complex, which can coordinate both CO_2 and the alkyne in two different positions. An intramolecular oxidative coupling between the ligated CO_2 and alkyne gives two isomeric cyclic Ni(II) carboxylates. The exchange by Mg^{2+} cations produced at a sacrificial Mg anode and the cleavage of the Ni−C bond by protons release the α,β-unsaturated carboxylic acids and the $Ni(bpy)_3^{2+}$ precursor, which is recycled back to the active Ni(0) complex by reduction at the cathode. Therefore, the activation of intermediate organometallic species is not required. The electrons are only used to generate and regenerate the active Ni(0) complex at each catalytic cycle, and the electrolyses are carried out at the reduction potential of the Ni(II) precursor.[214]The same group has developed the electroreductive hydrocarboxylation of non conjugated diynes (catalyst, $Ni(bpy)_3(BF_4)_2$) or $NiBr_2$(PMDTA), PMDTA = pentamethyldiethylenetriamine),[215] 1,3-diynes (catalyst, $NiBr_2$(PMDTA),[216] 1,3-enynes (catalyst, $NiBr_2$(PMDTA) or $Ni(bpy)_3(BF_4)_2$),[217] alkenes (catalyst, $NiBr_2$(PMDTA), P_{CO_2} = 1 atm),[218,219] and allenes (catalyst, $NiBr_2$(PMDTA) or $Ni(bpy)_3(BF_4)_2$; P_{CO_2} = 1−5 atm).[220] Terminal alkynes are more reactive than internal alkynes and alkenes.

3.3.1.2. Nickel-Catalyzed Electroreductive Hydroarylation of Electron-Deficient Alkenes. Nickel(II) salts catalyze the electroreductive hydroarylation of electron-deficient alkenes CH_2═CH-EWG (EWG = CO_2R,[221] COR,[221,222] and CN[222]) (Scheme 104), as reported by Condon et al. The electrolyses are performed in an undivided cell equipped with a sacrificial Fe anode. A tentative mechanism is proposed by the same group.[222] The electrochemical reduction of the Ni(II) salt or pyridine complex to a Ni(0) moieties occurs at the very beginning of the electrolysis. A complex $ArCH_2$-CH(EWG)-$Ni^{II}X$ would be formed as in a Heck reaction, but the β-hydride elimination does not take place. The saturated final product $ArCH_2$-CH_2-EWG is released together with a Ni(II) moiety, which is reduced back to the active Ni(0) at the cathode. The electrolyses are conducted at the reduction potential of the Ni(II) precursor, and no organonickel intermediate is described as being activated by electron transfer.

Condon et al. have extended their reactions to heteroaryl halides[223] and vinylic halides.[224,172] The electrosyntheses from aryl halides have also been performed in protic solvents, such as ethanol (catalyst, $NiBr_2$ and dpa, 1:1),[171] or in ionic liquids without any pyridine or ligands since the methylimidazolium may serve as ligand for Ni(II) and Ni(0) centers.[166]

The $NiBr_2$-catalyzed electroreductive hydroarylation of electron-deficient alkenes has been used as the first step toward the synthesis of aromatic lactones.[225] The intramolecular version of the $NiBr_2$-catalyzed hydroarylation of electron-deficient alkenes from aryl halides tethered to an

Scheme 103

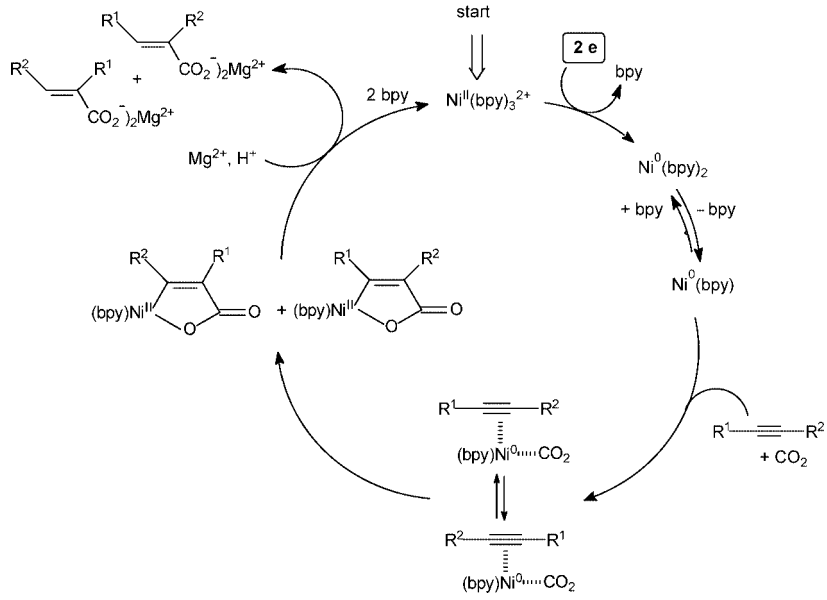

Scheme 104

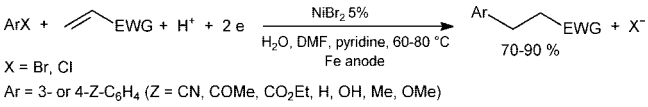

Scheme 105

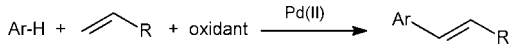

Scheme 106

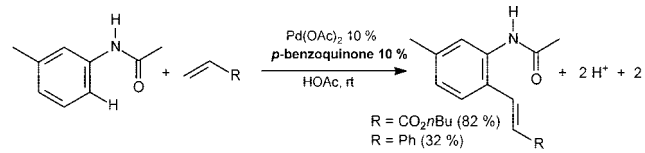

acrylic or fumaric moiety through an ester or amide function has been developed by Nédélec et al.[226] Similar reactions catalyzed by $CoBr_2$ associated with the bpy ligand have been reported by Gosmini et al.[227]

Other examples of such metal-catalyzed electrosyntheses where the electrons are not used to activate intermediate organometallic species but to recycle the catalyst are reported in reviews.[144,147,148]

3.3.2. Mediated Electrochemical Recycling of the Catalyst

3.3.2.1. Palladium/*p*-Benzoquinone-Catalyzed Electrooxidative Heck-Type Reactions from Arenes. Classical Heck reactions are performed from aryl halides, ArX, and are catalyzed by Pd(0) complexes, but halide ions are released as waste (Schemes 3, 51, and 54). Pd-catalyzed Heck-type reactions from arenes, ArH (widespread, cheap, no waste), as pioneered by Fujiwara et al.[228] but working under mild conditions, remained a challenge (Scheme 105).Such reactions indeed require a Pd(II) catalyst able to activate the Ar−H bond and a *stoichiometric* amount of oxidant (such as *p*-benzoquinone) to oxidize the Pd(0) formed in every catalytic cycle back to the active Pd(II) catalyst.[229]Amatore, Jutand, et al. have reported $Pd(OAc)_2$-catalyzed electrooxidative Heck-type reactions from an arene and alkenes (*n*-butylacrylate, styrene) in the presence of a *catalytic* amount of *p*-benzoquinone (or *p*-hydroquinone) (Scheme 106). The reactions are performed in acetic acid in a divided cell at room temperature.[230]

Most steps of the catalytic cycles are similar to those of a classical Heck reaction performed from ArX, except that the aryl−palladium(II) complex prone to react with the alkene is formed by activation of the Ar−H bond by $Pd(OAc)_2$ (Scheme 107). This key step is made faster when the arene has a substituent Z (the amido group in the present case)[229,230] able to coordinate $Pd(OAc)_2$ to favor an intramolecular orthopalladation (Scheme 107).[231]

After the classical carbopalladation, C−C internal rotation, and β-hydride elimination, a reductive elimination from HPd(OAc) generates a Pd(0) moiety,[232] which is oxidized to the active Pd(II) by *p*-benzoquinone (Scheme 107).[233] The latter is used in a catalytic amount because it is recycled by oxidation at the anode of the *p*-hydroquinone formed in the chemical oxidation of Pd(0) (Scheme 108). The catalytic cycle does not involve any activation of intermediate organopalladium complexes by electron transfer, but a stoichiometric amount of electrons is required to recycle the *p*-benzoquinone at every catalytic cycle.

In contrast to Heck reactions from aryl halides, which require high temperatures and a base, the reactions from ArH (Scheme 106) are performed at room temperature without any base. Indeed, the reversible reductive elimination from HPd(OAc) is shifted by the *p*-benzoquinone, which is both a ligand and a chemical oxidant of the transient Pd(0), as established by Bäckvall.[233] An electrolysis has been performed in the absence of *p*-benzoquinone via the direct oxidation of the Pd(0) at the anode, but the reaction is slower, due to catalyst desactivation.[230]

3.3.2.2. Palladium/*p*-Benzoquinone-Catalyzed Electrooxidation of Alcohols. Amatore, Jutand, et al. have reported electrochemical oxidations of primary or secondary alcohols to aldehydes or ketones, respectively, under anaerobic conditions in the presence of a base and a catalytic amount of $Pd(OAc)_2$ associated with catalytic *p*-benzoquinone (Scheme 109).[234]

The mechanism is displayed in Scheme 110.[234] The investigated secondary or primary alcohols do not exhibit any oxidation peak in DMF (potentials up to +2 V vs SCE

Scheme 107

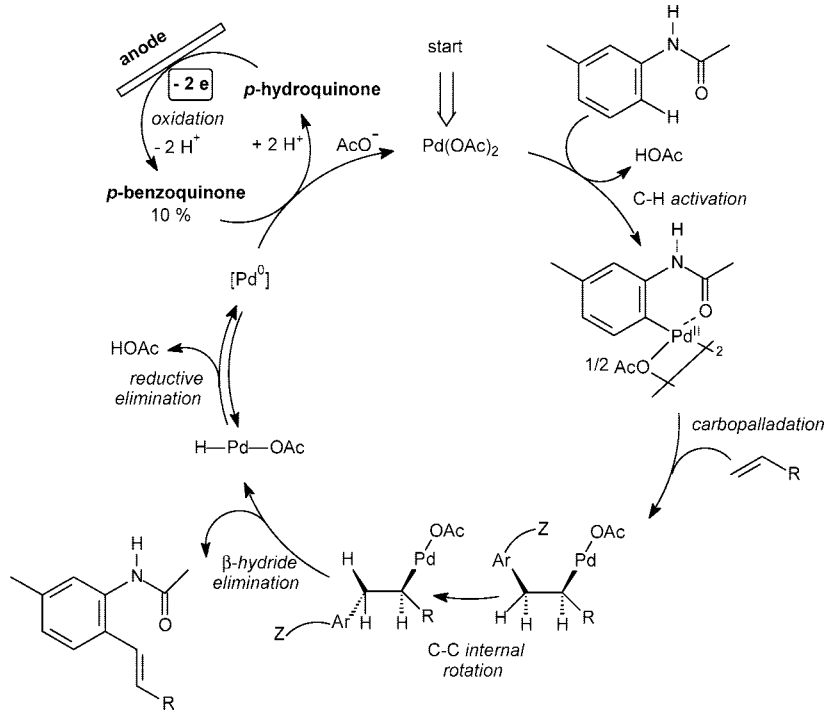

Scheme 108

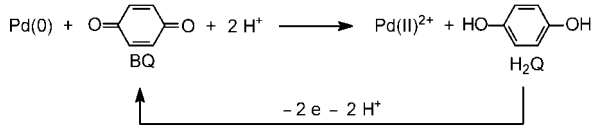

Scheme 109

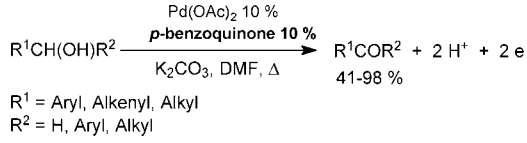

Scheme 110

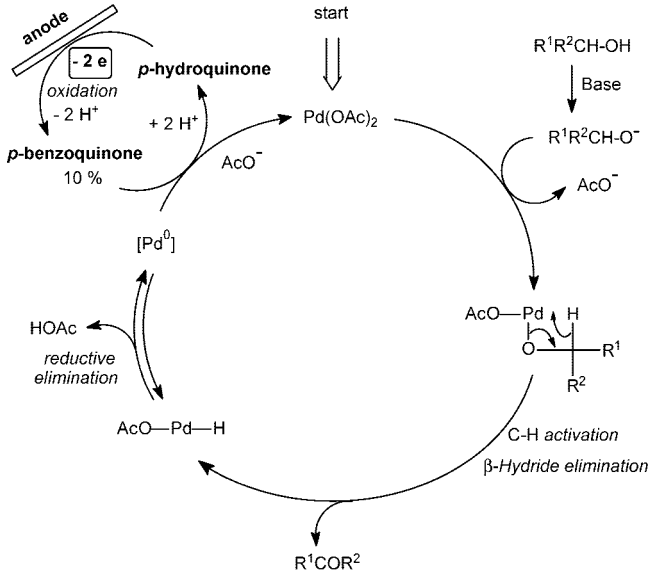

at a glassy carbon electrode). No oxidation peak is observed after addition of K_2CO_3 as a base, which is indicative of a slow deprotonation process at 25 °C. A Pd(II)-alkoxide is formed by substitution of one acetate ligand of $Pd(OAc)_2$ by the alkoxide at sufficiently high temperature (80 °C). It undergoes a β-hydride elimination, which generates the aldehyde or the ketone and HPd(OAc). A reductive elimination affords a Pd(0) moiety, which is oxidized to the active Pd(II) catalyst by *p*-benzoquinone. The latter is made catalytic by oxidation of *p*-hydroquinone at the anode (Scheme 108). $Pd(OAc)_2$ and $Pd^0(PPh_3)_4$ may be used as catalysts without any *p*-benzoquinone, but the reactions are slower due to catalyst decomposition.[234]

This anaerobic electrochemical process is quite general and selective and avoids the formation of H_2O_2, as generated in aerobic $Pd(OAc)_2$-catalyzed oxidation of alcohols whose rate is moreover limited by the rate-determining slow dissolution of O_2 into organic solvents.[235,236]

3.3.2.3. Palladium/*p*-Hydroquinone-Catalyzed 1,4-Electrooxidation of 1,3-Dienes. The electrooxidation of cyclohexa-1,3-diene in the presence of LiOAc is catalyzed by $Pd(OAc)_2$ associated with catalytic *p*-hydroquinone, as reported by Bäckwall and Gogoll.[237] The reaction leads to *cis*-1,4-diacetocyclohex-2-ene or to 1-aceto-4-chlorocyclohex-2-ene when performed in the presence of excess LiCl (Scheme 111). The catalytic cycle is initiated by reaction of

Scheme 111

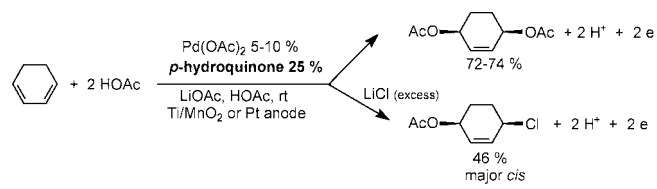

$Pd(OAc)_2$ with the diene. After two successive nucleophilic attacks of AcO^- (or AcO^- then Cl^-), a Pd(0) moiety is formed and is oxidized back to Pd(II) by *p*-benzoquinone. The latter is recycled by oxidation of *p*-hydroquinone at a Pt or Ti/MnO_2 anode. MnO_2 serves as a redox mediator.

3.3.2.4. Palladium-Catalyzed Electrooxidative Wacker Reactions. The Wacker process, oxidation of alkenes

$RCH{=}CH_2$ to aldehydes or ketones is catalyzed by $Pd^{II}X_2$ salts (e.g., $PdCl_2$).[10] The mechanism involves a complexation of the alkene to the Pd(II) salt, followed by the external nucleophilic trans attack of H_2O onto the ligated alkene (two possible attack sites according to the R group).[238] A β-hydride elimination from RCH(PdX)-CH_2OH or RCH(OH)-CH_2 PdX delivers the aldehyde or the ketone, respectively, and HPdX whose reductive elimination gives a Pd(0) moiety. The latter must be recycled back to the active Pd(II) by an oxidation process. The chemical oxidant is often a Cu(II) salt (e.g., $CuCl_2$) used in catalytic amount because it is recycled by the oxidation of Cu(I) by O_2.

Torii et al. have reported the electrochemical version using $PdCl_2$ or $Pd(OAc)_2$ as catalysts and a catalytic amount of $(4\text{-Br-}C_6H_4)_3N$ as redox mediator (Scheme 112).[239] Tanaka

Scheme 112

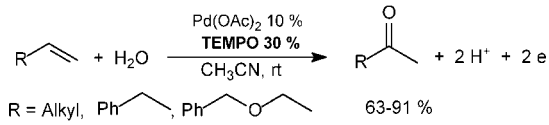

et al. have reported similar reactions using $Pd(OAc)_2$ as catalyst and a catalytic amount of TEMPO as redox mediator (Scheme 112).[240] According to Tanaka et al., a more reactive cationic $Pd(CH_3CN)_4^{2+}$ complex is formed via the oxidation of the acetate ligands of $Pd(OAc)_2$ at the very beginning of the electrolysis. The oxidation of TEMPO at the anode generates $TEMPO^+$, which oxidizes the Pd(0) formed at the end of each catalytic cycle back to the active Pd(II). TEMPO is regenerated in this homogeneous oxidation and can therefore be used in a catalytic amount.[240]

3.3.2.5. Osmium-Catalyzed Asymmetric Dihydroxylation of Alkenes. Osmium(VIII) (OsO_4) associated with a chiral ligand (e.g., L* = dihydroquinidine (DHQD), dihydroquinine (DHQ), or their derivatives such as $(DHQD)_2PHAL$) catalyzes the asymmetric dihydroxylation of alkenes, as reported by Sharpless et al.[241] The reactions are made catalytic in the presence of a chemical oxidant used in a stoichiometric amount to oxidize Os(VI) species formed in the catalytic cycle back to Os(VIII) species (e.g., *N*-methylmorpholine *N*-oxide (NMO) associated with catalytic OsO_4[241] or $K_3Fe(CN)_6$[241,242] or oxygen[242] associated with catalytic $K_2OsO_2(OH)_4$ in *t*BuOH/H_2O) (Scheme 113). An

Scheme 113

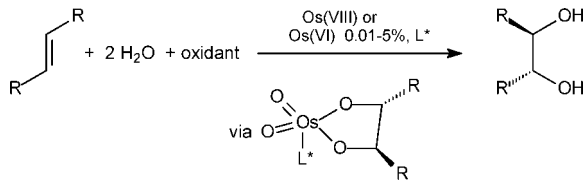

electrochemical oxidation has been developed as an alternative to regenerate OsO_4 from Os(VI) species, either directly[243,244] or mediated by a chemical oxidant used in a catalytic amount ($K_4Fe(CN)_6$,[243–245] I_2[246]), which is recycled by oxidation at the anode of its reduced form. The electrosyntheses are performed in basic medium in undivided cells. The proton is reduced at the cathode. The enantioselectivity is similar to that obtained in the presence of a stoichiometric amount of the oxidant (Scheme 114).

3.3.2.6. Palladium-Catalyzed Electrocarbonylation of Aryl Halides: Electrosynthesis of Aromatic Aldehydes.

Scheme 114

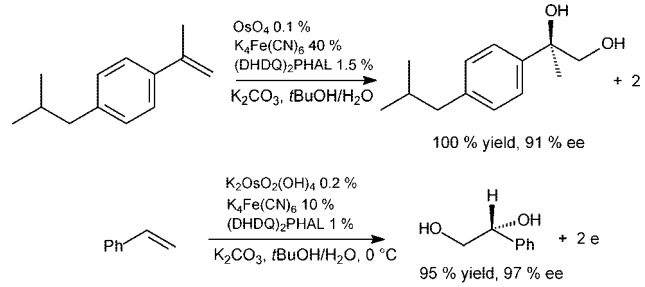

$PdCl_2(PPh_3)_2$ or $Pd^0(PPh_3)_4$ catalyze the electrosyntheses of aromatic aldehydes from aryl iodides and carbon monoxide in the presence of formic acid (Scheme 115), as reported by

Scheme 115

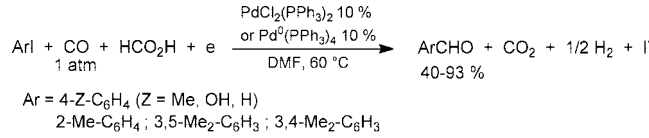

Carelli et al.[100] The electrosyntheses consume one electron per mole of aryl iodide and are all performed at the same potential (−1.5 V vs SCE).

The mechanism of the reaction catalyzed by $Pd^0(PPh_3)_4$ has been investigated by Amatore, Jutand, et al. (Scheme 116).[100,103] The oxidative addition of PhI is slower in the

Scheme 116

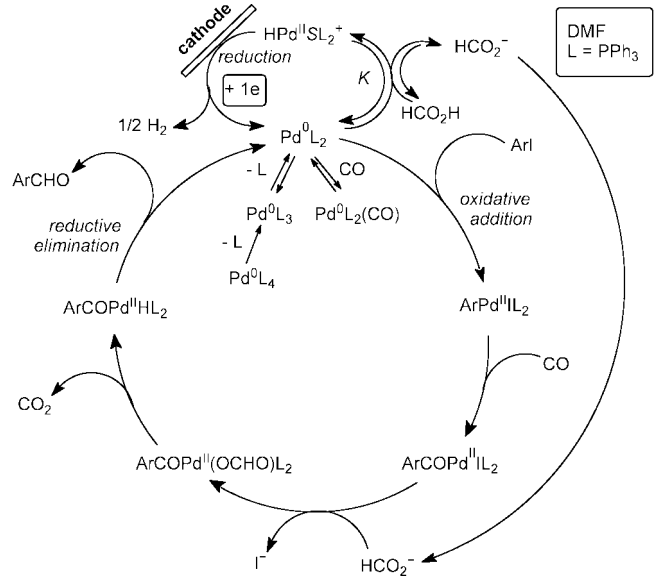

presence of CO by formation of nonreactive $Pd^0(PPh_3)_2(CO)$. An acyl−palladium(II) complex, $ArCOPdI(PPh_3)_2$, is generated in the carbonylation of $ArPdI(PPh_3)_2$ formed in the oxidative addition of $Pd^0(PPh_3)_2$ to ArI. Whatever the aryl iodides, the electrolyses are performed at the same potential, which is less negative than the reduction potential of $ArCOPdI(PPh_3)_2$,[247] suggesting that the latter is not reduced in the reaction. $ArCOPdI(PPh_3)_2$ reacts with formate ions, HCO_2^-, which are generated in the reversible oxidative addition of $Pd^0(PPh_3)_2$ to formic acid (Scheme 44 in section 2.6.3).[103] A classical decarboxylation in ArCOPd(OCHO)$(PPh_3)_2$ generates $ArCOPdH(PPh_3)_2$ and eventually the aromatic aldehyde and $Pd^0(PPh_3)_2$ by reductive elimination. Therefore, part of the Pd(0) is consumed in its reversible

oxidative addition to formic acid. The reaction also generates the hydrido complex, $HPd^{II}(DMF)(PPh_3)_2^+$ evidenced by conductivity measurement (Scheme 44 in section 2.6.3).[103] The latter is reduced at the cathode back to the active $Pd^0(PPh_3)_2$ at −0.99 V vs SCE, as established by cyclic voltammetry.[100]

Interestingly, the Pd(0) complex catalyzes the reduction of the protons of acetic acid to H_2 via the reduction of $HPd^{II}(DMF)(PPh_3)_2^+$ (−0.99 V instead of −2.0 V for acetic acid at a glassy carbon electrode in DMF).[100]

4. Conclusion

Electrochemical techniques have been used in association with spectroscopic techniques (mainly ^1H, ^{31}P NMR) to investigate the mechanism of transition metal-catalyzed reactions, even if they do not involve any electron transfer at an electrode, as shown in section 2 for palladium-catalyzed reactions (Heck, C−C and C−S cross-coupling, Stille, and Sonogashira reactions, etc.).

Electrochemistry has been used as an analytical technique to characterize the true reactive organometallic species (often present at very low concentration) generated from unreactive precursors or unreactive organometallic species. Their reactivity has been characterized by the determination of rate constants, as well. Electrochemistry has been used to characterize or mimic chemical reductions occurring in situ in elemental steps of catalytic cycles. Fast reactive organometallic species have been generated by electrochemical techniques, and their reactivity has been investigated by the same techniques.

The mechanism of all steps has been investigated under experimental conditions as close as possible to those of catalytic reactions (same precursor, ligand, reagents, additive, and solvent). The unexpected key role of precursors (precatalysts) has been established. Indeed, precursors have a great impact on the rate of elemental steps of catalytic cycles and consequently on the efficiency of catalytic reactions by delivering either anions (I^-, Br^-, Cl^-, AcO^-) or neutral ligands (dba, phosphine), which can coordinate reactive Pd(0) or Pd(II) complexes or control their concentration. Catalytic cycles of palladium-catalyzed reactions are proposed that involve unexpected organometallic species (anionic Pd(0) or Pd(II) complexes, $ArPd(OAc)L_2$ complexes, etc.). The existence of literature-postulated organometallic species has been confirmed by means of electrochemical techniques (Pd^0L_2, $HPdSL_2^+$, $ArPdSL_2^+$, (η^3-allyl)PdL_2^+, etc.).

Electrochemical techniques can of course be used to investigate the mechanism of transition metal-catalyzed electrosyntheses, as shown in section 3.

Electrons are used as stoichiometric reagents in transition metal-catalyzed electrosynthesis. Transition metal catalysts are required when the organic substrates are not electroactive or when their direct activation by electron transfer does not generate the desired product. Transition metal-catalyzed electrosyntheses proceed via a succession of chemical activation of organic substrates by the catalyst and activation of organometallic intermediates by electron transfer (one- or two-electron transfer). Those two kinds of activation are required to achieve the desired electrosynthesis. Electrons are also used as stoichiometric reagents for the recycling of unreactive species formed in a catalytic cycle to active ones, either by direct or by mediated electrochemical processes. Activation by both transition metal and electron transfer are quite complementary and synergistic.

5. Abbreviations

Binap	2,2′-bis(diphenylphosphino)-1,1'binaphthyl
bpy	2,2′-bipyridyl
COD	1,5-cyclooctadiene
Cy	cyclohexyl
dba	(*E*,*E*)-dibenzylideneacetone
DBP	1-phenyldibenzophosphole
$(DHQD)_2PHAL$	hydroquinine 1,4-phthalazinediyl diether
DMF	dimethylformamide
dpa	2,2′-dipyridylamine
dppe	1,2-diphenylphosphinoethane
dppb	1,4-diphenylphosphinobutane
dppf	1,1′-bis(diphenylphosphino)ferrocene
dppp	1,3-diphenylphosphinopropane
diop	*O*-isopropylidene-2,3-dihydroxy-1, 4-bis(diphenylphosphino)butane
EDG	electron-donating group
EWG	electron-withdrawing group
ferrocene	dicyclopentadienyliron
HMPA	hexamethylenephosphorotriamide
NHC	*N*-heterocyclic carbene
NMP	*N*-methyl-2-pyrrolidone
o-Tol	*ortho*-tolyl
PMDTA	pentamethyldiethylenetriamine
pte	1,2-phenylthioethane
RDE	rotating disk electrode
rds	rate-determining step
SCE	saturated calomel electrode
TEMPO	2,2′-tetramethylpiperidyloxide
TFP	tri-2-furylphosphine
THF	tetrahydrofuran
TMU	tetramethylurea

6. References

(1) *Principles and Applications of Organotransition Metal Chemistry*; Collman, J. P., Hegedus, L. S., Norton, J. R., Finke, R. G., Eds.; Oxford University Press: Mill Valley, CA, 1987.
(2) *Comprehensive Organometallic Chemistry III*; Crabtree, R., Mingos, M., Eds.; Elsevier: Amsterdam, 2006, Vols *1*−*13*.
(3) Amatore, C.; Jutand, A. *J. Organomet. Chem.* **1999**, *576*, 254.
(4) Kozuch, S.; Amatore, C.; Jutand, A.; Shaik, S. *Organometallics* **2005**, *24*, 2319.
(5) Faulkner, L. R. *J. Chem. Educ.* **1983**, *60*, 262.
(6) Bard, A. J.; Faulkner, L. R. *Electrochemical Methods. Fundamentals and Applications*, 2nd ed.; Wiley: New York, 2001.
(7) Savéant, J.-M. *Elements of Molecular and Biomolecular Electrochemistry. An Electrochemical Approach to Electron Transfer Chemistry*; Wiley: Hoboken, NJ, 2006.
(8) Amatore, C. In *Electrochemistry at Ultramicroelectrodes in Physical Electrochemistry*; Rubinstein, I., Ed.; Marcel Dekker, New York, 1995; Chapter 4.
(9) Atkins, P. W. *Physical Chemistry*, 5th ed.; University Press: 1994.
(10) *Handbook of Organopalladium Chemistry for Organic Synthesis*; Negishi, E.-i., Ed.; Wiley-Interscience, New York, 2002, Vols. *I and II*.
(11) For the history of Pd-catalyzed reactions, see: Tsuji, J. *New J. Chem.* **2000**, *24*, 127.
(12) Mizoroki, T.; Mori, K.; Ozaki, A. *Bull. Soc. Chim. Jpn.* **1971**, *44*, 581.
(13) Heck, R. F.; Nolley, J. P., Jr *J. Org. Chem.* **1972**, *37*, 2320.
(14) Cassar, L. *J. Organomet. Chem.* **1975**, *93*, 253.
(15) Dieck, H. A.; Heck, R. F. *J. Organomet. Chem.* **1975**, *93*, 259.
(16) Sonogashira, K.; Tohda, Y.; Hagihara, N. *Tetrahedron Lett.* **1975**, *50*, 4467.
(17) Fauvarque, J.-F.; Jutand, A. *Bull. Soc. Chim.* **1976**, 765.
(18) Negishi, E.-i.; King, A. O.; Okukado, N. *J. Org. Chem.* **1977**, *42*, 1821.
(19) Fauvarque, J.-F.; Jutand, A. *J. Organomet. Chem.* **1977**, *132*, C17.
(20) Milstein, D.; Stille, J. K. *J. Am. Chem. Soc.* **1979**, *101*, 4992.
(21) Miyaura, N.; Suzuki, A. *J. Chem. Soc., Chem. Commun.* **1979**, *19*, 866.
(22) Hatanaka, Y.; Hiyama, T. *Tetrahedron Lett.* **1988**, *29*, 97.

(23) Fitton, P.; Johnson, M. P.; McKeon, J. E. *J. Chem. Soc., Chem. Commun.* **1968**, 6.
(24) Fitton, P.; Rick, E. A. *J. Organomet. Chem.* **1971**, *28*, 287.
(25) Mann, B. E.; Musco, A. *J. Chem. Soc., Dalton Trans.* **1975**, 1673.
(26) Fauvarque, J. F.; Pflüger, F.; Troupel, M. *J. Organomet. Chem.* **1981**, *208*, 419.
(27) Amatore, C.; Jutand, A.; Khalil, F.; M'Barki, M. A.; L.; Mottier, L *Organometallics* **1993**, *12*, 3168.
(28) Amatore, C.; Pflüger, F. *Organometallics* **1990**, *9*, 2276.
(29) Tsou, T. T.; Kochi, J. K. *J. Am. Chem. Soc.* **1979**, *101*, 6319.
(30) Jutand, A.; Mosleh, A *Organometallics* **1995**, *14*, 1810.
(31) Ritter, K. *Synthesis* **1993**, 735.
(32) Sakamoto, T.; Kondo, Y.; Mutura, N.; Yamanaka, H. *Tetrahedron* **1993**, *49*, 9713.
(33) Kakino, R.; Yasumi, S.; Shimizu, I.; Yamamoto, A. *Bull. Chem. Soc. Jpn.* **2002**, *75*, 137.
(34) Jutand, A.; Negri, S.; de Vries, J. G. *Eur. J. Inorg. Chem.* **2002**, 1711.
(35) Amatore, C.; Godin, B.; Jutand, A.; Ferber, B.; Top, S.; Jaouen, G. *Organometallics* **2007**, *23*, 3887.
(36) Yamamura, M.; Moritani, S. I.; Murahashi, J. *J. Organomet. Chem.* **1975**, *91*, C39.
(37) Fauvarque, J.-F.; Jutand, A *J. Organomet. Chem.* **1981**, *209*, 109.
(38) Jutand, A.; Negri, S. *Organometallics* **2003**, *22*, 422.
(39) Amatore, C.; Jutand, A. *Coord. Chem. Rev.* **1998**, *178*−*180*, 511.
(40) Amatore, C.; Jutand, A.; Meyer, G. *Inorg. Chim. Acta* **1998**, *273*, 76.
(41) Amatore, C.; Jutand, A.; Meyer, G.; Atmani, H.; Khalil, F.; Ouazzani Chahdi, F. *Organometallics* **1998**, *17*, 2958.
(42) Amatore, C.; Jutand, A.; Thuilliez, A. *J. Organomet. Chem.* **2002**, *643*−*644*, 416.
(43) Amatore, C.; Bucaille, A.; Fuxa, A.; Jutand, A.; Meyer, G.; Ndedi Ntepe, A. *Chem.*−*Eur. J.* **2001**, *7*, 2134.
(44) Yin, J.; Rainka, M. P.; Zhang, X.-X.; Buchwald, S. L. *J. Am. Chem. Soc.* **2002**, *124*, 1162.
(45) Amatore, C.; Broeker, G.; Jutand, A.; Khalil, F. *J. Am. Chem. Soc.* **1997**, *119*, 5176.
(46) Paladino, G.; Madec, D.; Prestat, G.; Maitro, G.; Poli, G.; Jutand, A *Organometallics* **2007**, *26*, 455.
(47) Amatore, C.; Fuxa, A.; Jutand, A. *Chem.*−*Eur. J.* **2000**, *6*, 1474.
(48) Macé, Y.; Kapdi, A. R.; Fairlamb, I. J. S.; Jutand, A. *Organometallics* **2006**, *25*, 1795.
(49) Amatore, C.; Carré, C.; Jutand, A.; Medjour, Y. *Organometallics* **2002**, *21*, 4540.
(50) Amatore, C.; Bensalem. S.; Ghalem, S.; Jutand, A.; Medjour, Y. *Eur. J. Org. Chem.* **2004**, 366.
(51) Jutand, A. *Pure Appl. Chem.* **2004**, *76*, 565.
(52) Yoshida, T.; Otsuka, S. *Inorg. Synth.* **1990**, *28*, 113.
(53) Paul, F.; Patt, J.; Hartwig, J. F. *Organometallics* **1995**, *4*, 3030.
(54) Galardon, E.; Ramdeehul, S.; Brown, J. M.; Cowley, A.; Hii, K. K.; Jutand, A. *Angew. Chem., Int. Ed.* **2002**, *41*, 1760.
(55) Kurbangalieva, A.; Hii, K. K.; Galardon, E.; Carmichael, D.; Brown, J. M.; Jutand, A. Manuscript in preparation.
(56) Hartwig, J. F.; Paul, F. *J. Am. Chem. Soc.* **1995**, *117*, 5373.
(57) Amatore, C.; Azzabi, M.; Jutand, A. *J. Organomet. Chem.* **1989**, *363*, C41.
(58) Amatore, C.; Azzabi, M.; Jutand, A. *J. Am. Chem. Soc.* **1991**, *113*, 8375.
(59) Amatore, C.; Azzabi, M.; Calas, P.; Jutand, A.; Lefrou, C.; Rollin, Y. *J. Electroanal. Chem.* **1990**, *288*, 45.
(60) Kozuch, S.; Shaik, S.; Jutand, A.; Amatore, C. *Chem.*−*Eur. J.* **2004**, *10*, 3072.
(61) Negishi, E.-i.; Takahashi, T.; Akiyoshi, K *J. Chem. Soc., Chem. Commun.* **1986**, 1338.
(62) Amatore, C.; Jutand, A. *Acc. Chem. Res.* **2000**, *33*, 314.
(63) Negishi, E.-i *Bull. Soc. Chim. Jpn* **2007**, *80*, 233.
(64) Herrmann, W. A.; Elison, M.; Fischer, J.; Köcher, C.; Artus, G. R. J. *Angew. Chem., Int. Ed. Engl.* **1995**, *34*, 2371.
(65) Cloke, F. G. N.; Geldbach, T.; Hitchcock, P. B. *Organometallics* **1999**, *18*, 3228.
(66) Titcomb, L. R.; Caddick, S.; Clocke, F. G. N.; Wilson, D. J.; McKerrecher, D. *Chem. Commun.* **2001**, 1388.
(67) Guinness, D. S.; Cavell, K. J.; Skelton, B. W.; White, A. H. *Organometallics* **1999**, *18*, 1596.
(68) Caddick, S.; Cloke, F. G. N.; Hitchcock, P. B.; Leonard, J.; Lewis, A. K. K.; McKerrecher, D.; Titcomb, L. R. *Organometallics* **2002**, *21*, 4318.
(69) Lewis, A. K. K.; Caddick, S.; Cloke, F. G. N.; Billingham, N. C.; Hitchcock, P. B.; Leonard, J. *J. Am. Chem. Soc.* **2003**, *125*, 10066.
(70) Pytkowicz, J.; Roland, S.; Mangeney, P.; Meyer, G.; Jutand, A. *J. Organomet. Chem.* **2003**, *678*, 166.
(71) Roland, S.; Mangeney, P.; Jutand, A. *Synlett* **2006**, 3088.
(72) Dieck, H. A.; Heck, R. F. *J. Am. Chem. Soc.* **1974**, *96*, 1133.
(73) Heck, R. F. *Org. React.* **1982**, *27*, 345.
(74) Amatore, C.; Jutand, A.; M'Barki, M. A. *Organometallics* **1992**, *11*, 3009.
(75) Osawa, F.; Kubo, A.; Hayashi, T. *Chem. Lett.* **1992**, 2177.
(76) Amatore, C.; Carré, E.; Jutand, A.; M'Barki, M. A.; Meyer, G *Organometallics* **1995**, *14*, 1818.
(77) Amatore, C.; Jutand, A.; Lemaître, F.; Ricard, J. L.; Kozuch, S.; Shaik, S. *J. Organomet. Chem.* **2004**, *689*, 3728.
(78) Amatore, C.; Jutand, A.; Medeiros, M. J. *New J. Chem.* **1996**, *20*, 1143.
(79) Amatore, C.; Blart, E.; Genêt, J. P.; Jutand, A.; Lemaire-Audoire, S.; Savignac, M. *J. Org. Chem.* **1995**, *60*, 6829.
(80) Gélin, E.; Amengual, R.; Michelet, V.; Savignac, M.; Jutand, A.; Genêt, J. P. *Adv. Synth. Catal.* **2004**, *346*, 1733.
(81) Amatore, C.; Carré, E.; Jutand, A.; M'Barki, M. A.; Meyer, G. *Organometallics* **1995**, *14*, 5605.
(82) Cabri, W.; Candiani, I. *Acc. Chem. Res.* **1995**, *28*, 2.
(83) Amatore, C.; Jutand, A.; Thuilliez, A. *Organometallics* **2001**, *20*, 3241.
(84) Herrmann, W. A.; Brossmer, C.; Öfele, K.; Reisinger, C.-P.; Priermeier, T.; Beller, M.; Fischer, H. *Angew. Chem., Int. Ed.* **1995**, *34*, 1844.
(85) Herrmann, W. A.; Böhm, V. P. W.; Reisinger, C.-P. *J. Organomet. Chem.* **1999**, *576*, 23.
(86) Louie, J.; Hartwig, J. F. *Angew. Chem., Int. Ed.* **1996**, *35*, 2359.
(87) Sundermann, A.; Uzan, O.; Martin, J. M. L. *Chem.*−*Eur. J.* **2001**, *7*, 1703.
(88) Beller, M.; Riermeier, T. H. *Eur. J. Inorg. Chem.* **1998**, 29.
(89) Böhm, V. P. W.; Herrmann, W. A. *Chem.*−*Eur. J.* **2001**, *7*, 4191.
(90) d'Orlyé, F.; Jutand, A. *Tetrahedron* **2005**, *61*, 9670.
(91) Farina, V.; Krishnan, B. *J. Am. Chem. Soc.* **1991**, *113*, 9585.
(92) Amatore, C.; Bahsoun, A. A.; Jutand, A.; Meyer, G.; Ndedi Ntepe, A.; Ricard, L. *J. Am. Chem. Soc.* **2003**, *125*, 4212.
(93) Amatore, C.; Carré, C.; Jutand, A. *Acta Chem. Scand.* **1998**, *52*, 100.
(94) For a review on the characterization of coordination compounds by conductivity measurements, see: Geary, W. J. *Coord. Chem. Rew.* **1971**, *7*, 81.
(95) Jutand, A.; Mosleh, A. *J. Org. Chem.* **1997**, *62*, 261.
(96) Farina, V.; Krishnan, B.; Marshall, D. R.; Roth, G. P. *J. Org. Chem.* **1993**, *58*, 5434.
(97) Hii, K. K.; Thornton-Pett, M.; Jutand, A.; Tooze, R. P *Organometallics* **1999**, *18*, 1887.
(98) Trost, B. M.; Pfrengle, W.; Urabe, H.; Dumas, J. *Acc. Chem. Res.* **1990**, *23*, 34.
(99) Zargarian, D.; Alper, H. *Organometallics* **1993**, *12*, 712.
(100) Carelli, I.; Chiarotto, I.; Cacchi, S.; Pace, P.; Amatore, C.; Jutand, A.; Meyer, G. *Eur. J. Org. Chem.* **1999**, 1471.
(101) For a review on hydrido complexes of palladium, see: Grushin, V. V *Chem. Rev.* **1996**, *96*, 2011.
(102) Trost, B. M. *Chem.*−*Eur. J.* **1998**, *4*, 2405.
(103) Amatore, C.; Jutand, A.; Meyer, G.; Carelli, I.; Chiarotto, I. *Eur. J. Inorg. Chem.* **2000**, 1855.
(104) Tsuji, J. *Palladium Reagents and catalysts*; John Wiley & Sons: Chichester, U.K., 1996, p 290.
(105) Trost, B. M. *Acc. Chem. Res.* **1996**, *29*, 355.
(106) Trost, B. M.; Verhoeven, T. R.; Fortunak, J. F.; McElvain, S. M. *Tetrahedron Lett.* **1979**, *25*, 2301.
(107) For seminal works on the use of $Pd(dba)_2$ with monodentate phosphines in allylic substitutions, see: Ferroud, D.; Genêt, J. P.; Muzart, J. *Tetrahedron Lett.* **1984**, *25*, 4379.
(108) For seminal works on the use of $Pd(dba)_2$ with bidentate phosphines in allylic substitutions, see: Fiaud, J.-C.; Hibon de Gournay, A.; Larchevêque, M. *J. Organomet. Chem.* **1978**, *154*, 175.
(109) Amatore, C.; Jutand, A.; Meyer, G.; Mottier, L. *Chem.*−*Eur. J.* **1999**, *5*, 466.
(110) Amatore, C.; Gamez, S.; Jutand, A. *Chem.*−*Eur. J.* **2001**, *7*, 1273.
(111) Amatore, C.; Gamez, S.; Jutand, A.; Meyer, G.; Mottier, L. *Electrochim. Acta* **2001**, *46*, 3237.
(112) Agenet, N.; Amatore, C.; Gamez, S.; Gérardin, H.; Jutand, A.; Meyer, G.; Orthwein, C *ARKIVOC* **2002**, 92; http://www.arkat-usa.org/
(113) Amatore, C.; Jutand, A.; Mensah, L.; Fiaud, J.-C.; Legros, J.-Y. *Eur. J. Org. Chem.* **2006**, 1185.
(114) Bäckvall, J.-E.; Granberg, K. L.; Heumann, A. *Isr. J. Chem.* **1991**, *31*, 17.
(115) Granberg, K. L.; Bäckvall, J.-E *J. Am. Chem. Soc.* **1992**, *114*, 6858.
(116) Tsuji, J. *Tetrahedron* **1986**, *42*, 4361.
(117) Amatore, C.; Gamez, S.; Jutand, A.; Meyer, G.; Moreno-Mañas, M.; Morral, L.; Pleixats, R *Chem.*−*Eur. J.* **2000**, *6*, 3372.
(118) Moreno-Mañas, M.; Morral, L.; Pleixats, R. *J. Org. Chem.* **1998**, *63*, 6160.
(119) Jutand, A. *Eur. J. Inorg. Chem.* **2003**, 2017.
(120) Hayashi, T.; Kubo, A.; Ozawa, F. *Pure Appl. Chem.* **1992**, *64*, 421.

(121) de Meijere, A.; Meyer, F. E. *Angew. Chem., Int. Ed. Engl.* **1994**, *33*, 2379.
(122) Beletskaya, I. P.; Cheprakov, A. V. *Chem. Rev.* **2000**, *100*, 3009.
(123) Farina, V. *Adv. Synth. Catal.* **2004**, *346*, 1553.
(124) Amatore, C.; Godin, G.; Jutand, A.; Lemaitre, F. *Chem.—Eur. J.* **2007**, *13*, 2002.
(125) Amatore, C.; Godin, G.; Jutand, A.; Lemaitre, F. *Organometallics* **2007**, *26*, 1757.
(126) Mo, J.; Xu, L.; Xiao, J. *J. Am. Chem. Soc.* **2005**, *127*, 751.
(127) Farina, V.; Roth, G. P., *Recent Advances in the Stille Reaction in Advances in Metal-Organic Chemistry*; JAI Press Inc.: 1996, Vol, *1*.
(128) Farina, V.; Krishnamurthy, V.; Scott, W. J. *The Stille Reaction in Organic Reactions*, Wiley: New York, 1997; Vol *50*, p 1.
(129) Casado, A. L.; Espinet, P. *J. Am. Chem. Soc.* **1998**, *120*, 8978.
(130) Alvarez, R.; Faza, O. N.; Lopez, C. S.; de Lera, A. R. *Org. Lett.* **2006**, 35.
(131) Nova, A.; Ujaque, G.; Maseras, F.; Lledos, A.; Espinet, P. *J. Am. Chem. Soc.* **2006**, *128*, 14571.
(132) Tougerti, A.; Negri, S.; Jutand, A. *Chem.—Eur. J.* **2007**, *13*, 666.
(133) Alami, M.; Ferri, F.; Linstrumelle, G. *Tetrahedron Lett.* **1993**, *34*, 6403.
(134) Jutand, A.; Negri, S.; Principaud, A. *Eur. J. Inorg. Chem.* **2005**, 631.
(135) Moreno-Mañas, M.; Pérez, M.; Pleixats, R. *J. Org. Chem.* **1996**, *61*, 2346.
(136) For dppp as ligand, see: Yoshida, H.; Yamaryo, Y.; Ohshita, J.; Kunai, A. *Tetrahedron Lett.* **2003**, *44*, 1541.
(137) Miyaura, N. *Advances in Metal-Organic Synthesis*; JAI Press Inc.: 1998, Vol *6*, p 187.
(138) Adamo, C.; Amatore, C.; Ciofini, I.; Jutand, A.; Lakmini, H. *J. Am. Chem. Soc.* **2006**, *128*, 6829.
(139) Moreau, X.; Campagne, J. M. *J. Organomet. Chem.* **2003**, *687*, 322.
(140) For the seminal use of dppf ligand in C-S coupling, see: Ciattini, P. G.; Morera, E.; Ortar, G. *Tetrahedron Lett.* **1995**, *36*, 4133.
(141) Moreau, X.; Campagne, J. M.; Meyer, G.; Jutand, A. *Eur. J. Org. Chem.* **2005**, 3749.
(142) Lund, H. In *Organic Electrochemistry*, 4th ed.; Lund, H., Hammerich, O., Eds.; Marcel Dekker Inc: New York, 2001.
(143) *Organic Electrochemistry*; Schäfer, H. J., Ed.; Wiley-VCH: Weinheim, Germany, 2004.
(144) Torii, S. *Synthesis* **1986**, 873.
(145) Steckhan, E. *Angew. Chem., Int. Ed. Engl.* **1986**, *25*, 683.
(146) Chaussard, J.; Folest, J.-C.; Nédélec, J.-Y.; Périchon, J.; Troupel, M. *Synthesis* **1990**, *5*, 369.
(147) Nédélec, J.-Y.; Périchon, J.; Troupel, M. *Top. Curr. Chem.* **1997**, *18*, 5–141.
(148) Duñach, E.; Franco, D.; Olivero, S. *Eur. J. Org. Chem.* **2003**, 1605.
(149) Sock, O.; Troupel, M.; Périchon, J. *Tetrahedron Lett.* **1985**, *26*, 1509.
(150) Troupel, M.; Rollin, Y.; Périchon, J.; Fauvarque, J.-F. *Nouv. J. Chim.* **1981**, *5*, 621.
(151) Fauvarque, J.-F.; Chevrot, C.; Jutand, A.; François, M.; Périchon, J. *J. Organomet. Chem.* **1984**, *264*, 273.
(152) Amatore, C.; Jutand, A. *J. Am. Chem. Soc.* **1991**, *113*, 2819.
(153) Amatore, C.; Jutand, A. *J. Electroanal. Chem.* **1991**, *306*, 141.
(154) Fauvarque, J.-F.; Jutand, A.; François, M.; Petit, M. A. *J. Appl. Electrochem.* **1988**, *18*, 116.
(155) Fauvarque, J.-F.; Jutand, A.; François, M. *Nouv. J. Chim.* **1986**, *10*, 119.
(156) Fauvarque, J.-F.; Jutand, A.; François, M. *J. Appl. Electrochem.* **1988**, *18*, 109.
(157) Fauvarque, J.-F.; De Zélicourt, Y.; Amatore, C.; Jutand, A. *J. Appl. Electrochem.* **1990**, *20*, 338.
(158) Fauvarque, J.-F.; De Zélicourt, Y.; Amatore, C.; Jutand, A., Compagnie Générale d'Electricité, CGE SA,French Patent 86/0571, 1986.
(159) Amatore, C.; Jutand, A. *Organometallics* **1988**, *7*, 2203.
(160) Amatore, C.; Jutand, A.; Mottier, L. *J. Electroanal. Chem.* **1991**, *306*, 125.
(161) Amatore, C.; Jutand, A. *Acta Chem. Scand.* **1990**, *44*, 755.
(162) Rollin, Y.; Troupel, M.; Tuck, D. G.; Périchon, J. *J. Organomet. Chem.* **1986**, *303*, 131.
(163) Meyer, G.; Troupel, M.; Périchon, J. *J. Organomet. Chem.* **1990**, *393*, 137.
(164) Courtois, V.; Barhdadi, R.; Troupel, M.; Périchon, J. *Tetrahedron* **1997**, *53*, 11569.
(165) Raynal, F.; Barhdadi, R.; Périchon, J.; Savall, A.; Troupel, M. *Adv. Synth. Catal.* **2002**, *344*, 45.
(166) Barhdadi, R.; Courtinard, C.; Nédélec, J.-Y.; Troupel, M. *Chem. Commun.* **2003**, 1434.
(167) Mellah, M.; Gmouh, S.; Vaultier, M.; Jouikov, V. *Electrochem. Commun.* **2003**, *5*, 591.
(168) de França, K. W. R.; Navarro, M.; Léonel, E.; Durandetti, M.; Nédélec, J.-Y. *J. Org. Chem.* **2002**, *67*, 1838.
(169) de França, K. W. R.; de Lira Oliviera, J.; Florêncio, T.; da Silva, A. P.; Navarro, M.; Léonel, E.; Nédélec, J.-Y. *J. Org. Chem.* **2005**, *70*, 10778.
(170) Durandetti, M.; Devaud, M.; Périchon, J. *New J. Chem.* **1996**, *20*, 659.
(171) Courtois, V.; Barhdadi, R.; Condon, S.; Troupel, M. *Tetrahedron Lett.* **1999**, *40*, 5993.
(172) Cannes, C.; Labbé, E.; Durandetti, M.; Devaud, M.; Périchon, J. J. *Electroanal. Chem.* **1996**, *412*, 85.
(173) Cannes, C.; Condon, S.; Durandetti, M.; Périchon, J.; Nédélec, J.-Y. *J. Org. Chem.* **2000**, *65*, 4575.
(174) Fauvarque, J.-F.; Petit, M. A.; Pflüger, F.; Jutand, A.; Chevrot, C.; Troupel, M. *Makromol. Chem.* **1983**, *4*, 455.
(175) Fauvarque, J.-F.; Digua, A.; Petit, M. A.; Savard, J. *Makromol. Chem.* **1985**, *186*, 2415.
(176) Aboukassim, A.; Chevrot, C. *Polymer* **1993**, *34*, 401.
(177) Mellah, M.; Labbé, E.; Nédélec, J.-Y.; Périchon, J. *New J. Chem.* **2002**, *26*, 207.
(178) Zotti, G.; Schiavon, G.; Comisso, N.; Berlin, A.; Pagani, G. *Synth. Met.* **1990**, *36*, 337.
(179) Utley, J. H. P.; Gao, Y.; Gruber, J.; Lines, R. *J. Mater. Chem.* **1995**, *5*, 1297.
(180) Amatore, C.; Gaubert, F.; Jutand, A.; Utley, J. H. P. *J. Chem. Soc., Perkin Trans.* **1996**, *2*, 2447.
(181) Kijima, M.; Sakai, Y.; Shirakawa, H. *Chem. Lett.* **1994**, 2011.
(182) Conan, A.; Sibille, S.; d'Incan, E.; Périchon, J. *J. Chem. Soc., Chem. Commun.* **1990**, 48.
(183) Durandetti, M.; Sibille, S.; Nédélec, J.-Y.; Périchon, J. *Synth. Commun.* **1994**, *24*, 145.
(184) Durandetti, M.; Nédélec, J.-Y.; Périchon, J. *J. Org. Chem.* **1996**, *61*, 1748.
(185) Durandetti, M.; Périchon, J.; Nédélec, J.-Y. *Tetrahedron Lett.* **1997**, *38*, 8683.
(186) Durandetti, M.; Périchon, J.; Nédélec, J.-Y. *J. Org. Chem.* **1997**, *62*, 7914.
(187) Gomes, P.; Gosmini, C.; Périchon, J. *Tetrahedron* **2003**, *59*, 2999.
(188) Buriez, O.; Nédélec, J.-Y.; Périchon, J. *J. Electroanal. Chem.* **2001**, *506*, 162.
(189) Polleux, L.; Labbé, E.; Buriez, O.; Périchon, J. *Chem.—Eur. J.* **2005**, *11*, 4678.
(190) Gomes, P.; Gosmini, C.; Périchon, J. *J. Org. Chem.* **2003**, *68*, 1142.
(191) Gomes, P.; Buriez, O.; Labbé, E.; Gosmini, C.; Périchon, J. *J. Electroanal. Chem.* **2004**, *562*, 255.
(192) Scheffold, R.; Dike, M.; Dike, S.; Herold, T.; Walder, L. *J. Am. Chem. Soc.* **1980**, *102*, 3642.
(193) Scheffold, R.; Abrecht, S.; Orfinski, R.; Ruf, H.-R.; Stamouli, P.; Tinembart, O.; Walder, L.; Weymuth, C. *Pure Appl. Chem.* **1987**, *59*, 363.
(194) Torii, S.; Tanaka, H.; Hamatani, T.; Morisaki, K.; Jutand, A.; Pflüger, F.; Fauvarque, J.-F. *Chem. Lett.* **1986**, 169.
(195) Amatore, C.; Jutand, A.; Khalil, F.; Nielsen, M. F. *J. Am. Chem. Soc.* **1992**, *114*, 7076.
(196) Jutand, A.; Négri, S. *Eur. J. Org. Chem.* **1998**, 1811.
(197) Jutand, A.; Négri, S.; Mosleh, A. *J. Chem. Soc., Chem. Commun.* **1992**, 1729.
(198) Jutand, A.; Négri, S. *Synlett* **1997**, 719.
(199) Kamekawa, H.; Senboku, H.; Tokuda, M. *Tetrahedron Lett.* **1998**, *39*, 1591.
(200) Senboku, H.; Fujimura, Y.; Kamekawa, H.; Tokuda, M. *Electrochim. Acta* **2000**, *45*, 2995.
(201) Kamekawa, H.; Senboku, H.; Tokuda, M. *Electrochim. Acta* **1997**, *42*, 2117.
(202) Kamekawa, H.; Kudoh, H.; Senboku, H.; Tokuda, M. *Chem. Lett.* **1997**, 917.
(203) Torii, S.; Tanaka, H.; Morisaki, K. *Tetrahedron Lett.* **1985**, *26*, 1655.
(204) Amatore, C.; Carré, E.; Jutand, A.; Tanaka, H.; Ren, Q.; Torii, S. *Chem.—Eur. J.* **1996**, *2*, 1729.
(205) Marzouk, H.; Rollin, Y.; Folest, J. C.; Nédélec, J.-Y.; Périchon, J. *J. Organomet. Chem.* **1989**, *369*, C47.
(206) Amatore, C.; Jutand, A.; Périchon, J.; Rollin, Y. *Monatsh. Chem.* **2000**, *131*, 1293.
(207) Sengmany, S.; Léonel, E.; Paugam, J.-P.; Nédélec, J.-Y. *Tetrahedron* **2002**, *58*, 271.
(208) Léonel, E.; Paugam, J.-P.; Condon-Gueugnot, S.; Nédélec, J.-Y. *Tetrahedron* **1998**, *54*, 3207.
(209) Oudeyer, S.; Léonel, E.; Paugam, J.-P.; Nédélec, J.-Y. *Tetrahedron* **2003**, *59*, 1073.
(210) Oudeyer, S.; Léonel, E.; Paugam, J.-P.; Sulpice-Gaillet, C.; Nédélec, J.-Y. *Tetrahedron* **2006**, *62*, 1583.
(211) Duñach, E.; Périchon, J. *J. Organomet. Chem.* **1988**, *352*, 239.
(212) Labbé, E.; Duñach, E.; Périchon, J. *J. Organomet. Chem.* **1988**, *353*, C51.

(213) Duñach, E.; Derien, S.; Périchon, J. *J. Organomet. Chem.* **1989**, *364*, C33.
(214) Derien, S.; Duñach, E.; Périchon, J. *J. Am. Chem. Soc.* **1991**, *113*, 8447.
(215) Derien, S.; Duñach, E.; Périchon, J. *J. Organomet. Chem.* **1990**, *385*, C43.
(216) Derien, S.; Clinet, J.-C.; Duñach, E.; Périchon, J. *J. Chem. Soc., Chem. Commun.* **1991**, 549.
(217) Derien, S.; Clinet, J.-C.; Duñach, E.; Périchon, J. *J. Organomet. Chem.* **1992**, *424*, 213.
(218) Derien, S.; Clinet, J.-C.; Duñach, E.; Périchon, J. *Tetrahedron* **1992**, *48*, 5235.
(219) Derien, S.; Clinet, J.-C.; Duñach, E.; Perichon, J. *J. Org. Chem.* **1993**, *58*, 2578.
(220) Derien, S.; Clinet, J.-C.; Duñach, E.; Périchon, J. *Synlett* **1990**, 361.
(221) Condon-Gueugnot, S.; Léonel, E.; Nédélec, J.-Y.; Périchon, J. *J. Org. Chem.* **1995**, *60*, 7684.
(222) Condon, S.; Nédélec, J.-Y.; Périchon, J. *Eur. J. Org. Chem.* **2002**, 105.
(223) Condon, S.; Dupré, D.; Lachaise, I.; Nédélec, J.-Y. *Synthesis* **2002**, 1752.
(224) Condon-Gueugnot, S.; Dupré, D.; Nédélec, J.-Y.; Périchon, J. *Synthesis* **1997**, 1457.
(225) Métay, E.; Léonel, E.; Condon, S.; Nédélec, J.-Y. *Tetrahedron* **2006**, *62*, 8515.
(226) de Mendonça Cavalcanti, J. C.; Goulart, M. O. F.; Léonel, E.; Nédélec, J.-Y. *Tetrahedron Lett.* **2002**, *43*, 6343.
(227) Gomes, P.; Gosmini, C.; Nédélec, J.-Y.; Périchon, J. *Tetrahedron Lett.* **2002**, *43*, 5901.
(228) Jia, C.; Fujiwara, Y. *Pure Appl. Chem.* **2001**, *73*, 319.
(229) Boele, M. D. K.; van Strijdonck, G. P. F.; de Vries, A. H. M.; Kamer, P. C. J.; de Vries, J. G.; van Leeuwen, P. W. N. M. *J. Am. Chem. Soc.* **2002**, *124*, 1586.
(230) Amatore, C.; Cammoun, C.; Jutand, A. *Adv. Synth. Catal.* **2007**, *349*, 292.
(231) For a review on orthometallation, see: Pfeffer, M. *Pure Appl. Chem.* **1992**, *64*, 335.
(232) Heck, R. F. *J. Am. Chem. Soc.* **1969**, *91*, 6707.
(233) Grennberg, H.; Gogoll, A.; Bäckvall, J.-E. *Organometallics* **1993**, *12*, 1790.
(234) Amatore, C.; Cammoun, C.; Jutand, A. *Synlett* **2007**, 2173.
(235) Peterson, K. P.; Larock, R. C. *J. Org. Chem.* **1998**, *63*, 3185.
(236) Steinhoff, B. A.; Stahl, S. S. *J. Am. Chem. Soc.* **2006**, *128*, 4348.
(237) Bäckvall, J.-E.; Gogoll, A. *J. Chem. Soc., Chem. Commun.* **1987**, 1237.
(238) Bäckvall, J.-E.; Åkermark, B.; Ljunggren, S. O. *J. Am. Chem. Soc.* **1979**, *101*, 2411.
(239) Inokuchi, T.; Ping, L.; Hamaue, F.; Izawa, M.; Torii, S. *Chem. Lett.* **1994**, 121.
(240) Mitsudo, K.; Kaide, T.; Nakamoto, E.; Yoshida, K.; Tanaka, H. *J. Am. Chem. Soc.* **2007**, *129*, 2246.
(241) Kolb, H. C.; VanNieuwenhze, M. S.; Sharpless, K. B. *Chem. Rev.* **1994**, *94*, 2483.
(242) Mehrman, S. T.; Abdel-Magid, A. F.; Maryanoff, C. A.; Medaer, B. P. *Topics III, Organometallic Chemistry 06, Organometallics in Process Chemistry*; Larsen, R. D., Ed.; Springer-Verlag: Berlin-Heidelberg, 2004; p 153.
(243) Gao, Y.; Zepp, C. M.; Wai, J. S. M. *Abstr. Pap. Am. Chem. Soc.* **1990**, *199*, 15.
(244) Gao, Y.; Zepp, C. M. World Patent WO9317150 1993.
(245) Torii, S.; Liu, P.; Tanaka, H. *Chem. Lett.* **1995**, 319.
(246) Torii, S.; Liu, P.; Bhuvaneswari, N.; Amatore, C.; Jutand, A. *J. Org. Chem.* **1996**, *61*, 3055.
(247) Amatore, C.; Carré, E.; Jutand, A.; Tanaka, H.; Torii, S.; Chiarotto, I.; Carelli, I. *Electrochim. Acta* **1997**, *42*, 2143.

CR068072H